Ao.Univ.Prof. Alois Lugstein | Ao.Univ.Prof. Günther Fafilek

TECHNISCHE UNIVERSITÄT WIEN
Vienna University of Technology

DISSERTATION

Nucleation and Growth of Germanium Nanostructures using Unusual Metal Seeds

ausgeführt zur Erlangung des akademischen Grades eines
Doktors der technischen Wissenschaften

unter der Leitung von
Privatdoz. Dipl.-Chem. Dr.rer.nat. Sven Christian Barth

E165
Institut für Materialchemie

eingereicht an der Technischen Universität Wien
Fakultät für Technische Chemie

von

Dipl.-Ing. Patrik Pertl
0630352
Andreasgasse 5/4/5, 1070 Wien

Wien, November 2017 | Dipl.-Ing. Patrik Pertl

“Everything will be okay in the end. If it's not okay, it's not the end.”

John Lennon *(1940-1980)*

Statutory declaration

I herewith declare that I have authored this thesis independently, that I have not used other than the declared sources / resources, and that I have explicitly marked all material which has been quoted either literally or by content from the used sources.

Eidesstattliche Erklärung

Ich erkläre hiermit an Eides statt, dass ich die vorliegende Dissertation selbstständig und ohne fremde Hilfe verfasst, andere als die angegebenen Quellen und Hilfsmittel nicht benutzt und die den benutzten Quellen wörtlich und inhaltlich entnommenen Stellen als solche erkenntlich gemacht habe.

Parts of this work have been published

- *"Lead-supported germanium nanowire growth"*
  M. S. Seifner, P. Pertl, J. Bernardi, S.Biswas, J. D. Holmes, S. Barth, *Materials Letters*, **2016**, 173, 248-251

I. Acknowledgement

I would like to thank all those people who made this thesis possible and an unforgettable experience:

First of all, I would like to thank my supervisor Privdoz. Sven Barth for giving me the opportunity to work in this fascinating research field; countless SEM and TEM measurements, his inexhaustible patience and positive attitude when chemistry appeared beyond control and his always open door, enabling fruit-full discussions, small tips and hints whenever required. Without your encouragement, this thesis would look rather different.

Prof. Alois Lugstein and Prof. G. Fafilek should be acknowledged for reviewing my thesis.

I also want to thank.....

...MSc. Masiar Sistani and Prof. A. Lugstein for providing the electrical measurements.

...the USTEM and X-Ray Centre of the TU Vienna for providing infrastructure for numerous measurements at their facilities.

...my PhD buddies Felix Biegger and Michael S. Seifner for being great colleagues, sharing their thoughts about rising questions and great lunch breaks at the canteen of the Theater an der Wien. It was great sharing lab and office with you.

...Michael S. Seifner once again for the time and expertise he provided to measure my nanowire samples at the TEM and some awesome-looking EDX mappings.

...Lukas Hrachowina for being a great lab fellow, several chess tips and his humorous attitude.

...the members of the AG Eder, especially Oliver W., Leonie D., Greta H. and Dennis D. for being great colleagues during the Synthesepraktikum and for funny discussions during tea and coffee breaks.

...Stephan R.-P., Harald S. and Ruppert K. of the institutes staff.

...Felix J, as we had several great bouldering sessions at the Boulderbar

... Felix B. once more for proof reading a major part of this thesis.

...my family, namely my parents Erich and Claudia, my sister Corinna as well as Hansjörg, Michaela and Maximilian for supporting me spiritually throughout the time in Vienna and always being there for me.

...my love Carmen, listed last for the third time, but still number one on the importance scale.

Thank you, for all your encouragement!

II. Abstract

The fast progress in the electronic industry regarding enhanced performance and miniaturisation leads to an increased demand for new materials exhibiting superior electronic properties. Elongated nanostructures of the well-known group IV element germanium stay in focus of intense research efforts due to the high charge carrier mobility's, achievable with this material. Usually, germanium nanowires are grown via the gas-phase on substrates or in solution using a gold-assisted growth process. However, the usage of gold as growth promoter leads to many drawbacks, such as decreasing semiconducting properties due to incorporation of seed atoms into the nanowire material. Therefore, various metals have been investigated as alternative growth promoters, nevertheless some interesting elements have not been examined yet.

In the first part of this thesis, the application of lead as an alternative growth promoter for germanium nanowires is investigated. Nanowire growth is conducted via liquid-seeded growth in the vapour phase and under supercritical fluid conditions. Obtained single crystalline nanowires with approx. 15 nm in diameter exhibit no seed material incorporation. Additionally, solid-seeded growth in the supercritical regime is investigated. Therein, metal-amide precursors are used, to achieve sufficient thermolysis at lower growth temperatures.

In another study, low temperature growth for germanium nanorods and nanowires is examined. Gallium seeds, which induced nanowire growth, are generated *in situ* by the thermal decomposition of pentamethylcyclopentadienyl gallium (I) in toluene. Gallium seeds seem to catalyse the decomposition of the germanium precursor, which enables decreasing the growth temperature as low as 170 °C, which is the lowest reported temperature for germanium nanowire grown via CVD. The obtained nanostructures exhibited a high crystallinity, despite low growth temperatures. Elemental maps obtained from STEM EDX measurements exhibit an incorporation of up to 3.6 % gallium into the nanowire matrix. Ga incorporation in germanium is known to result in a p-doping effect of the material. Electrical characterisation of single nanowires revealed a very high conductivity compared to pristine germanium nanowires.

Lastly, the defect transfer from solid silver seeds to germanium nanowires is used to gain control over the nanowires' crystal structure. Silver bipyramids exhibiting a defined twin structure are synthesised via the polyol-method and used to promote nanowire growth via a solid-seeded mechanism. Unfortunately, nucleation as well as nanowire growth is strongly inhibited, which is related to the capping agent, used for the polyol method. Large fractions of the obtained nanowires exhibit strong kinking or diameters not matching to the synthesised silver seeds. Nevertheless, hints towards a successful defect transfer are found.

III. Kurzfassung

Schnell fortschreitende Entwicklungen in der Elektronikindustrie hinsichtlich erhöhter Leistung und Miniaturisierung führt zu einer vergrößerten Nachfrage nach neuen Materialien mit immer besseren elektronischen Eigenschaften. Nanostrukturen des Gruppe-IV Elements Germanium sind in diesem Zusammenhang von besonderem Interesse, da sie überdurchschnittlich hohe Ladungsträgermobilitäten aufweisen. Für gewöhnlich werden Germanium-Nanodrähte mittels Gold-unterstütztem Wachstum hergestellt. Diese Methode hat jedoch mehrere Nachteile. Zum Beispiel, dass in den Nanodraht eingebaute Goldatome die Halbleitereigenschaften des Materials verschlechtern. Aus diesem Grund werden alternative Materialien als Wachstumskeim für elongierte Germanium-Nanostrukturen untersucht.

Im ersten Teil der Arbeit wird das Blei-unterstützte Wachstum von Germanium-Nanodrähten beschrieben. Nanodrähte wurden mit Hilfe von flüssigen Bleikeimen auf Siliziumsubstraten, in überkritischem Lösungsmittel, sowie mittels chemischer Gasphasenabscheidung synthetisiert. Die erhaltenen einkristallinen Drähte zeigten Durchmesser um 15 nm und wiesen keinen Einbau von Bleiatomen auf. Des Weiteren wurde das Nanodrahtwachstum mittels festen Bleikeimen unter überkritischen Bedingungen untersucht. Zu diesem Zweck wurden Germanium- und Bleiamid Vorstufen eingesetzt, die sich bei den vorherrschenden niedrigen Temperaturen bereits ausreichend zersetzen.

Ein weiterer Abschnitt der Dissertation befasst sich mit der Niedertemperatursynthese von Germanium Nanostäbchen und Nanodrähten. Dazu wurden Keime aus Gallium *in situ* durch die Thermolyse von Pentamethylcyclopentadienyl Gallium(I) in Toluol erzeugt, die das Nanodrahtwachstum initiieren. Die Wachstumstemperatur der Nanostrukturen konnte auf Grund der katalysierten Zersetzung der Germaniumvorstufe durch die Galliumkeime auf bis zu 170 °C verringert werden, was zum heutigen Zeitpunkt die niedrigste Temperatur für Germanium-Nanodrahtwachstum mittels CVD darstellt. Die erhaltenen Nanodrähte zeigten trotz der niedrigen Wachstumstemperatur eine sehr hohe Kristallinität. Des Weiteren konnte ein Einbau von bis zu 3.6 % Gallium in die Germaniumstrukturen beobachtet werden. Eine elektrische Charakterisierung von Einzeldrähten ergab aus diesem Grund eine, im Vergleich zu reinen Germaniumdrähten, stark erhöhte Leitfähigkeit.

Im letzten Teil wird die Kontrolle über die Kristallstruktur von Germanium-Nanodrähten mit Hilfe von Defekttransfer fester Silberkeime auf Germanium-Nanodrähte untersucht. Zu diesem Zweck wurden verzwillingte Silberbipyramiden mittels der Polyolmethode hergestellt und anschließend als Wachstumskeime für Germanium-Nanodrähte verwendet. Durch das in der Polyolmethode verwendete Tensid kam es zu einem stark erschwerten Wachstumsprozess, der sich in einer verschlechterten Nukleation, sowie dem Auftreten von defektreichen Drähten, die viele Wechsel der Wachstumsrichtung aufweisen äußerte, was die Untersuchung des Defekttransfers stark erschwert. Trotzdem konnten Indizien für einen erfolgten Defekttransfer gefunden werden.

IV. TOC

1. One-Dimensional Nanostructures

Over the last 25 years, nanotechnology has gained a massive upward trend evolving from a small research niche to one of the most future-oriented topics. Many of nowadays inventions, such as new methods for controlled drug delivery[1], functional coatings[2] or high performance electronic components[3] had been induced by the investigation of nanoscopic objects exhibiting specific properties. Usually, nanotechnology is referred to structures exhibiting at least one dimension which is sized below 100 nm.

Nanostructures can be classified by their dimensionality.[4] Objects are described to be zero, one or two dimensional. Needless to say that objects with a missing dimension do not exist in reality, it became custom practice to categorize objects by the number of dimensions which are bigger than 100 nm. Therefore, clusters and particles with a particle diameter below 100 nm are denoted as zero dimensional objects or quantum dots, while thin films and platelets exhibiting a thickness below 100 nm represent the group of two dimensional objects. One dimensional objects in contrast, show a wider variety of possible morphologies. Nanowires (NWs) or whiskers are anisotropic, solid objects with an aspect ratio (i.e. the ratio between length and diameter) above 100. Nanorods (NRs) in contrast, show lower aspect ratios, usually up to ten. Nanotubes are hollow objects, which show anisotropic dimensions similar to nanorods or NWs. They are very well-known for carbon and represent a separate research topic in the group of 1D materials. Finally, nanobelts show an additional lateral expansion, making their cross-section rather rectangular than quadratic or circular. Examples for 1D-nanostructures and their corresponding cross-sections are illustrated in Figure 1.

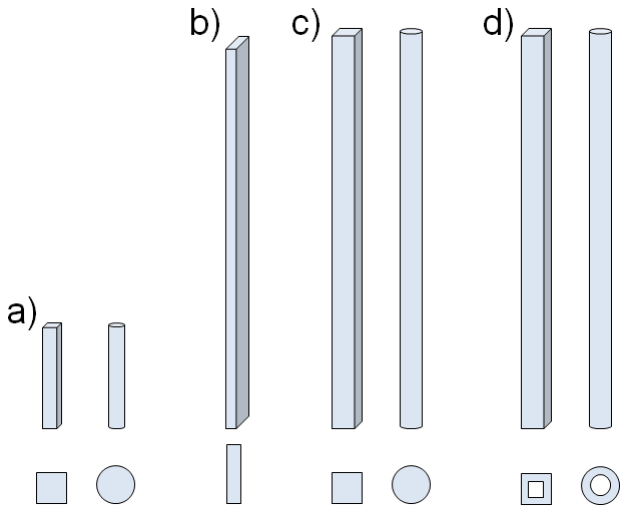

Figure 1: Nanostructures and corresponding cross-sections: a) nanorods, b) nanobelts, c) nanowires and d) nanotubes.

Semiconducting properties are the most important material feature for a broad number of applications. Electronic and photonic devices such as transistors[5], light emitting diodes[6] or photovoltaic cells[7] as

well as photocatalytic applications[8] like water splitting or carbon dioxide reduction require a semiconductor with distinct electronic properties. Many processes of the aforementioned fields of application show only low or limited performance, when using a bulk semiconductor instead of a nanomaterial. Furthermore, the increase in performance of new electronic circuits generates an emerging demand for nano-scaled materials, as they often enable features which cannot be obtained from the corresponding bulk materials. Inorganic semiconductors for instance, show interesting modulations of their electronic properties, if their size decreases below a critical value.[9]

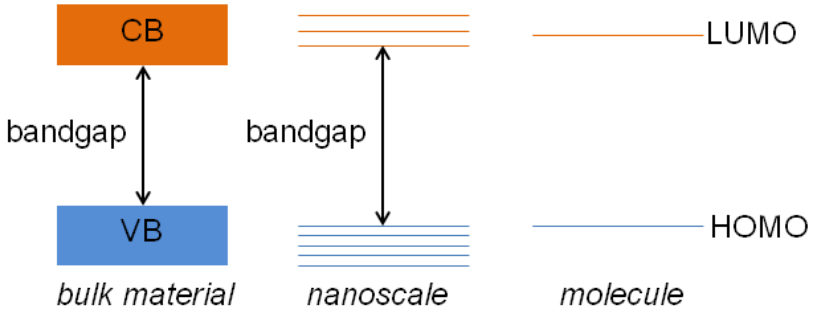

Figure 2: Band structure of various sized objects.

If a structure becomes diminished in size, the decreasing number of atoms and with it the decreasing number of overlapping orbitals in the structure lead first to an increase of the bandgap. With further decreasing size, the remaining orbitals are no longer sufficient to generate a continuous valence and conduction band. As a result only a small number of discrete energetic states remain (quantum confinement). A comparison between the band structure of a bulk material, nanoscale object and molecule is illustrated in Figure 2. This feature enables to alter the electronic properties directly by adjusting the morphology of the nanostructure.[10] Therefore, it should be at least possible in theory to create the material exhibiting the "ideal" band structure for each purpose.

2. Synthesis Methods and Growth Mechanisms for 1D-Nanostructures

Basically, every method applied to produce 1D-nanostructures is based either on a top-down or a bottom-up growth strategy. A brief overview about distinct features, advantages and disadvantages for each growth strategy and the underlying growth mechanisms should be given in the following chapters.

2.1. Top-Down Approaches

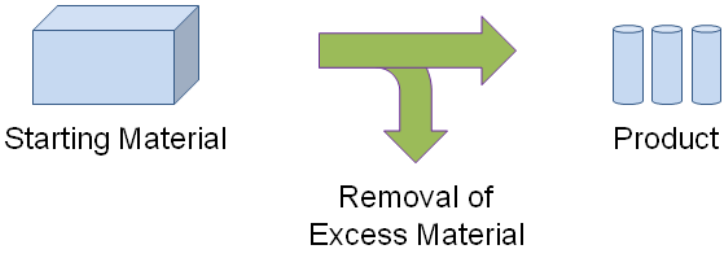

Figure 3: Scheme of the top-down approach.

In top-down approaches, the manufacturing process of nanostructures starts from a bulk material. The desired structure is created by the successive removal of excess material (Figure 3). As the dimensions of nanostructures are very small, conventional top-down techniques such as cutting, milling or drilling are not feasible, hence mostly photolithography-based methods are applied. In a first step a resist is applied onto the material, which is a light sensitive coating. The resist is than exposed to a pattern of intensive light, which induces a chemical reaction in the resist molecules. The illuminated areas become soluble (positive resist) or insoluble (negative resist) for the subsequently applied developer solution, leaving only the desired structures covered by the resist. In the following etching step, the non-covered material is removed using chemical or ion etching techniques.[11] The applied method depends on the starting material and desired structure of the product. Finally the resist can be removed from the remaining nanostructures. The basic sequence of a lithography-based synthesis process is depicted in Figure 4. The major drawback of lithography-based manufacturing methods is that they require multiple steps as well as specific equipment, especially if the desired structures have dimensions near the wavelength of the light used during resist exposure. In this size regime, diffraction starts to limit the resolution of the patterning process. Nevertheless, the lithographic approach is state of the art in nowadays in semiconductor industry and therefore huge effort is expended to further improve this technique. In June 2017 for instance, a research alliance around IBM, Samsung and Globalfoundries demonstrated the potential of advanced lithography techniques by manufacturing a 5 nm nanostructure using extreme ultraviolet lithography.[12]

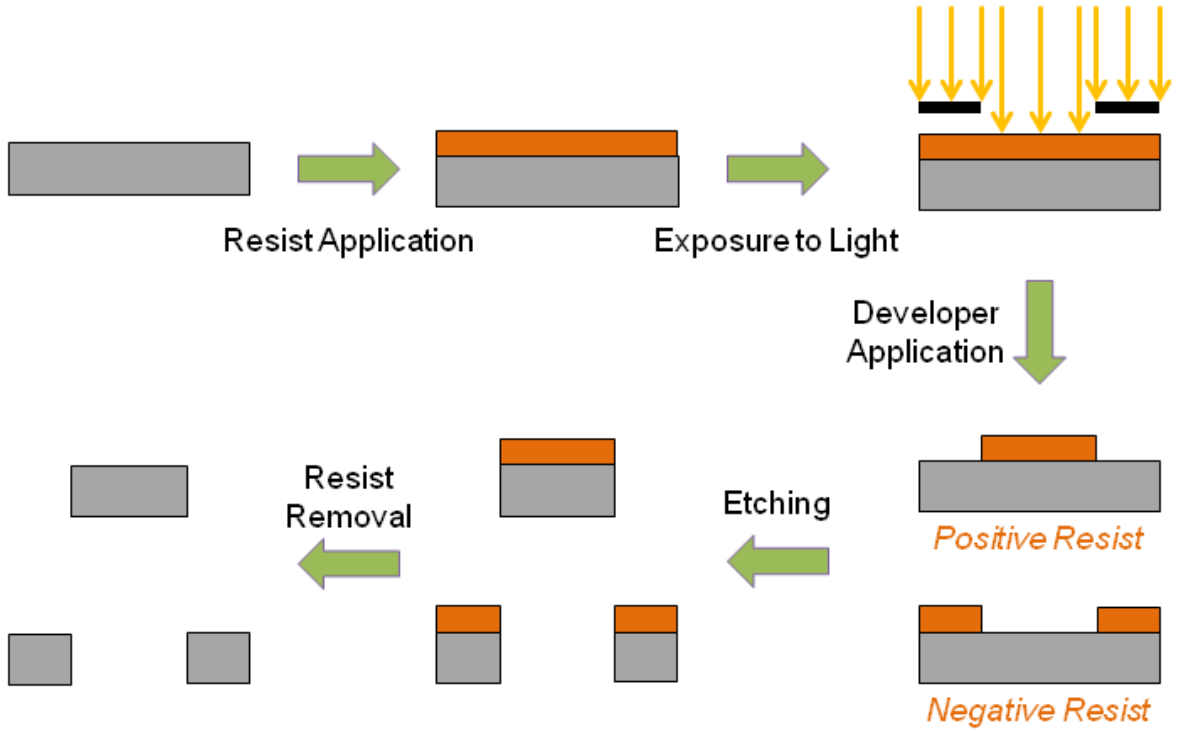

Figure 4: Basic scheme of a lithography-based process.

Another top-down approach, which makes use of site-selective etching is metal-assisted chemical etching.[13] Noble metal particles such as silver[14], gold[15], platinum[16] or a gold/palladium alloy[15] are deposited onto the substrate, mostly silicon. To conduct the etching process, the substrate is placed into a solution containing variable amounts of HF, HNO_3, H_2O_2 and ethanol. Areas covered by the noble metal are dissolved significantly faster, which leads to a selective removal of material. Depending on the process conditions, a porous layer, Si needles or NWs can be obtained. The dissolution process occurs similar to an electrochemical reaction in a galvanic cell. Substrate, metal particles and growth solution act as anode, cathode and electrolyte respectively. However, the details of the growth mechanism are still under discussion.[15-18]

The last top down method which should be mentioned, is focused ion beam (FIB) milling. Thereby material is removed by a beam of accelerated ions such as gallium[19, 20], helium[21] or xenon[22, 23]. Ion beams can be focused very well, which enables the production of very small structures including 1D nanostructures. Shape as well as location of the desired structure can be controlled with a very high accuracy, similar to an electron beam in a scanning electron microscope (SEM). However, FIB techniques are very time consuming and therefore only rarely used to grow nanostructures. Nevertheless the technique is well applied in electron microscopy, as it enables the production of thin lamellae or cross-sections where electrons are capable to pass through.[24, 25] Furthermore, a FIB can be used for post-growth modification of nanostructures and bulk materials. For instance, the implantation of Ga atoms into group IV semiconductors to alter the electronic properties can be achieved via a beam of focused Ga ions.[19, 26, 27]

2.2. Bottom-Up Approaches

In bottom-up approaches, nanostructures are generated from atomic or molecular building blocks. (Figure 5). Hence, an anisotropic growth is mandatory to ensure the formation of an elongated structure. Over the years, a huge variety of growth methods have been published, whereas the underlying mechanisms can be assigned to three major strategies shaping and subsequent conversion, self-induced and seeded growth. As this thesis is aimed on seeded growth methods using metal seeds to promote the formation of elongated nanostructures, other approaches are just briefly discussed, whereas the applied growth strategy will be discussed in more detail.

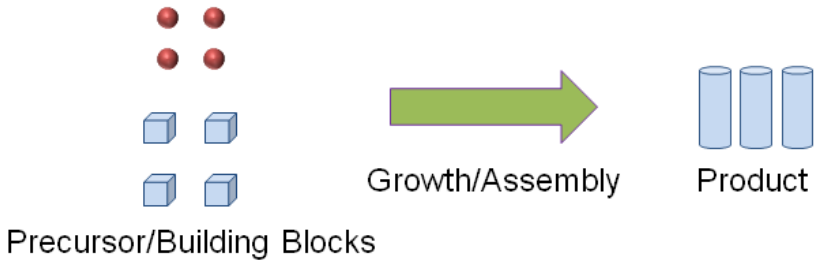

Figure 5: Scheme of the bottom-up approach.

Bottom-up approaches, especially seed-mediated growth require an elaborated supply of adatoms, otherwise the growth process terminates or results in non-reproducible phenomena. While solvent-based approaches are limited to the injection of a precursor solution or electrochemical techniques, a wide variety of techniques had been developed for vapour phase-based approaches. Discussing all techniques in detail would go beyond the scope of this introduction. Therefore, only chemical vapour deposition (CVD) should be discussed in the following chapter, which was the applied method for the vapour phase-based approach.

2.2.1. Chemical Vapour Deposition

Over the years a huge variety of techniques emerged facilitating the deposition of material onto substrates, by using the vapour phase as transport medium. The majority of methods are based on physical vapour deposition (PVD), which can be described as bringing the material from a condensed state into the vapour phase and subsequent condensation of the vapour at the target substrate.

A completely different approach is CVD. In contrast to PVD, exhibits CVD a dissociation process or a chemical reaction of a gaseous species at a thermally activated substrate. The first industrial application of a CVD process dates back to the 1890s, where a patent had been applied, describing the deposition of tungsten onto filaments in light bulbs, by using WCl_6 and H_2 as gaseous precursors.[28] Over the years, CVD emerged to one of the most important coating techniques, enabling the deposition of a vast amount of materials, reaching from simple metals (Al, Pt, Rh, etc) over semiconductors (Si, Ge) as well as compound semiconductors (III-V, II-VI) to ceramics (oxides, nitrides, silicides, borides,

etc.).[29] Even the synthesis of synthetic diamonds via CVD had already become an applied process.[30] Needless to say, that the huge variety of materials cannot be obtained via one CVD process, hence several modifications had been developed to meet specific requirements. Nevertheless, the basic steps remain the same in all CVD methods:

A) Generation of a gaseous precursor and its transport into the CVD chamber.
B.1) Homogenous gas-phase reaction and subsequent formation of particles.
B.2.a) Diffusion through the boundary layer towards the substrates surface.
B.2.b) Adsorption to the surface.
B.2.c) Heterogeneous decomposition to adatoms and byproducts.
B.2.d) Formation of a deposit due to nucleation.
B.2.e) Desorption and subsequent diffusion of by-products through the boundary layer.
C) Removal of the by-products from the CVD chamber.

A schematic view of a basic CVD process is depicted in Figure 6.

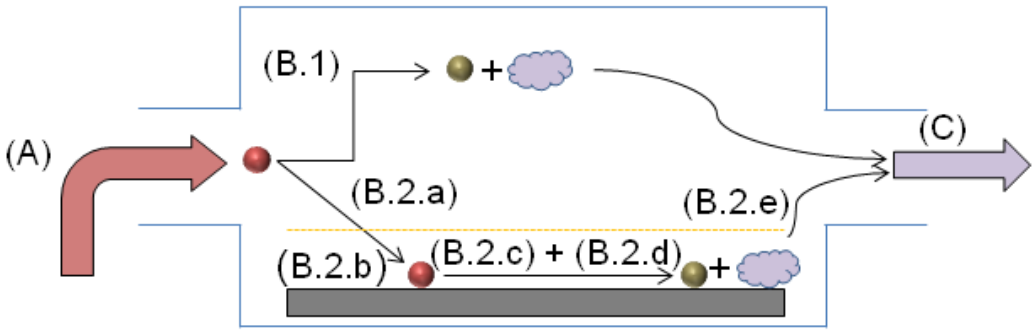

Figure 6: Schematic illustration of the key steps in the CVD process. Redrawn in the style of reference[29].

Depending on the location of the precursor decomposition, two type of reaction take place. The heterogeneous reaction on top of the substrate leads to the formation of deposit directly at the substrate (illustrated as B.2-path in Figure 6). Therefore, precursor molecules must diffuse through the boundary layer, which describes the diffusion-controlled layer in close vicinity to the substrate surface. Homogeneous gas-phase reactions on the other hand, occur in the gas phase and lead to the formation of particles. Growth processes making use of homogenous gas-phase reactions are often related to chemical vapour synthesis (depicted as B.1-path in Figure 6). Process conditions are the main factors determining whether heterogeneous or homogeneous gas-phase reactions take place. For the deposition of dense films or coatings, the CVD process is usually optimized to favour the heterogeneous decomposition reaction.[29]

As precursor decomposition is thermally induced, it is necessary to heat the area where deposition should occur. Therefore, two different approaches have emerged. In the so-called hot-wall CVD, the entire reaction chamber is heated to the growth temperature, whereas in cold-wall approaches exclu-

sively the deposition area is maintained at growth temperature. In hot-wall CVD, the precursor concentration is much more influenced by the reaction chamber as decomposition and the resulting loss of precursor molecules can occur along the entire reaction chamber. Furthermore, the tendency to homogenous gas-phase reactions is much more pronounced. In cold-wall CVD the precursor concentration is not affected by the reactor sidewalls, as the area where deposition can occur is much smaller. Nevertheless, a depletion of precursor along the substrate can occur, if flow conditions are unfavourable.

Another aspect which should be briefly discussed is the supply of precursor. Compounds which are already gaseous under ambient conditions are usually introduced as gas mixture, using an inert gas diluting the precursor to reasonable concentrations. Control over the gas flow can be easily maintained via mass flow controllers or aerometers. For precursors exhibiting higher boiling points, the pressure in the CVD system can be reduced, which is known as low pressure (LP)CVD. Nevertheless, LPCVD is also used for precursors which are gaseous at ambient pressure to minimise effects induced by mass transport and flow dynamics. Solid precursors, which cannot be evaporated by pressure reduction can be also applied by using aerosol-assisted CVD.[31]

From the process engineers view, growth temperature, pressure and precursor flow rate are the most important process parameters in a CVD process, as they can be used to manipulate the morphology and composition of the obtained product. Kinetics and thermodynamics of the growth process are mainly controlled by the applied temperature. Figure 7 illustrates the temperature dependence of the deposition rate for a simplified CVD process, which includes adsorption/desorption of molecules at the substrate as well as deposit formation due to precursor thermolysis. Further effects such as a finite precursor feed or the homogenous gas phase reaction are excluded. At lower deposition temperatures, the deposition reaction appears to be the rate-limiting step of the entire process. Therefore, it is called the kinetically controlled regime. For higher temperatures, the deposition reaction is accelerated until diffusion becomes the rate limiting step, making the CVD process mass transport-controlled. In this regime, the diffusion of precursor molecules through the boundary layer as well as surface diffusion of adatoms on the substrate surface governs the deposition rate. Further temperature increase shifts the process into the thermodynamically controlled regime. Desorption events are favoured at higher temperatures, leading to a steady decrease of the deposition rate with increasing temperatures. An exothermic reaction would further decrease the deposition rate, due to the temperature-dependence of the Gibbs free energy.

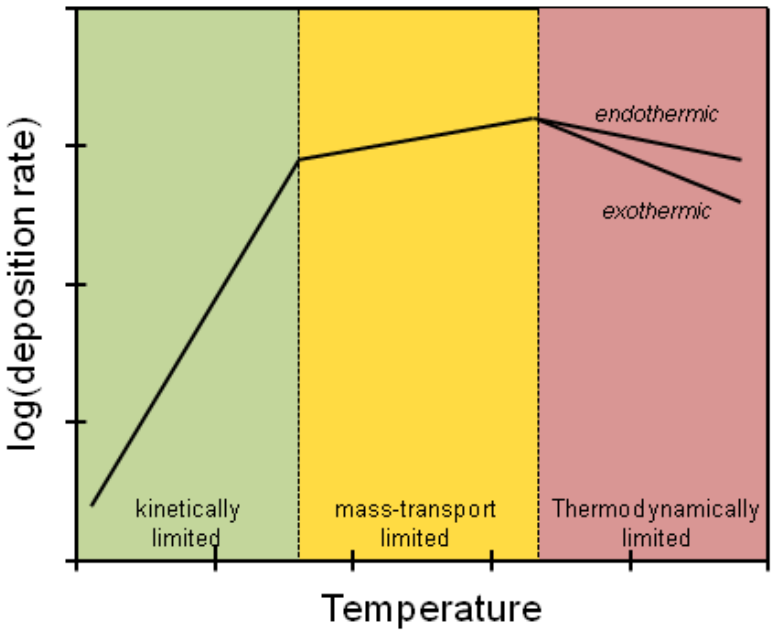

Figure 7: Temperature dependence of deposition rate and growth regimes. Redrawn in style of reference[29].

Regarding metal-assisted NW growth using CVD, the entire growth process becomes more complicated as it includes a lot more steps (discussed in chapter 2.2.6), all exhibiting their own kinetics. However, NW growth is usually conducted in the kinetic regime, which implies that the precursor decomposition reaction is the rate limiting step of the entire growth process.

2.2.2. Shaping and Subsequent Conversion into the Material

The first bottom-up strategy for the synthesis of elongated nanostructures, which should be discussed, consists two growth steps to obtain the final structure. In the first part, the shape of the later structure is directed, while during the second step the final material is obtained.

2.2.3. Electrospinning

Electrospinning is a common technique used for the synthesis of polymer fibres with diameters ranging from few nanometers to several microns.[32] However, it can be adapted for the growth of elongated inorganic/organic hybrid materials as well as pure inorganic nanostructures by adding a conversion step subsequent to the electrospinning process. The method makes use of electrostatic forces impacting on polar liquids at very high electric field strengths. Therein, a solution containing an inorganic component such as a precursor[33-36] or nanoparticles and a polymer is provided through a hollow, conductive needle on which high voltage is applied. Due to the high electric field strength, a hemispherical tip of the solution is pointing towards the metal sheet counter electrode. Further increase of the voltage leads to a stream containing prealigned polymer molecules being pulled out of the needle (taylor jet). As the solvent evaporates, the stream solidifies to nanoscale fibres, which can be collected from the counter electrode. In the fibres, the inorganic component is embedded within the

polymer matrix, resulting in an inorganic/organic hybrid material. In a subsequent thermal treatment under oxygen, the hybrid material is converted into pure inorganic fibres by burning off the organic matrix and/or converting the precursors to the desired material. The treatment is also the major drawback of this process, as it limits the process to oxide materials. Nevertheless a wide variety of ceramic fibres could be produced via this method.[37]

2.2.4. Growth via Templates

A growth strategy, which makes use of the basic idea of the lithography-based top-down approach is the so-called growth via templates. Similar to the idea of lithography, the desired elongated shape of the nanostructure is generated first, which functions like a mould in casting. Subsequently, the template is filled with the desired material. Finally, the template is removed and the elongated structure can be obtained. Essentially, all templates can be categorized in two types, called hard and soft templates. Hard templates such as anodised aluminium oxide or polycarbonate membranes provide predefined pores. The pores can be either filled with the desired material or with the materials precursor, which is then converted to the material in a subsequent step. The filling of these pores can be a challenging task, especially for membranes containing small pore diameters. Therefore, different approaches have been published, ranging from methods making use of high pressure injection[38], supercritical fluid inclusion[39], electrolysis[40, 41] or capillary force[42]. Hard templates can also act as structure directing component during metal-assisted growth (the metal-assisted growth process is discussed in chapter 2.2.6), which enables the production of aligned NW arrays.[43-45] Furthermore, the template-assisted synthesis of hollow 1D nanostructures can be facilitated via two basic strategies. In the first strategy, the pores of the template are coated instead of completely filled, resulting in hollow nanostructures when the template is removed.[46, 47] The second strategy makes use of a nanowire, which is coated with the material of the final nanotube, yielding in an intermediate core-shell structure. Subsequently, the template, represented by the core, is removed by etching[48] or thermal annealing in an oxidising atmosphere[49] resulting in nanotubes.

Soft templates in contrast, are mesophasic structures such as micelles which are formed via self-assembly above the critic micelle concentration. Material synthesis can be performed within such structures, where size and morphology is governed by the micelles. This approach enables the possibility to grow a wide variety of differently shaped nanostructures.[50] Growth systems using soft templates require a stable emulsion, where shape and size of the micelles can be efficiently controlled. However, the formation of an elongated structure via soft templates is not only attributed to the shape of the micelles. 1D growth can be also the result of irreversible fusion of micro emulsion droplets.[51] In this case, anisotropic growth is the result of different exchange rates between the centre of the elongated structure, where surfactant molecules are stronger bonded to the nanocrystal and its tips, where a higher number of water-enriched domains is located between surfactant layer and nanostructure. The

surfactant as well as the compositions of the involved phases play a crucial role in this growth approach, limiting it to materials such as barium sulfate[51] or calcium carbonate[52].

2.2.5. Self-Induced-Growth

As mentioned before, the synthesis of an elongated nanostructure requires a process, which favours anisotropic growth. Therefore, adatoms must preferentially attach to a certain site (also called growth front), which can be for instance a crystallographic facet. From the thermodynamic point of view, crystal growth can be seen as the result of the decrease in the chemical potential, if diffusing adatoms are incorporated into a crystal lattice. The amount of energy, which can be gained from the incorporation process, depends on the type of facet where the atom is incorporated. Generally, the differences in energies are extremely low, when compared to the total energy of the entire growth system. As a result, isotropic growth is much more likely, which leads to particles or thin films, rather than elongated structures. Nevertheless, under certain growth conditions, a small number of materials exhibit preferential growth facets.[53] A possibility to influence the energy of crystallographic facets is the addition of surfactants. These can be either small molecules or polymers, which coordinate preferentially to a specific facet. As a result, the facet is shielded stronger from the environment, meaning that the growth of other facets becomes more favourable. Surfactants play a key role in the growth of metal NWs via the polyol method[54-56] as well as in the hydrothermal synthesis of elongated ZnO nanostructures.[57] In the latter case mentioned, anisotropic growth is not only induced by a surfactant. The crystal structure of ZnO (wurzite) exhibits an elongated c-axis. Such an intrinsic feature of the crystal structure can also be capable to induce 1D growth. However, only in a small number of materials such as Se[58-60], Te[61] as well as their alloys[62] show growth of 1D structures exclusively by the feature of an elongated crystal structure.

The growth front of the aforementioned self-induced growth processes always consists of a crystallographic facet. The smooth surface of such an ideal facet exhibits only a very limited of potential nucleation centres making desorption events for diffusing adatoms very likely. Crystal growth can only proceed in a slow layer-by-layer growth mode. In reality, a crystal surface is rather rough exhibiting atomic steps and defects such as kinks or dislocations, which can act as potential binding sites for diffusing adatoms. These features can induce site-selective nucleation and therefore mediate anisotropic growth. The first report about such a defect-induced growth of an anisotropic material had been reported by Sears in 1955.[63] He could demonstrate the formation of mercury whiskers during resublimation at low supersaturation (amount of diffusing atoms). The small number of adatoms diffusing on the substrate appeared to be insufficient to induce film growth. However, defects on the substrate could mediate crystal nucleation at low supersaturation and therefore induce the formation of an elongated structure. He supported his conclusion by an additional report describing the formation of needle-like structures of Zn, Cd, Ag and CdS at lower pressures (i.e. low supersaturation), whereas higher pressures led to the expected film growth.[64]

The growth method, which Sears conducted, is a so-called vapour transport growth. The source material is evaporated in a hot area and transported via the vapour phase to a cooler substrate, where it deposits. The deposition via such a growth method can be seen as a simple resublimation process, where parameters such as substrate type, temperature, gas-phase composition and pressure influence the product morphology. Over the years, vapour transport growth has become a popular synthesis method for a wide variety of oxide nanostructures.[65]

Another synthesis method where anisotropic growth is initiated without any external growth promoter is the so-called oxide-assisted growth.[66] Similar to the vapour transport process, the material is provided via the vapour phase, though redox reactions are involved in the formation of the gaseous precursor species and its decomposition at the substrate. Thermal energy, which is applied to a mixture of the desired material and its oxide leads to the formation of gaseous sub-oxide clusters. The clusters are transported to a substrate, where a disproportion reaction takes place leading to the formation of NWs with a pure material core and a thin oxide shell.[67] The formation of an elongated structure is related to the aspect that the growth front consists of highly reactive sub-oxide species, which act as nuclei that absorb other sub-oxide clusters from the vapour phase and facilitate NW nucleation.[70] Oxygen atoms of the sub-oxide clusters are dispelled by atoms of the NW material and diffuse to the edges of the growth front, where they form an inert oxide layer preventing lateral growth. The growth mechanism was mainly investigated for the formation of Si[65-[67]] as well as Ge[68] NWs and was supported by theoretical calculations.[69] In the case of Si, the formation of pure Si in the NW core was explained by the theoretically predicted preferential formation of Si-Si bonds instead of Si-O bonds during adsorption of silicon sub-oxide clusters.[69] Besides group IV NWs, the oxide-assisted growth mechanism had been also proposed to be feasible for the growth of III/IV compound NWs[70-72], which is remarkable as these materials exhibit distinct properties ranging from the crystallographic system to available sub-oxide clusters. The conclusive proof for this assumption is still missing.

2.2.6. Seeded Growth

Compared to other methods, seeded growth enables the best control over the growth of elongated nanostructures. This strategy makes use of a seed or growth promoter, which mediates the nucleation event and facilitates the site-selective crystallisation of material to elongate the nanostructure. The growth mechanism was first reported by Wagner and Ellis, who observed sub-micrometer sized silicon whiskers emerging from a gold-decorated substrate during CVD using a mixture of $SiCl_4$ and H_2 as precursor.[73] From their observations they proposed the vapour liquid solid (VLS) mechanism, which has since been extensively studied. The mechanism explains the growth of an elongated nanostructure (**S**olid) promoted by a liquid seed droplet (**L**iquid), where the NW material is provided via the gas phase (**V**apour). Figure 8 illustrates the VLS mechanism using the example of Si NWs grown via Au seeds and the corresponding binary phase diagram. For the purpose of simplification, nanoscale ef-

fects, kinetic phenomena as well as dissolution of the substrate material into the growth promoter are neglected.

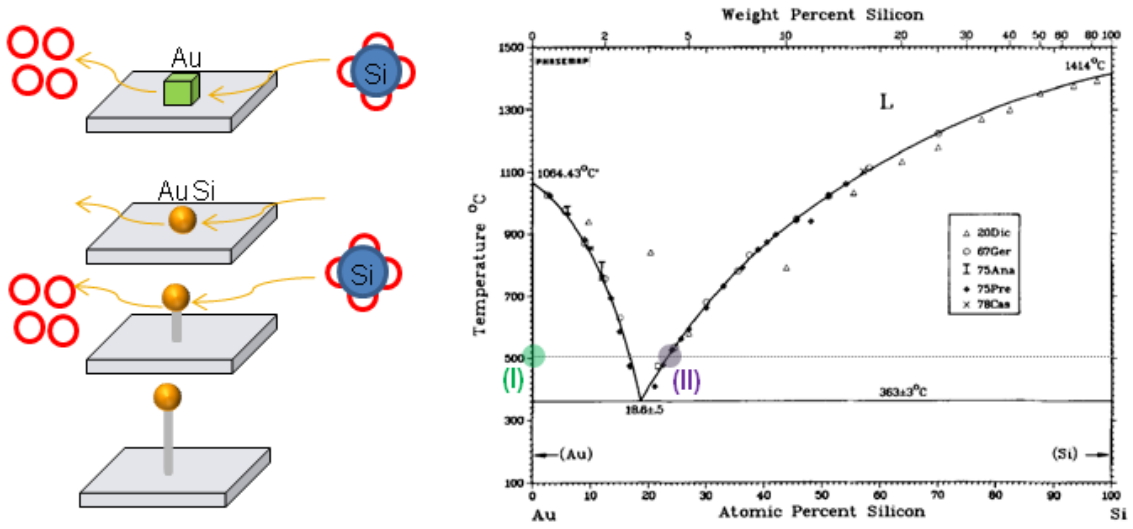

Figure 8: Schematic illustration of Si NW growth via the VLS mechanism and the corresponding binary phase diagram. Reprinted with permission from reference[74].

VLS growth is usually facilitated on a substrate decorated by a particulate growth promoter. Usually, seeded growth is facilitated at elevated growth temperatures (I in Figure 8), though the growth promoter does not necessarily have to be liquid at this stage. The Si precursor, which is provided via gas phase, decomposes at the hot substrate and starts to alloy with the Au seeds. The growth promoter starts to melt due to the lower melting point of the emerging Au/Si alloy. The Si concentration in the seeds increases further due to continuing dissolution until the solubility limit is reached (II in Figure 8). As a consequence, a solid Si layer starts to precipitate at the energetically most favoured position, which is the interface between the droplet and the substrate. Due to further Si supply and the resulting continuing precipitation, an elongated structure emerges consisting of an elongated Si crystal with an Au/Si alloy droplet on its tip. Extension of the Si NWs can occur as long as Si atoms are provided.

The aforementioned growth mechanism is distinctly simplified, thus several aspects must be considered to obtain a more realistic model. Besides ensuring the precipitation of NW material at the growth interface, the growth promoter must facilitate the adsorption of adatoms from the gas phase as well as from the substrate surface. The growth promoter is often described as growth catalyst, i.e. it lowers the activation energy for the decomposition reaction and enhances the NW growth rate in CVD. This aspect was already suggested by Wagner and Ellis[73] and subsequently observed by several groups.[75, 76] However, catalytically enhanced precursor decomposition at the growth promoter is not absolutely necessary for metal-assisted NW growth. Whether a catalytic decomposition effect occurs or not and how pronounced it is, depends on the reaction of the precursor thermolysis and is therefore depending on the precursor and growth promoter.

A synthesis, which exhibits a tremendously enhanced catalytic effect is the gold-seeded growth of GaP NWs using trimethylgallium as Ga source.[77] The partial decomposition of trimethylgallium on the Au seeds leads to the formation of monomethylgallium, which is known to be relatively stable.[78] As a consequence, partially decomposed precursor molecules can desorb from the surface and are removed from the system. Reabsorbtion on neighbouring growth promoters however, leads to an increased chance for complete thermolysis. The synergistic effect of neighbouring growth promoters resulted in a correlation of wire spacing and growth length, where NWs with small spacing (many growth promoters in the vicinity) exhibited increased growth rates than separate ones. An increased growth rate was also observed for NWs grown in the proximity of thicker ones, as the larger growth promoter of the thicker NW also provides the synergistic effect. Nevertheless, such a tremendously enhanced catalytic effect is limited to growth systems where a relatively stable intermediate can occur during the precursor thermolysis.

The substrate-based NW growth process via VLS mechanism can be also seen as a deposition experiment using a substrate contaminated with metal particles. Therefore, film growth would be the result, which is expected at the first view. Actually, axial- (NW-) and lateral (film-) growth are competing growth modes in metal-assisted growth processes, if the temperature is high enough to facilitate thin film growth. Whether one or the other growth mode is prevalent depends on the diffusion length. Process parameters such as temperature, precursor composition or substrate type can directly influence the diffusion length of the resulting adatoms and with it the dominant growth mode.[79] As long as diffusing species are able to reach the growth promoter, they are going to contribute to axial growth. If the diffusion length is too small, the atoms will contribute to lateral growth, which results in NWs exhibiting a broader diameter at the base than at the tip, so-called tapering. The influence of surface diffusion was investigated for InAs nanowires by lithographically prealigned gold seeds on InAs(111)B substrates. Jensen *et al.* could show that up to 80% of the growth was resulting from diffusion of In adatoms on the substrate surface to the growth promoter.[80]

Kinetic phenomena also play a significant role during the NW nucleation and growth process. Similar to the nucleation of nanoparticles (the corresponding LaMer model[81] is discussed in chapter 5.2.2), the crystallisation of an atomic layer in the NW is kinetically hindered and requires a certain amount of activation energy. As a result, the precipitation does not immediately occur if the solubility limit, i.e. the liquidus line, in the phase diagram is reached, which leads to a certain degree of supersaturation in the seed. The achievable degree of supersaturation is depending on the surface free energies of the involved phases. Therefore, the behaviour of the triple phase boundary (TPB) is eminently important. A first kinetic model describing the VLS mechanism had been reported by Givargizov and Sheftal.[82, 83] They provided also a model to describe essential steps in the gold-seeded growth of Si NWs, such as the decomposition of precursor molecules at the particle surface, the formation of the Si/Au

alloy, the diffusion of NW material through the catalyst and the nucleation of the NW at the catalyst/substrate interface.

The opinion that NW growth proceeds in a layer-by-layer fashion, where the nucleation of the next atomic step is initiated at the TPB emerged relatively early. However, a clear proof could not be given before *in situ* transmission electron microscopy (TEM) became available. As such, Hofman *et al.* conclusively demonstrated layer-by-layer growth for Au-seeded Si NWs for the first time in 2008.[84] They observed the advance of the NW/seed interface via recurring propagation of ledges due to phase separation. Nevertheless, the nucleation front is not propagated from the TPB, rather from a spot located inside the NW/seed interface, which is connected to the TPB via other facets.[85, 86] Gamalski *et al.* observed similar behaviour of the growth front and proposed a model explaining the propagation of new atom layers at the NW/seed interface as a cyclic process in NW growth[87] As illustrated in Figure 9, the NW growth cycle begins with the precipitation of Ge preferentially at the TPB, which results in the formation of a rough facet(A). The emerging facet leads also to an increase of the wetting angle ($\Theta_{contact}$) and an increasing supersaturation in the NW seed (B). The progressing increase of supersaturation continues until the kinetic barrier for the bilayer formation is reached. At this point (C), the step nucleation is initiated, which leads to a swift reduction of the supersaturation in the seed. As a result, the emerging facet at the TPB is partially redissolved in the growth promoter (D). Subsequently, the next growth cycle begins with the new precipitation of Ge at the TPB (E). Despite to the fact that Gamalski *et al.* proposed this mechanism for single element NWs such as Si or Ge, a similar growth behaviour was also observed for compound NWs such as GaAs[88] or sapphire.[86]

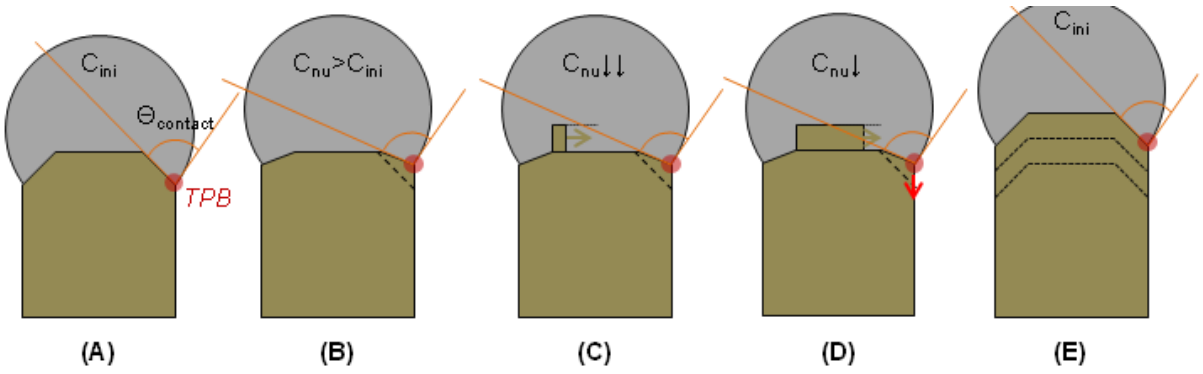

Figure 9: Behaviour of the TPB during the NW step growth according to Gamalski *et al.*.[87]

The growth of single element nanostructures such as Si or Ge NWs in CVD can be well explained by the discussed VLS mechanism, where nucleation of the NWs occurs when the concentration of the NW atoms exceeds the solubility limit in the growth seed. However, when trying to explain the metal-assisted growth of compound NWs such as GaAs or InP, the growth and especially the nucleation cannot be referred to a similar mechanism, since many of them do not form a ternary alloy with the seed. Additionally, the requirement of multiple precursors as it is the case for many III/V semiconductors shows that a typical alloying of both components might not be necessary. Regarding the growth of

GaAs for instance, the Ga/Au alloy is known, while a Ga/As alloy is not known to be stable. Nevertheless, gold promoted growth of GaAs NWs had been observed.[89] Detailed explanation of the growth mechanism suggests an interaction between the group V species and the Ga/Au compound and a resulting incorporation at elevated temperatures, or a surface diffusion mechanism to the growth interface, where the crystallisation occurs. In summary, the functionality of the growth promoter is highly depending on the discussed system, albeit it always provides an energetically favourable interface, where nucleation of the NW is facilitated.

Up to this point, the growth promoter for the metal-assisted growth mechanism was always considered as a liquid droplet. However, a solid particle can also be a feasible growth seed. The so-called vapour-solid-solid (VSS) mechanism describes the solid-seeded counterpart to the VLS mechanism and had been reported for Si[90], Ge[91], as well as for GaAs[92], GaN[93] and ZnO[94] NWs. Regarding the VSS mechanism, a first assumption on the feasibility of a growth promoter can be made from the binary phase diagram of the seed and NW material. First, adatoms generated by the precursor decomposition must be capable to diffuse through the solid seed, which is usually ensured, if the binary phase diagram contains a pocket at the metal-rich side, i.e. the NW material has a certain degree of solubility in the solid seed. Second, the melting point of the seed must be sufficiently high. This aspect becomes even more important when aiming on NWs with very small diameters, as the Gibbs Thomson effect tremendously influences the melting point of nanoscaled materials. The VSS mechanism exhibits some features distinct to the corresponding VLS growth mode. Due to the fact that the transport of adatoms towards the growth front mostly occurs via solid-state diffusion, VSS growth exhibits significantly slower growth rates when being compared to the VLS mechanism.[75] The reduced growth temperature and the solid-state of the seed inhibit coalescence of the growth promoter, which helps maintaining narrow diameter distributions.[95] Also the unintentional incorporation of seed material into the NW might be reduced as the diffusivity and solubility is usually significantly lower in solid state.[95]

Besides vapour-based growth methods, metal-assisted NW growth can also be conducted in liquid phase and in supercritical environment. As the VLS and VSS growth mechanisms occur in vapour phase, solution-liquid-solid (SLS) and the solution-solid-solid (SSS) mechanism have been described for the liquid phase.[96, 97] Furthermore, growth strategies in supercritical fluid have been denoted as supercritical fluid-liquid-solid (SFLS) and supercritical fluid-solid-solid (SFSS) mechanism in literature. In contrast to vapour-phase approaches, mechanisms based on the liquid-phase do not necessarily require a substrate. In such a substrate-free growth process, the NW nucleation occurs in a slightly different manner, as the energetically favourable growth promoter/substrate interface is not available. In addition, the required supersaturation to initiate NW nucleation is supposed to be different, since the surface free energy is only determined by the seed/solvent interface. Substrate-free growth methods usually make use of a growth promoter, which is dispersed in an appropriate solvent. As the supersaturation in the growth promoter approaches the kinetic limit for NW nucleation, a small crystal of

the nanowire material precipitates at the growth promoter generating a so-called heterodimer. This species already provides a TPB and with it a liquid/solid interface, where further crystallisation of NW atoms can take place.

Liquid-phase-based methods require an inert solvent, which should have a decomposition point high enough to withstand thermolysis during NW growth. In the case of supercritical fluid approaches, the critical point must be well below the achieved pressure and growth temperature. If growth is not conducted on a substrate, the growth promoter must be dispersible in the solvent. In substrate-based growth processes, the emerging NWs are bonded to the substrate and therefore immobilised. As a result, coalescence is limited to growth seeds before NW nucleation occurs. In substrate-free methods, diffusion is significantly more pronounced as the nanostructures are capable to move freely through the growth environment. To overcome this drawback, surfactants are often added, which form a shell around the emerging nanostructures and protect them from fusing together. The molecules of the capping agent can be bonded to the NW- and growth seed and isolate the surface from the environment. Usually, steric demanding, long chained amines[98] or thiols[99, 100] as well as organophosphorous compounds such as trioctylphosphine oxide[101] and polymers like polyvinylpyrrolidone derivates[102] have been reported to provide a feasible stabilisation. The capping function can be also assumed by the solvent. Besides inhibiting agglomeration during the growth process, the added capping agent also protects the emerging nanostructures against oxidation due to oxygen. However, capping agents do not only provide beneficial effects. Considering the fact that capping molecules bond to surface atoms of the nanostructure, they influence the electron distribution of them. As a greater part of atoms in nanoscaled objects is located at the structures surface, the surface termination can influence optic and electronic properties of the material significantly.[103]

2.2.7. Seed Formation

Metal-assisted growth processes require stable metal seeds to facilitate nucleation and growth of 1D nanostructures. As the size of the seed determines the diameter of the emerging NW, control over the particle size is required. Over the years, a huge variety of synthesis strategies for nanoparticles has been reported, though the separate synthesis of seeds (the so-called *ex situ* approach) is not the only strategy to obtain a feasible NW growth promoter. Over the years, three basic strategies for seed formation have been developed. The approaches as well as their specific features are discussed in the following chapters:

2.2.7.1. Vapour Deposition

Vapour deposition methods are the most common techniques used to prepare substrates for seeded NW growth. Physical vapour deposition (PVD)[104] as well as CVD[91] enable the deposition of high purity metal onto substrates. As in all non-epitactic coating processes, deposit formation occurs via island growth mode[105], where the material starts to nucleate at specific sites and subsequently forms a

closed layer as the islands grow larger. This growth mode is favourable for seed-formation as it provides separated metal islands. However, also a thin film can be converted into separate islands by a subsequent annealing step if cohesion forces are larger than the adsorption onto the substrate.[106] Therefore, it is required that the deposited film thickness is not too high. The formation of separated islands is related to the minimisation of the surface energies in the system.[106] A second phenomenon, which can be observed during thermal annealing, is that larger particles grow at the expense of smaller ones. The so-called particle coalescence or Ostwald ripening had been extensively investigated by in situ TEM experiment and molecular simulations.[107-110] Both techniques showed that coalescence also occurs due to the minimisation of surface energies.[111] Regarding the fact that annealing steps are often conducted at temperatures below the melting point of the seeds, surface diffusion phenomena are expected to be the dominant mass transport mechanism in this regime.[112] The amount of coalescence is related to the particle density, where a higher density leads to an enhanced coalescence.[113] This aspect is very important due to the fact that NW diameters are highly depending on the size of the growth seeds.[114] In conclusion, it can be said that vapour deposition methods enable growth promoter preparation with the highest purity, albeit its application is limited to substrate-based growth.

2.2.7.2. In Situ Formation

The simplest way to obtain a growth promoter is its production directly in the growth solution. This strategy does not require additional synthesis steps or equipment, as the formation of the growth promoter as well as NW growth is facilitated in the same process. The *in situ* method is mainly used for solvent-based growth processes. Usually, the precursors for growth promoter and NW are mixed with the solvent and the reaction solution is heated to the desired growth temperature, but also an injection into the preheated solvent is conceivable. Therefore, the precursor must be soluble in the solvent. Growth processes making use of the *in situ* generation for the growth promoter require a defined sequence for precursor decomposition. To provide a growth promoter in time, its precursor has to decompose before the NW precursor. This requirement can be easily fulfilled when using a precursor injection method, though in a batch process, the decomposition temperature of the precursor has to be lower than the decomposition onset of the NW precursor. Additionally, there are requirements regarding the chemistry of the entire process: First of all, the precursors must not react with each other to yield indecomposable products, even at elevated temperatures. However, a reaction of the precursors to an "active species" is conceivable and sometimes necessary.[98, 115] By-products deriving from the seed precursor decomposition must not react with the NW precursor or influence the growth process.

Another aspect which requires attention is the size control of the emerging structures. Decomposition of precursor in an inert solvent is equivalent to an uncontrolled growth process. The size of the emerging particles is merely controlled by precursor concentration and reaction time. To overcome this drawback, surfactants can be added. In some cases, NW growth with *in situ* generated growth promoter does not require the addition of surfactants. Thereby, the emerging NW nucleus stabilises the

growth promoter. The stabilisation is not facilitated in similar manner as surfactants do. The part of the growth promoter where the NW nucleates is coated with NW material. As a consequence, the active area where collisions with other seeds could result in coalescence is decreased. Needless to say that such a stabilisation effect is less pronounced when being compared with surfactants, though it is sometimes sufficient to facilitate controlled growth.

2.2.7.3. Ex Situ Formation

This approach summarizes all methods where the growth promoter is produced via a separate reaction step, enabling the possibility of choosing the desired nanoparticle synthesis and purification method without influencing the growth process itself. Usually, nanoparticles are stored as dispersions in an appropriate solvent. Therefore, they can be used for substrate-based as well as substrate-free growth processes.

For NW growth on substrates, seeds are usually applied from dispersions via simple coating techniques, such as drop-casting or spin-coating. The achieved seed density as well as the resulting NW density is governed by the concentration of the applied dispersion. Matching in polarity of solvent and substrate ensures good wetting behaviour, which is required to facilitate a homogenous particle density on the substrate. Furthermore, seed agglomerates, which usually emerge during storage of nanoparticle dispersions must be prevented. Therefore, dispersions are homogenised using an ultrasonic bath or simple stirring. In the case of substrate-free NW growth processes, the seeds are simply dispersed in the required solvent, which can be facilitated using solvent exchange methods.

As nanoparticles are usually stabilised using surfactants, it is necessary to consider their influence on the NW growth process. As growth is usually conducted at higher temperatures, which is favourable for desorption or degradation of surfactants, partially desorbed or decomposed species can still hinder the incorporation of adatoms into the seeds. Also, a contamination of the substrate/seed interface can be induced by the surfactants, which can inhibit or aggravate the crystallisation process. Therefore it is necessary to choose growth seeds, whose surfactants are easily desorb- or decomposeable.

Since a part of this thesis investigates the growth of Ge NWs using Ag bipyramids as growth seeds, the synthesis of Ag nanoparticles should be discussed in the following paragraphs:

Silver Nanoparticles

Silver nanoparticles are among researchers interest for nearly 25 years. A vast amount of applications gained benefits due to their unique properties, reaching from the application as a conductive material for solar cells[116] or printable electronics[117] to health care applications in virtue of their anti-microbial behaviour.[118, 119] In addition, surface plasmons can be observed in silver nanostructures, making them an interesting material for optical applications such as surface enhanced raman scattering. [120, 121]

Over the years, a huge variety of synthesis methods for silver nanoparticles emerged, reaching form non-polar to polar solvents. Basically, the components of a typical synthesis procedure are: the solvent, a precursor and a reduction agent, which provide the necessary silver atoms and a capping agent to prevent excessive growth. To obtain control over the resulting morphologies, a structure directing agent is necessary, which stabilises a certain type of facets. For silver nanoparticles, the citric acid is known to stabilise the <111> facets.[122, 123] In contrast to citrate, polyvinylpyrrolidone is a feasible stabilisation agent for the <100> facets in a silver crystal.[124]

Obtaining shape-control is a demanding challenge; however, the group around Younan Xia at Berkeley reported a method for a shape-controlled synthesis of silver nanostructures in a modified polyol process.[125] The polyol process is one of the most common synthesis methods for silver nanoparticles. Herein, silver nitrate is reduced in 1,2-ethanediol. Polyvinylpyrrolidone acts as capping agent suppressing uncontrolled crystal growth. The nature of the reducing species was identified as glycolaldehyde, which is produced by the thermal oxidation of 1,2-ethanediol at reaction temperature. The product of a standard polyol process consists of <100> facetted silver nanostructures, mainly cubes, bipyramides, decahedrons and nanowires. Looking into the crystal structure of the obtained product, single crystalline, single-twinned and multiple-twinned structures can be identified. Decahedrons for instance, show a five-fold-twinned structure intersected by five <111> twin planes. They are considered as the preliminary structure of the observed nanowires, which show a similar cross section.[126] The observed nanocubes are single-crystalline structures, while bipyramides exhibit a single <111> twin plane.[127]

Shape control is facilitated by oxidative etching, which is facilitated by the addition of small amounts of chloride and bromide ions to the reaction solution. In combination with oxygen, the halides facilitate the oxidation and dissolution of emerging nuclei containing defects such as twins or stacking faults. Chloride ions are the stronger etching agent, shifting the product morphology to single crystalline structures,[128] whereas the addition of bromide ions can result in single twinned morphologies.[127] As a consequence, the polyol process is very sensitive to solvent impurities such as salts. It is well known that iron ions can suppress the adsorption of bromide and chloride onto silver facets and therefore hinder the oxidative etching.[129] Therefore, it is necessary to work with high purity chemicals. Oxidative etching can be enforced by bubbling oxygen through the reaction solution.[130]

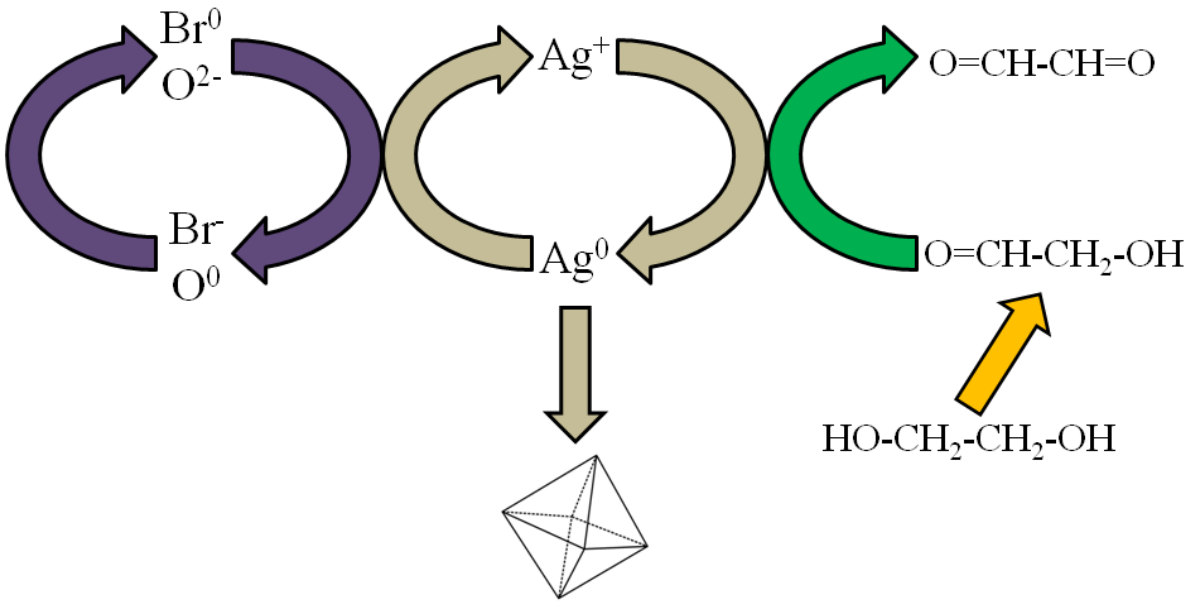

Figure 10: Scheme of the reaction mechanism for the silver bipyramid synthesis using polyol method and oxidative etching.

A reaction scheme for the synthesis of silver bipyramids via the polyol method is illustrated in Figure 10. Due to the fact, that the desired bipyramides contain only one twin plane, they are neither the kinetic product, which would be decahedrons or pentagonaly twinned NWs, nor the thermodynamic product, i.e. cubes. As a consequence, reduction rate, nucleation and etching rate have to be adjusted to the point where the growth of single-twinned particles is favourable.[131] At this point, the etch rate is too small to dissolve single crystalline particles, which means a certain contamination of the final product with nanocubes cannot be excluded.

3. Germanium

Germanium, the third element in the group of tetrels has been discovered by the German chemist Clemens Winkler in 1886.[132] Similar to silicon, it crystallises preferentially in a cubic diamond lattice, but also a hexagonal allotrope exhibiting different electronic and optic properties has been predicted.[133] Bulk germanium shows intrinsic semiconducting properties with an indirect bandgap of 0.67 eV[134] and a direct bandgap of 0.8 eV[135] at room temperature. It was used for the first semiconducting electronic devices such as diodes or transistors, before being replaced by silicon, which is the most prevalent material in today's electronic industry. Nevertheless, the upcoming demand for new materials with enhanced properties makes Ge interesting again. The larger exciton bohr radius (24.3 nm)[136] facilitates quantum confinement in much larger structures, when being compared with Si (4.9 nm)[137] and enables a direct influence on the materials band structure by adjusting the crystal size.[138] Additionally, the high intrinsic carrier mobility[139] and density[140] promises faster switching in high-frequency applications and the usage in components for power electronics. Furthermore, it shows a good compatibility with III/V compound semiconductors such as GaAs[141] and high dielectric constant materials. Up to the present day, several research groups have reported the synthesis of elongated Ge nanostructures such as rods and wires exhibiting polycrystalline as well as single crystalline features. An overview over synthesis methods published is given in the following chapter.

3.1. Germanium Nanowire Growth

Vapour transport growth techniques enable an easy, scalable way to produce Ge NWs. They differ from CVD techniques as they usually do not include a chemical reaction step at the substrate, hence germanium powder or germanium oxide/graphite mixtures are used as source material.[142] However, oxide-assisted growth methods constitute an exception, since adatoms are obtained from the decomposition of a gaseous germanium suboxide. NW growth via vapour transport processes can be achieved seed-mediated[143] using Au, Ag, In, Cu or Ni as well as via self-seeded growth processes on Si, silicon oxide or Ge substrates.[144] Basically, the source material is evaporated by simply adding thermal energy. Gaseous Ge atoms are then transported to the substrate, which is usually held at lower temperatures. This growth technique leads to crystalline NWs surrounded by a 1-3 nm thick amorphous oxide shell.[145] When using pure GeO_2 powders as source material, a slightly different growth mechanism occurs. GeO sublimates from the GeO_2 source and is transported to a substrate, which must contain gold seeds as growth promoter. As germanium oxide approaches the substrate, oxygen atoms are rejected, predominantly at the surface of the gold-rich seeds, yielding in elemental Ge which is subsequently alloyed for growth via VLS mechanism. The obtained NWs are single crystalline and show excellent structural and electric properties.[146] Self-seeded growth of Ge NWs on Si substrates has been reported by Li *et al.*[144] Either amorphous, poly- or single crystalline NW structures could be obtained by controlling the evaporation rate and adjusting the substrate temperature between room

temperature and 330°C. A subsequent rapid thermal annealing step under nitrogen atmosphere could further alter the NW morphology and crystallinity.[144] Furthermore, the oxide shell can be removed from the NWs by treating the product with HBr.[142]

Vapour transport growth becomes more controllable when using laser ablation to vaporise the source material. Morales *et al.* reported the controlled growth of Si and Ge NWs with diameters ranging from 6 to 20 nm and 3 to 9 nm respectively, by using this growth technique.[147] They used a pulsed, frequency-doubled Nd–yttrium-aluminium garnet laser (wavelength: 532 nm) to ablate atoms from a $Fe_{0.1}Ge_{0.9}$ target inside a tube furnace. The vaporised Fe and Ge species condensate during cooling and form supersaturated clusters, which subsequently grow into pure Ge NWs via the VLS mechanism. Growth ceases as the NWs pass out the hot zone of the tube furnace. Analysis of the obtained product showed crystalline Ge NWs growing in <111> direction with a tip containing $FeGe_2$, which was expected due to the binary phase diagram of Ge and Fe. HRTEM analysis also exhibited twining along the <111> plane for Ge NWs, which was not observed for the Si structures. The reported method constitutes an exception as it is a vapour-based process, which does not require a substrate.

Mixtures containing pure Ge and germanium oxide have been reported to be also feasible for laser ablation growth of Ge NWs without using a metal growth promoter.[68] Obtained NWs exhibited a core shell structure, containing a pure Ge core and a germanium oxide shell. Also the growth direction differs, as the core wire shows growth in <211> direction with <111> facets on the core/shell interface. During further investigation of the growth process, it was shown that the presence of germanium oxide in the laser target was mandatory for 1D growth. Despite to the lack of a metal seed, growth could not occur via the VLS mechanism. On basis of these findings, an oxide-assisted growth mechanism had been proposed, which is discussed in chapter 2.2.5.

Despite the variety of vapour transport growth processes, the most popular synthesis strategy for Ge NWs is based on CVD. CVD processes enable the usage of a wide variety of Ge sources. Decomposition temperatures of these compounds enable growth processes conducted at much lower temperatures. To obtain sufficient control, Ge NW growth via CVD is usually facilitated via seed-mediated growth processes, using either a liquid or solid growth promoter. Depending on the phase of the growth promoter, NW growth occurs via the VLS or VSS mechanism. Basically, growth seeds can be classified by their binary phase diagram with germanium:[148]

A-type Eutectic with more than 1 % Ge concentration. No germanide phases.
B-type Eutectic with less than 1 % Ge concentration. No germanide phases.
C-type Germanide phases present in the binary phase diagram.

Figure 11 illustrates the periodic table of elements with A-type seeds coloured in red, B-type seeds green and C-type seeds grey. All three seed types are feasible to promote the NW growth process, as

long as the corresponding binary phase diagram contains a non-horizontal phase boundary. In the case of VLS, this is usually maintained by a v-shaped liquidus curve, whereas in solid-seeded growth mode a limited solubility of Ge in the seed material must be given.

									Al	Si	
Ti	V	Cr	Mn	Fe	Co	Ni	Cu	Zn	Ga	Ge	
Zr	Nb	Mc	Tc	Ru	Rh	Pd	Ag	Cd	In	Sn	Sb
Hf	Ta	W	Re	Os	Ir	Pt	Au	Hg	Tl	Pb	Bi

Figure 11: Periodic table of elements with potential growth promoters for Ge NWs classified by their phase diagrams. Redrawn in the style of reference [149].

Similar to Si NWs, Au is the most frequently used seed to promote Ge NW growth. The binary phase diagram of the Au-Ge system[150] (depicted in Figure 12) reveals the typical feature of an A-type growth promoter with an eutectic point at 360 °C and ~28 % Ge concentration.

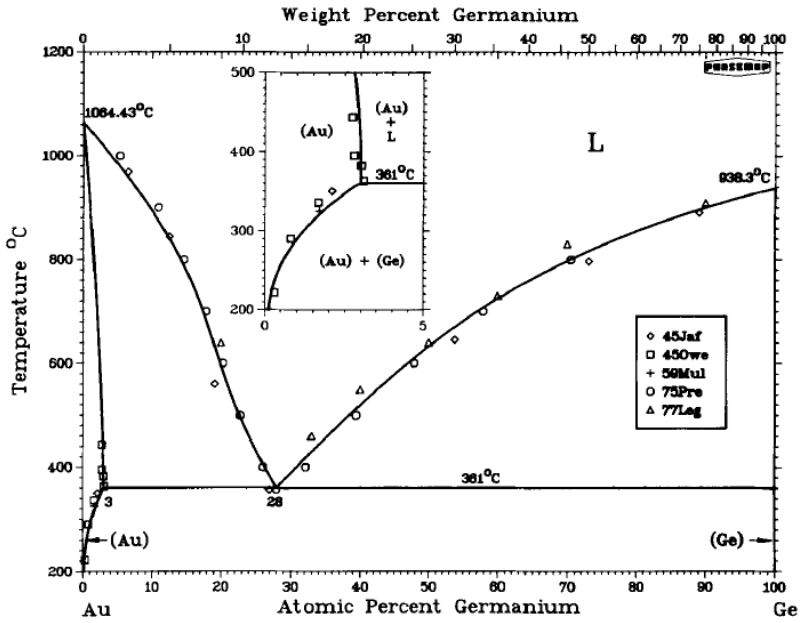

Figure 12: The binary phase diagram of the Au-Ge system reprinted with permission from reference[150].

Due to the fact that Ge precursors such as germane already decompose at lower temperatures, Au-promoted growth can also occur in the subeutectic regime.[75] The phase of the growth promoter and the resulting growth mechanism during subeutectic growth have been extensively studied. On one

hand, melting point depression due to the Gibbs Thomson effect leads to a melting temperature decrease and therefore to VLS growth occurring below the eutectic temperature.[151] On the other hand, liquid seeded growth had been also observed at ~50 °C below the eutectic point. This temperature is too low to result from melting point depression due to nanoscopic effects. Particular investigation of the process conditions led to the conclusion that the phase of the growth promoter is influenced by the growth pressure, its thermal history,[75] as well as by species trapped at the promoters surface.[152, 153] Especially the thermal history of the growth promoter is an important feature, as growth of high quality Ge NWs can be facilitated via a two-step growth process.[154-156] In the first step, the NW nucleation is initiated at higher temperature, which improves the yield of the nucleation process and ensures a proper NW orientation if an epitaxial growth is targeted.[154, 155] The subsequent elongation is facilitated at lower temperature, as the enhanced precursor decomposition during nucleation would lead to tapering.[154]

The popularity of gold as growth promoter poses the question why this metal is so extensively used?" The first advantage of gold is related to practical reasons, as gold is one of the standard materials in electronic industry and therefore widely available. The coating of a thin gold layer onto electric contacts is a basic procedure and poses no major obstacle in this field. Furthermore, Au nanoparticles with sizes ranging from 2 to several 100 nm are commercially available. The high chemical stability of gold makes handling easy, as the growth promoter does not oxidise under ambient conditions. Also technical requirements for the growth process are lowered, especially regarding the maximum oxygen background pressure. Gold is also non-toxic and therefore no safety hazard. Besides practical reasons, the binary phase diagram of the Au-Ge system also exhibits features, which are beneficial for the usage of gold: First, the low vapour pressure of gold prevents loss of growth promoter during NW growth, even under low pressure conditions.[148] Second, the relative high concentration of Ge in the eutectic indicates that the energetic cost for dissolving Ge atoms in Au is rather low. Also the energetic cost to achieve supersaturation seems to be relatively low (indicated by the low slope of the liquidus line). Concluding from this, the precursor pressure which is necessary to achieve a supersaturated state for NW growth must be low as well. However, the high Ge concentration in the eutectics of gold and other A-type seeds can be also a drawback, when aiming on the synthesis of axial NW heterostructures. The high solubility of NW atoms in the growth seed results in a so-called tailing effect, which describes the formation of a NW segment where the NW composition changes continuously from A to B, instead of a sharp interface. Another serious disadvantage which emerges from Au seeds is the incompatibility of gold with current semiconductor production standards. During the metal-assisted growth process, atoms of the seed can be incorporated into the NW material.[157] As a result, the NW is doped by the growth promoter. Gold is known to induce recombination centres into Ge, degrading its semiconducting properties.[158] Additionally, the high chemical stability and low vapour pressure of gold make a post-growth purification difficult. Therefore, huge efforts had been made to minimise seed material.

As discussed in chapter 2.2.6, one attempt to minimise the incorporation of growth promoter into the NW matrix is to apply a solid-seeded mechanism, i.e. VSS growth. Usually, VSS growth is carried out at lower temperatures. As a result, the diffusivity of atoms as well as the solid solubility is significantly decreased, which results in less incorporation of seed material. A second attempt is to simply replace gold by another growth promoter, which does not influence the electronic properties. Over the years, a huge variety of different growth promoters have been reported, ranging from pure elements to alloys. A summary of the reported growth promoters is given in the following:

Table 1:Growth promoters for Ge NW growth reported in literature.

Ag[149]	Co[159]	Ir[159]	Sn[160]	AgAu[161]
Al[162]	Cu[163]	Mn[91]	Sb[164]	AlAu[165]
Au[75]	Fe[166]	Ni[167]		FePt[159]
Bi[168]	In[169]	Pb[170]		$MnPt_3$[159]

Growth of Ge NWs can be also conducted in liquid media, enabling a highly flexible growth strategy regarding the process parameters.[171] Similar to CVD-based approaches, metal-assisted growth is the most popular growth strategy for liquid-based growth processes, but also self-seeded growth[172-174] has been reported. Growth is usually carried out in organic solvents, exhibiting a high boiling point, such as squalane[175], 1-octadecene[176] or trioctylphosphine[168]. Furthermore, growth processes making use of supercritical conditions captured researchers' interests. The pressurised environment enabled the usage of simple solvents such as pentane[177], cyclohexane[177] or toluene[159]. Even growth in SC carbon dioxide had been conducted.[178] Due to the fact that processes making use of SCFs require a high pressure, these synthesis methods are carried out in stainless steel or titanium vessels. While the introduction of precursor can be easily facilitated via manual syringe injection at ambient pressures, SCF methods require a high-pressure injection equipment such as a HPLC pump. Nevertheless, solvent-based Ge NW synthesis can be also carried out in a closed system, i.e. the reaction solution including precursors and growth promoter is completely prepared and the growth process is initiated by heating. The liquid environment enables NW growth localised on substrates[179] as well as in a colloidal manner[175], where the growth promoter is dispersed in the solvent. Especially latter mentioned enables the usage of a growth promoter, which is generated *in situ* before NW growth.[102, 180] Therefore, seed as well as NW synthesis can be conducted with minimal effort in a one-step process.

A special growth technique which makes also use of a high boiling point solvent is the so-called solvent vapour growth. In this substrate-based approach NW growth is conducted in the vapour phase of a high boiling point solvent, which enables an extension of the temperature window of solvent-based methods. Using the solvent vapour growth approach, Ge NWs[163] as well as elongated Ge/Si heterostructures[160] were grown using tin seeds[179] as well as via a self-induced growth mechanism on

copper substrates[163]. Another growth approach, which makes use of a similar process, has been reported by Mullane *et al.*[181] They describe the growth of Ge NWs via a simple thermolysis reaction by dropping a precursor solution onto a heated substrate. The process reported appears to be a hybrid between a solution and vapour-based growth strategy.

Another special strategy to obtain elongated Ge structures in a solution-based, metal-assisted process is growth via the so-called electrochemical liquid-liquid-solid (ecLLS) mechanism. The special attribute of the ecLLS mechanism is that adatoms are not supplied via thermal decomposition of a molecular precursor species, rather than by the electrochemical reduction of Ge^{4+} ions in aqueous medium, which derive from dissolved GeO_2.[182] A potential more negative than 1.6 V vs Ag/AgCl enables the reduction of Ge ions according to eq. (I)[183]

$$HGeO_3^-(aq) + 4e^- + H_2O \rightarrow Ge(s) + 5OH^- \quad \textbf{(I)}$$

The Ge atoms diffuse on the substrate and dissolve in the liquid growth promoter, which is deposited on the substrates. Due to the aqueous media conditions, the growth temperature is limited to 100 °C. This aspect affects also the number of available growth promoters. As a result, growth had only been reported by Hg[184], Ga-[182] as well as InGa alloy[185] seeds which exhibit liquid state in this temperature regime. Unfortunately, the reported structures were rather on the micrometer scale and suffered from a high degree of seed material incorporation. Furthermore, diffusion effects appeared to hinder the growth of structure with very high aspect ratio, as wires grown from Ga exhibited strong tapering as well as kink formation after a defined length.[186]

The process parameter which has only been little discussed until now is the Ge precursor. Basically the precursor must be capable of providing Ge atoms via its decomposition. Furthermore, by-products which derive from the decomposition reaction should be easily to remove from the growth environment. Therefore, decomposition by-products should be volatile for vapour-based approaches or soluble, if growth is conducted in a liquid medium. As mentioned before, processes based on vapour transport growth do not involve a chemical reaction at the substrate (oxygen-assisted growth excluded). Therefore, source material is limited to pure germanium and germanium oxide which is reduced by carbon.

For Ge NWs, obtained via CVD, the precursor variety is much wider. First experiments were conducted using $GeCl_4$, which was evaporated in the presence of hydrogen gas. The germanium halide was reduced at the heated substrate, leading to pure Ge and HCl. Over the years, simple germanes such as mono- (GeH_4)[187, 188], di- (Ge_2H_6)[189] and trigermane (Ge_3H_8)[190] have become very popular precursors. Due to their gaseous nature at ambient temperature, they can be easily supplied as gas mixtures with hydrogen gas. As the Ge-H bond is rather labile, it can be easily decomposed via thermolysis, leading to pure Ge deposits. Nevertheless, due to their pyrophoric nature and sensitivity towards oxygen, stringend air-free handling and extended protective equipment is necessary. Therefore, less

reactive germanes such as diphenyle germane (DPG) or tert. butyl germane (*t*BG) can be used. These compounds are liquids at ambient conditions, but exhibit a significant vapour pressure, hence they can be used for solution-based methods[171, 175] as well as for LPCVD processes[149, 170]. Another precursor, which is feasible for Ge NW growth via LPCVD is dicyclopentadienyl germanium. However, the thermal decomposition of the cyclopentadienyl ring is more difficult, which leads to a significant contamination of the NW surface.[166]

Besides germanes also germanium amide precursors are feasible for solution-based growth methods. Especially bis,bis hexamethyldisiliazane germanium (II) is frequently used for the growth of Ge NWs[191] as well as nanoparticles[192] in amine solvents. However, the species which ultimately provides the Ge atoms from the decomposition step is more likely a Ge amido-/imido-cuban species, which emerges from aminolysis due to the solvent.[98]

3.2. Defect Transfer

Planar defects, such as twin boundaries or stacking faults are often observed in III-V and group IV NWs.[193] However, control over the formation of such defects is still challenging and mainly obtained for III-V NWs.[194, 195] For Ge NWs, twin boundaries can be introduced intentionally, when using solid silver seeds as growth promoter.[149] During NW growth, the crystal/defect structure of the seed acts as template, transferring its lattice information to the emerging NW. During the layer-by-layer growth process, the introduction of a new step occurs in heteroepitaxial manner. In a first assumption, the growth seed must meet four major requirements to facilitate the defect transfer:

- Structure and lattice constant must be similar to the NW material, to enable heteroepitactic growth.
- The absence of germanide phases, as its formation could lead to major changes in the crystal structure.
- Solid solubility of NW material to ensure solid-seeded growth.
- High melting point to prevent liquid-seeded growth and recrystallisation.

Regarding the aforementioned requirements, silver and aluminium appear to be feasible seeds. However, due to the high energy required to form twins, aluminium was not pursued. In the reported procedure, Ag seeds were obtained from fusing small silver particles at ~400 °C.[196] This approach led to the formation of multiple twinned silver particles, exhibiting an irregular twin structure. NW growth has subsequently been conducted in supercritical toluene as well as via hot-wall CVD at ~400 °C growth temperature (eutectic temperature of the Ag-Ge system: 640 °C[197]). The temperature was sufficiently high to ensure the decomposition of the Ge precursor DPG as well as the growth of straight NWs. In addition, growth conditions did not induce a modification of the seeds crystal structure, for instance by recrystallisation. TEM investigation exhibited a large number of NWs with <111> twin planes along the entire NW length. A large fraction of NWs with <111> twins grow in <112>

direction, which is usually only an inferior growth direction for Au- and Ni-seeded Ge NWs in the observed diameter range.[198, 199] TEM micrographs of the NW tips, exhibited that the twin structure of the Ag seed had been transferred to the NW. However, fast fourier transformation (FFT) pattern revealed a minor offset (~2.9°) of the orientation of the Ag seed, which was attributed to strain due to lattice mismatch. The article reported by Barth *et al.* is the first publication describing a defect transfer from growth promoter to NW.[149] However, the reported method suffers from a lack of control over the defect density, as the crystal structure of the seeds could not be controlled.

A follow-up article described the manipulation of the defect density by using bimetallic seeds.[200] The influence on the defect density was attributed to different stacking fault and twinning energies, which could be adjusted by tuning the Ag and Au content of the growth promoter. Nevertheless, an absolute control could not be achieved via this method. Regarding the defect transfer mechanism, an absolute control over the NW crystal structure can only be achieved, if the crystal structure of the growth promoter is entirely under control. Therefore, a nanoparticle synthesis with sophisticated morphology control is necessary. Such an approach is for instance the so-called polyol method (discussed in detail in chapter 2.2.7.3), which enables the synthesis of Ag nanoparticles with controlled shapes and structures.[201]

3.3. Doping of Germanium

The application of germanium in electronic devices requires the modification of its band structure. Germanium itself already shows semiconducting properties and is therefore called an intrinsic (pure) semiconductor. However, only by adjusting the electronic structure, the formation of interfaces such as pn-junctions can be facilitated, which is mandatory for electronic devices such as diodes or transistors. The modification of the materials band structure can be facilitated via the incorporation of foreign atoms which is called doping. A semiconductor, which has been doped to alter its electronic properties is called extrinsic semiconductor. In general, two types of doping –called p- and n-doping, are interesting for electronic devices and therefore most common.

As illustrated in Figure 13, P-doping is achieved, if an element with less valence electrons than the host element is introduced into the semiconductor lattice. For Ge, which exhibits four valence electrons, elements of group III such as boron or aluminium can be incorporated to achieve p-doping. In industrial applications, Ga emerged as standard p-dopant for Ge wafers.[202] Incorporation results in a missing bond, which can be seen as a positively charged hole or electron acceptor state. These holes are capable to move through the semiconductor lattice by attracting electrons of other bonds. Regarding the band structure of the material, the introduced hole is related to an acceptor state, which is located slightly above the valence band.

N-doping in contrast, is achieved by incorporating atoms with more valence electrons into the semiconductor lattice. For germanium this can be achieved by elements of the group V, i.e. phosphorus,

arsenic and antimony. In industry, phosphorous as well as antimony emerged as standard n-dopants for Ge wafers.[202] The incorporation results in valence electrons, which are not required for binding. Thermal energy at room temperature is sufficient to liberate the electron from its core. As a result, the electron is capable to move freely through the lattice and carry current. Regarding the materials band structure, n-doping results in the introduction of donor states, slightly below the conduction band, which is also illustrated in Figure 13.

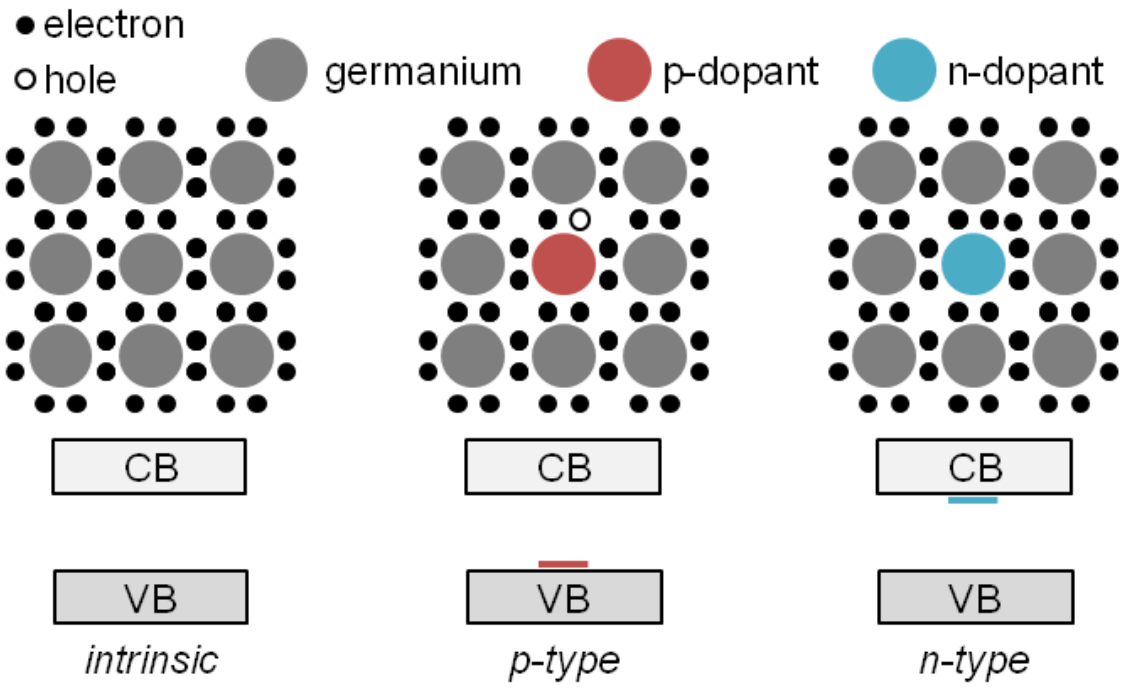

Figure 13: Illustrations of an intrinsic, p-doped and n-doped germanium crystal segment and the corresponding representation of energy bands (VB=valence band, CB=conduction band).

Donor- or acceptor states located near the band edges are also called shallow-level states. They are called shallow, as thermal energy (kT) is sufficient to remove electrons or holes from this state into the valence or conduction band. These states are favoured in electronics as they enable shifting of the band edges. Deep-level states, often called trap states, in contrast, are undesirable states in electronics. They are located further away from the band edges, so that thermal energy is no longer sufficient to remove charge carriers from these states. Due to their location, they offer an alternative state for free charge carriers and can act as recombination centres and therefore interfere with the operation of transistors or optoelectronic devices. Elements, which generate deep level states in Ge are usually transition metals such as gold, silver or nickel.[158]

In intrinsic Ge, the number of electrons and holes is equal. Incorporation of a dopant leads to a change in the number of electrons or holes and thus introduces charge carriers. An increase of charge carriers also leads to an increase in conductivity. Therefore, wafers are often characterised by their sheet resistance, rather than by doping levels. In general, dopant concentrations depend on the application, but

are usually in the range of 10^{13} to 10^{21} cm^{-3}. Ge substrates for epitaxial growth of GaAs as solar cells for instance, require a high conductivity and are therefore highly doped 10^{17}-$10^{18}cm^{-3}$.[202]

In general, there are three approaches to facilitate the introduction of dopants into Ge. The simplest method is to add the dopant into the melt before crystal growth. During the subsequent growth process, the emerging crystal obtains a homogenous dopant distribution.[203] This technique is favoured for substrate production, albeit it is not feasible to produce predefined areas with different dopant concentrations, as it is required for electronic components.

The second approach is based on thermally activated diffusion processes, where the substrate is brought into contact with the dopant at elevated temperatures.[204] This can be achieved via annealing in an atmosphere containing dopant atoms in the vapour phase, or by a coating containing the dopant and a subsequent thermal treatment. Dopant concentration as well as its penetration depth can be controlled via temperature and exposure time.[205]

The most versatile, and dominant method to introduce a dopant is ion implantation.[206, 207] In this approach the substrate is exposed to a bombardment of accelerated ions. Due to their high kinetic energy, the ions enter the crystal lattice where they get stuck by collisions with atoms or electronic interactions. As a result, the impurity atoms are mostly located on interstitials. In a subsequent thermal treatment, the implanted atoms move towards lattice sites and induce the discussed shifts in the materials band structure. Impurity distribution as well as concentration can be well controlled via kinetic energy and dose, respectively. However, the method has one major drawback. The ion bombardment causes the introduction of a sizeable amount of energy, which can cause major damage to the crystal lattice, ranging from sputtering of atoms over crystallographic damage to amorphisation of the material.[208] Some amount of the introduced damage can be cured by the thermal treatment, though a number of defects remains in the material.

Thermally activated diffusion as well as ion implantation techniques can be combined with lithographic techniques to achieve area-selective doping, which is required for electronic devices. Both doping techniques are used in today's semiconductor industry.

4. Motivation and Aim of the Thesis

Metal-assisted growth is a popular synthesis strategy for Ge NWs. Up to the present day, growth via a vast variety of metals had been demonstrated, each exhibiting its distinct features. However, Ge NW growth via lead seeds has not been demonstrated before. Therefore, procedures using liquid as well as solid lead seeds should be developed. Furthermore, the obtained materials should be characterised by various electron microscopy techniques as well as x-ray diffraction.

Gallium is also a potential growth promoter for Ge NWs. The metal exhibits interesting features, such as the low eutectic temperature in the Ge-Ga system, which theoretically enables liquid-seeded NW growth at body temperature. Moreover, Ga is a popular dopant for Ge, hence seed material incorporation potentially causes a p-doping effect on the material. Despite to these beneficial effects, Ga-assisted growth remained rather unexplored. In consequence, the development of synthesis procedures for Ga-seeded Ge NWs at temperatures below 200 °C was targeted. Furthermore, a potential incorporation of seed material in the NW matrix as well as its impact on the electrical properties, should be investigated, using elemental mappings and electrical measurements of single NWs.

In the third part of the thesis, the controlled transfer of a silver seeds crystal structure to a Ge NW during metal-assisted growth should be investigated. The procedure which has already been reported, suffers from a lack of control, as the applied seeds exhibited random defect structures. To obtain a growth promoter with a defined defect structure, the synthesis of single twinned silver bipyramids via the polyol method is targeted. In further consequence, the obtained nanoparticles should be used to promote the solid-seeded growth of Ge NWs via supercritical fluid as well and CVD techniques.

5. Results and Discussion

5.1. Lead-supported Growth

Comparing the binary phase diagrams of group IV elements and Ge reveals for Si that a growth of Ge NWs via Si seeds is not possible, as Si and Ge are completely miscible.[209] The addition of Ge atoms to a Si seed would only lead to the formation of a SiGe alloy, while no nucleation of a NW occurs. Regarding the binary phase diagram of Ge and its heavier homologue tin, a simple eutectic is present containing 99.7 % tin. Therefore, tin is denoted as B-type growth promoter according to Schmidt *et al.*[148]. Tin-seeded Ge NWs have been reported to grow via solvent-vapour-growth[179], via CVD[210] as well as in solution[98, 180, 211, 212]. However, the low eutectic temperature of 231.9 °C[213] makes growth via solid seeds difficult, as only a limited number of Ge precursors exhibits feasible decomposition rates in this temperature regime. The binary phase diagram of Ge and Pb (illustrated in Figure 14) in contrast, exhibits a significant higher eutectic temperature (T_e=327.5 °C)[214], which could enable solid-seeding for a wider precursor variety.

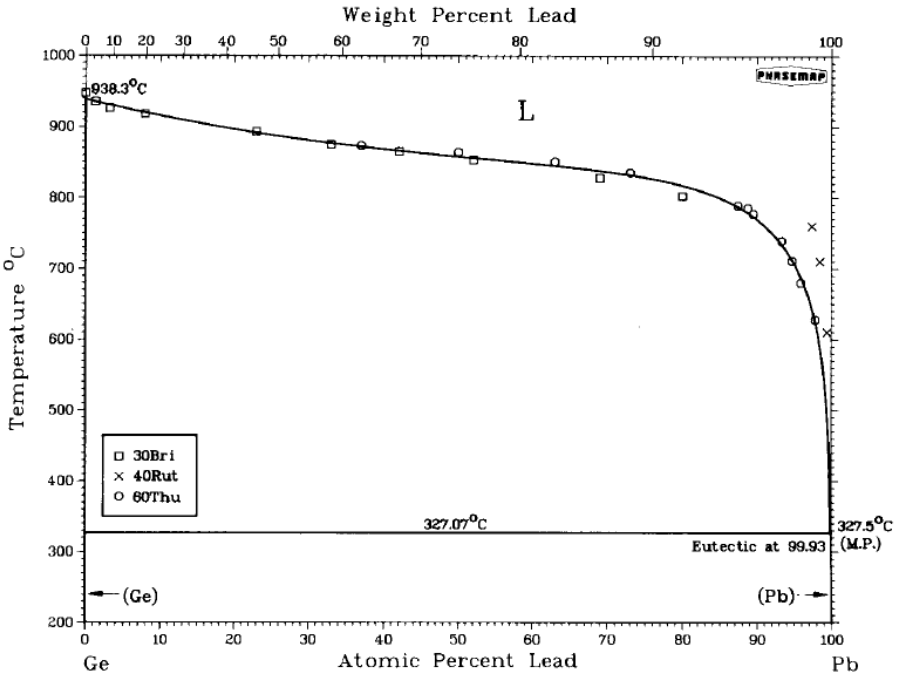

Figure 14: Ge-Pb binary phase diagram. Reprinted with permission from reference[214].

As the binary phase diagram exhibits no germanide phases and the eutectic contains only 0.07 % Ge, Pb can be also classified as type B growth promoter.[148] Therefore, only a negligible reservoir effect[165] can be expected, which makes Sn as well as Pb promising seeds for axial NW heterostructures with sharp interfaces. The reservoir effect describes the continuous transition in composition between two NW segments of axial heterostructures, which is facilitated by the solubility of NW adatoms atoms in the growth promoter. In more detail, adatoms for the previous segment, which had been

already dissolved in the growth promoter, are incorporated, when growth of the next segment is initiated. As a consequence, the composition of the next NW layers consists decreasing amounts of the previous segments material. To keep the transition regions almost atomically abrupt , the concentration of NW material in the seeds must be as low as possible.

Another considerable feature of the Ge-Pb system is the immiscibility of Pb in solid Ge. The binary phase diagram of Ge and Pb exhibits no solid solution at the Ge-rich site. Therefore, the incorporation of seed atoms into the NW matrix during growth can be excluded, as long as growth is conducted under thermodynamic conditions, which is required, since phase diagrams are only valid under these conditions. In contrast to gold, incorporation of Pb atoms into Ge NWs would not result in the formation of deep-level trap states in the materials band structure.[158] Those trap states are unfavourable, as they significantly alter the electronic properties of the NW.[215] Incorporation of group IV metals in contrast, results in an asymmetric decrease of the bandgap.[216-219] The direct bandgap decreases faster than the corresponding indirect bandgap, which could lead to a transformation to a direct bandgap material. As direct band gap semiconductors are favoured for opto-electronic applications, these group 14 alloys have gained high interest over the last years. Despite to the beneficial effects mentioned, literature concerning Pb-assisted growth of Ge NWs is limited to the result published from this thesis[170] and a second article, describing the usage of Pb-seeded Ge NWs in lithium ion batteries[220].

5.1.1. Growth via Liquid Seeds

Pb growth seeds were obtained from photolytic decomposition of $Pb(HMDS)_2$ in clear glass vials. Over a period of 14 days, a grey precipitate emerged in the glass vial, which could be isolated via multiple centrifugation and redispersion steps.

Ge NW growth was conducted via LP CVD using hot-wall and cold-wall setups, as well as in supercritical toluene at ~290-320 bar pressure. Diphenyl germane was used as Ge source, which was often reported to be used for NWs grown in solution[102, 175, 181], supercritical solvent[149, 221] as well as in vapour phase[200, 222]. DPG is known to decompose at elevated pressures via a phenyl redistribution mechanism, where monogermane is formed as an intermediate species.[175] As such a redistribution reaction requires multiple collisions, which are maintained due to the short mean free path lengths at elevated pressures, the mechanism is rather unlikely for low pressure growth processes such as in the applied CVD method. Therefore, a simple thermal cleavage of the Ge-C and Ge-H bonds similar to the decomposition of alkyl germanes such as methyl-[223] and ethyl germane[224] is more likely. According to this reaction scheme, the thermal decomposition of DPG leads to pure germanium and an organic by-product, most likely benzene.

Growth in the SCF led to the formation of NWs over a wide range of process parameters (precursor amount, temperature, and duration), albeit growth via CVD was more sensitive. This aspect was related to the lower precursor concentration achieved in the gas phase of the LPCVD process. An effi-

cient NW nucleation in CVD required a higher precursor concentration as it could be obtained from evaporation in a dynamic vacuum of $6 \cdot 10^{-2}$ mbar at room-temperature. Therefore, the precursor temperature had been maintained at 35 °C using a water bath. Cold-wall experiments in contrast, which were conducted under a vacuum $<10^{-3}$mbar did not show the formation of any NWs, even at 50 °C precursor temperature. Samples obtained from successful growth reactions showed brown precipitates on top of the substrates.

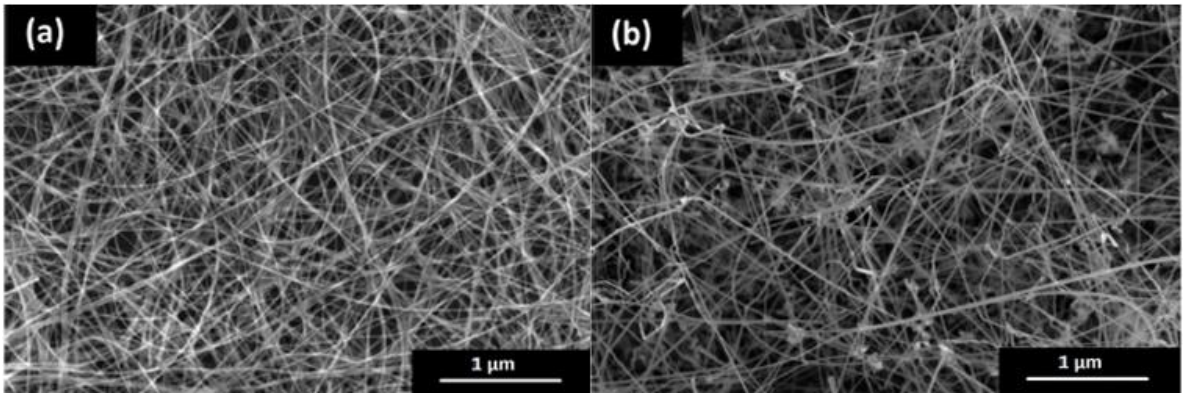

Figure 15: SEM image of Ge NWs grown via SFLS(a) and VLS(b) growth.

Figure 15 illustrates a typical SEM image of NWs obtained from the supercritical- and vapour-phase growth process. Both samples showed similar straight NWs, thus products obtained from the solution-based process exhibited a significant higher NW density than samples obtained from CVD. This aspect was attributed to seed deactivation due to partial oxidation of the Pb particles. While the handling of growth substrates could be maintained under exclusive inert condition in the case of the SF process, the substrates in the CVD process must be transferred into the reaction chamber under ambient conditions.

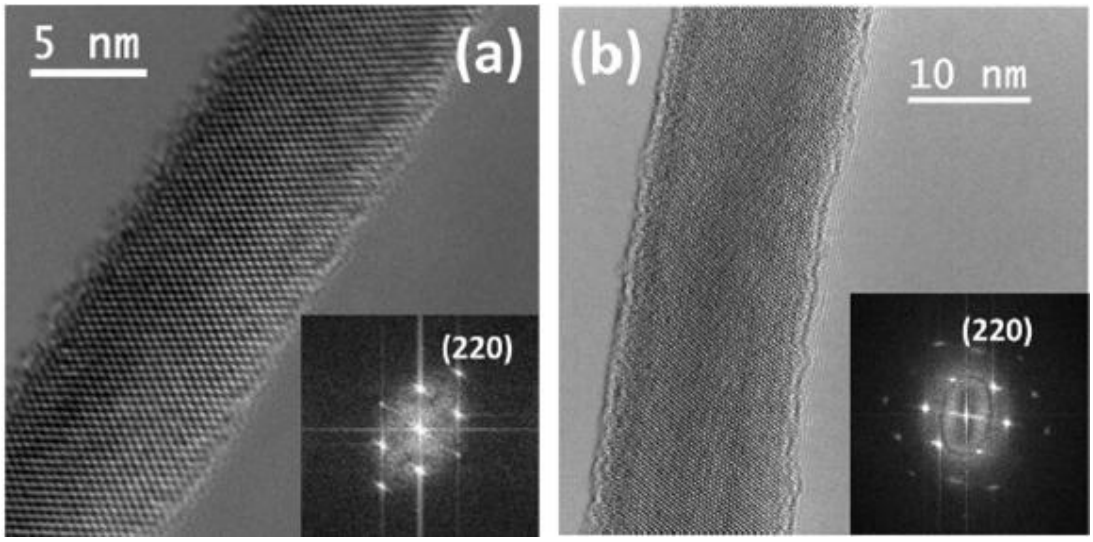

Figure 16: HRTEM images and corresponding FFTs of Ge NWs grown in SCF(a) and in vapour phase(b).

As shown in Figure 16, TEM investigation of the Pb-seeded NWs showed highly crystalline NWs with NW diameters in the range of 10-20 nm. Fast fourier transformation pattern exhibit that the majority of NWs (>90 %) grew along the <011> growth axis, which is common for group 14 NWs with diameters below 20 nm.[174, 225] However, a small fraction of NWs showed a <111> growth axis.

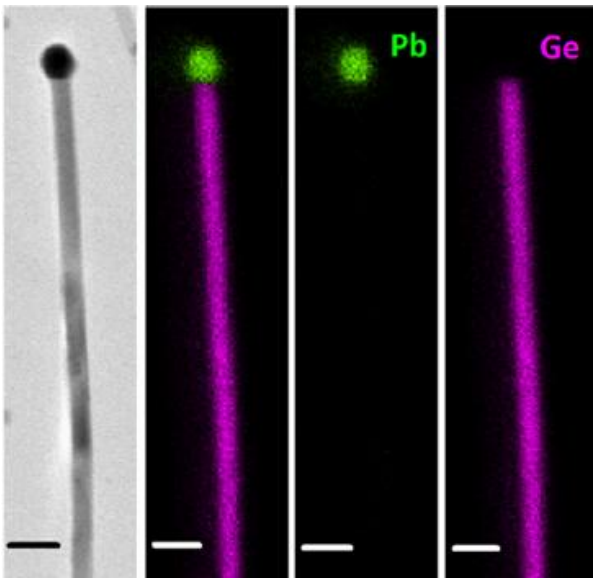

Figure 17: STEM EDX mapping of a Ge NW. The Scale bars are 50 nm.

In order to investigate the elemental distribution in the obtained NWs, scanning transmission electron microscopy-energy dispersive x-ray (STEM-EDX) mapping of a single NW had been carried out. As shown in Figure 17, the Pb signal was exclusively located to the NW tips, while in the NW bodies the signal dropped below the quantification limit of the measurement. Regarding the covalent radii of Ge (120 pm)[226] and Pb (146 pm)[226], the large mismatch of 26 pm would lead to a tremendous strain in the crystal lattice, if Pb atoms are incorporated into the Ge matrix. The formation of such a metastable phase cannot be explained via phase diagrams and require kinetically controlled low-temperature growth processes,[227] similar to the growth of GeSn-alloys.[98, 180, 210, 228-230] Addressing the incorporation of Pb into Ge, only a recently published article is known, which describes the incorporation of maximum 0.2 % Pb into crystalline Ge thin films via pulsed laser epitaxy.[231] Regarding the growth conditions of the obtained Pb-seeded NWs, a kinetic process control can be excluded, as growth temperatures were ~150 °C to high. However, a Pb-doping, therefore the incorporation of trace amounts of Pb cannot be completely excluded, as detection limit for STEM-EDX (~0.5 %) is out of range for very low concentrations.

5.1.2. Growth via Solid Seeds

As the eutectic temperature of the Pb-Ge system is 327.5 °C, growth via solid seeds must be realised at temperatures significantly below this temperature. For the obtained nanostructure sizes, melting point depression due to the Gibbs Thomson effect can be nearly neglected (~20 °C for 10 nm Pb particles).[232] Based on a temperature of 300 °C necessary to maintain growth via solid seeds, the de-

composition temperature for DPG is already at the lower edge. Additionally, the critical temperature of toluene is 320 °C[233], thus growth would no longer proceed in supercritical environment. To overcome these obstacles and maintain a feasible precursor decomposition under SC conditions, the Ge source had been changed to $Ge(HMDS)_2$ and n-hexane (T_C=234 °C)[234]was chosen as alternative solvent. $Ge(HMDS)_2$ is a known precursor for Ge nanostructures grown at lower temperatures.[180, 235, 236] Additionally, Pb seeds had been generated *in situ* from the decomposition of $Pb(HMDS)_2$. With these modifications, it was possible to obtain NWs at growth temperatures as low as 250 °C, which is ~80 °C below the eutectic temperature.

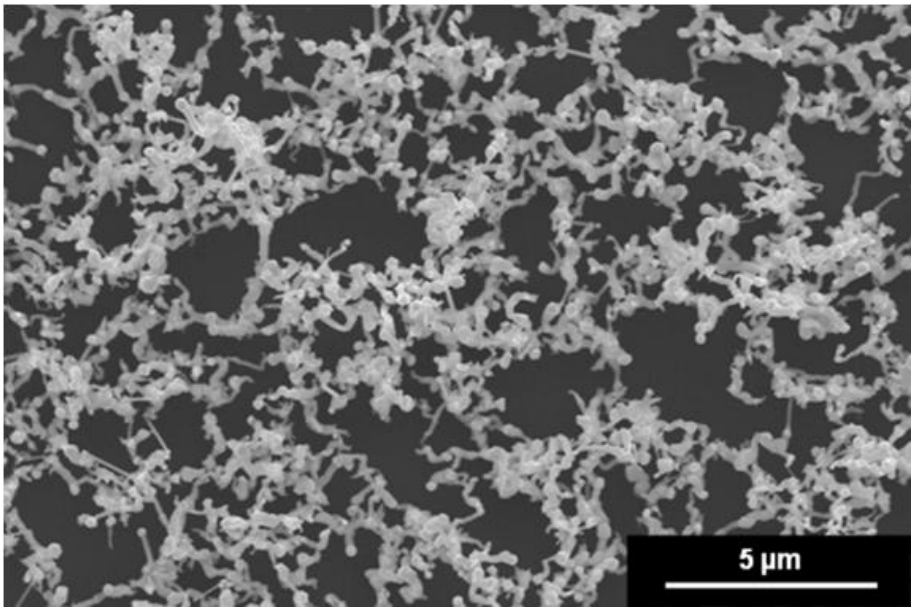

Figure 18: SEM image of Pb-seeded Ge NWs grown at 250 °C in solution.

Figure 18 illustrates a SEM micrograph of the product obtained from the low temperature growth process. The substrates showed a much lower NW density and significant more kinking compared to the NWs grown at higher temperatures.

The TEM micrograph in Figure 19 shows a growth seed of a NW grown via SFLS mechanism. It exhibits a nearly perfect spherical shape, which is common for NWs grown from liquid growth promoters. In contrast to this, tips of NWs grown via the SFSS mechanism showed facetted morphology. The possibility to grow Ge NWs via solid as well as liquid seeds using the same growth promoter had already been reported for gold nanoparticles via simple temperature reduction during growth and observation *in situ* TEM experiments.[75]

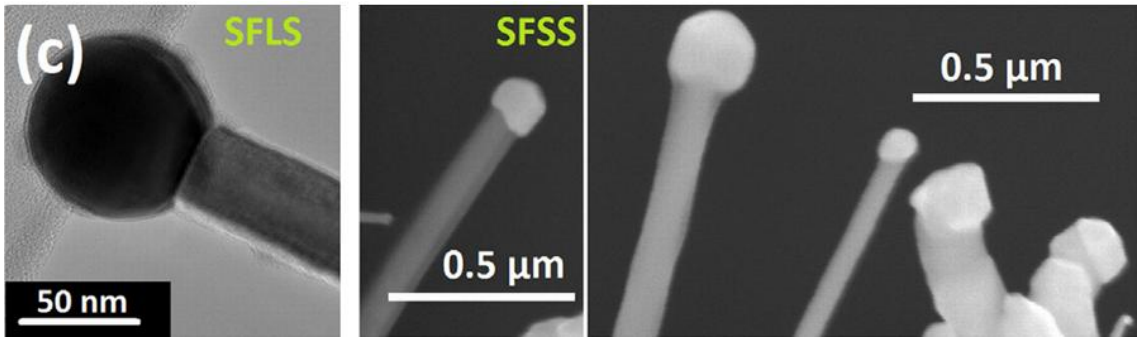

Figure 19: Comparison of Ge NW tips grown via SFLS and SFSS mechanism.

Additionally the growth on Pb foil as alternative growth substrates had been investigated. Therefore a Pb foil was placed into the reaction cell instead of the Si substrate. In this experiment, no growth seeds or lead precursor was added. Figure 20 shows NWs grown from bulk substrates at 320 °C which is close to the eutectic temperature. These NWs exhibited also a spherical seeds located on the NW tips. Therefore it can be concluded that NW growth did also occur via a seeded mechanism.

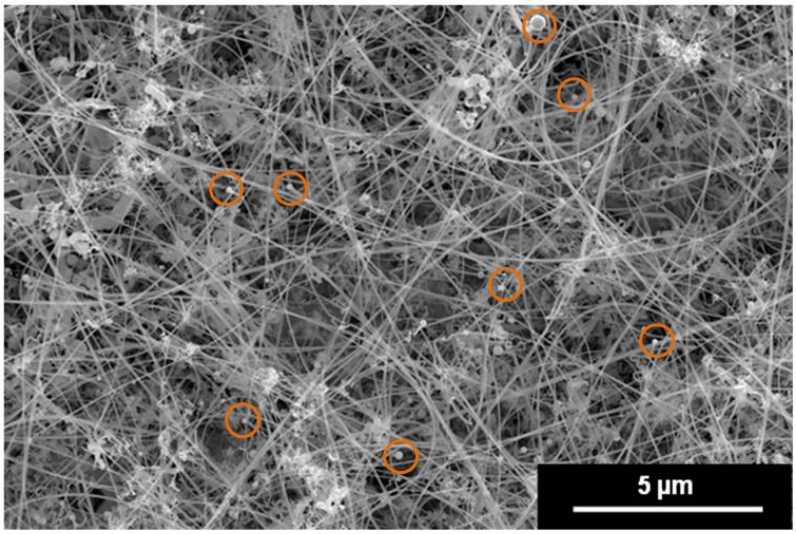

Figure 20: SEM micrograph of Ge NWs grown on a Pb foil at 320 °C. Orange circles mark spherical Pb droplets on NW tips

Such a self-induced growth mechanism had been demonstrated by various groups. Mathur *et al.* investigated such a growth mechanism on Fe substrates and proposed the formation of an intermetallic nuclei.[166] Similar findings were reported by Geaney *et al.*, who observed Cu_3Ge in the Ge NW seeds as well as on the Cu foil they used as substrate.[163] Also for Si NWs, growth from bulk metals had been reported and seed formation was most commonly attributed to the formation of intermetallic phases as nuclei.[237]

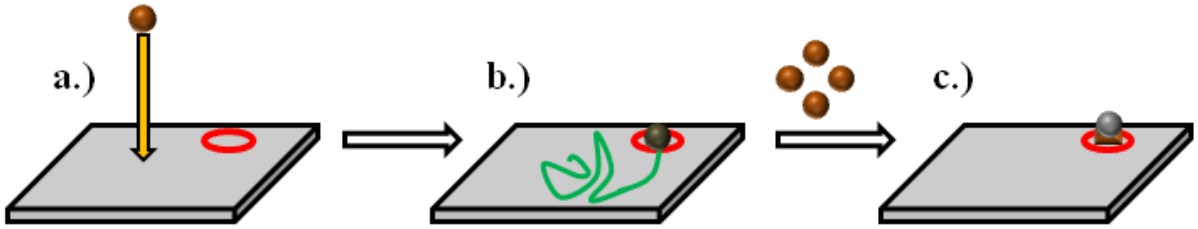

Figure 21: Scheme of the proposed seed formation mechanism by Dřínek *et al.*.[238]

Regarding the Pb-Ge system the formation of intermetallic nuclei as growth promoter can be excluded as there are no germanide phases existing in the binary phase diagram. Anyway, NW growth had occurred via a seeded mechanism, as NW tips exhibited Pb particles. A seed-formation mechanism for Ge-NWs grown from bulk metals which do not form intermetallic phases at growth conditions, had been reported by Dřínek *et al.*.[238] As shown in Figure 21, Ge adatoms are adsorbed at the bare substrate, thus a slight mobility remains until the atoms stick to a specific site. The density of such sticking sites on the substrate must be relatively low, as a too high number of sites would lead to thin film growth. The nature of the sticking site is still unknown. Dřínek *et al.* propose that it can be a defect or imperfection in the substrates surface such as a vacancy or grain boundary but also crystal edge or facet as well a surface chemical group at which the atom can adhere via Van der Waals interaction is conceivable. The sticking site traps further Ge atoms until a nucleus is formed.

Unfortunately, the reported mechanism does not discuss how single atoms which stick to a specific metal site are transformed into a metal nucleus on top of a Ge segment. Nevertheless, the observation that NW nucleation is limited to specific sites, applies also to Ge NWs grown on Pb substrates. When having a closer look at the Pb substrates, the surface is not comparable to an atomically flat facet of a single crystal. Due to its exposure to air and moisture, the substrate forms a rough passivation layer containing mostly lead oxide.[239] Furthermore, the surface exhibits a high number of steps as well as scratches and is contaminated with Pb particles exhibiting a similar passivation layer. When the substrate is heated to growth temperature, the passivation layers sustain cracks due to thermal expansion, enabling access of metallic Pb to the surface. Additionally, diffusion phenomena are significantly enhanced by the increased temperature, leading to a high mobility of Pb atoms and clusters on the surface. This environment is beneficial for the formation of new Pb seeds due to coalescence or Ostwald ripening. Furthermore, metallic Pb seeds might emerge from the reduction of the substrate by the Ge precursor. The Interfaces of the protruding Pb structures and the substrate could than act as preferential nucleation sites for Ge atoms, which derive from the precursor decomposition. As a result, Ge precipitates almost selectively at these interfaces, inducing the formation of a thin semiconductor layer between the substrate and the seed, which subsequently broadens due to metal-promoted precipitation.

5.2. Gallium-Seeding

Regarding group III elements, the metal-assisted growth of elongated Ge nanostructures is mostly investigated for aluminium and indium seeds. Literature about gallium-promoted growth is rather limited to Si NWs[115, 240] and the formation of elongated Ge structures via vapour transport growth[241] and the so-called electrochemical liquid–liquid-solid mechanism[182, 185, 186]. Last mentioned is a solution-based electrodeposition method which is discussed in chapter 3.1.

The usage of gallium possesses some valuable advantages in contrast to other seeds. As illustrated in Figure 22, the phase diagram of Ga and Ge exhibits a eutectic point at 0.006% Ge and no germanide phases. Therefore, Ga can be denoted as a type-B seed.[242] When considering the elevated temperatures necessary for sufficient precursor thermolysis, the gallium-germanium system is not limited by the solidification temperature of the seed. Low temperature growth enables deposition on flexible polymer substrates such as silicone or other plastics.

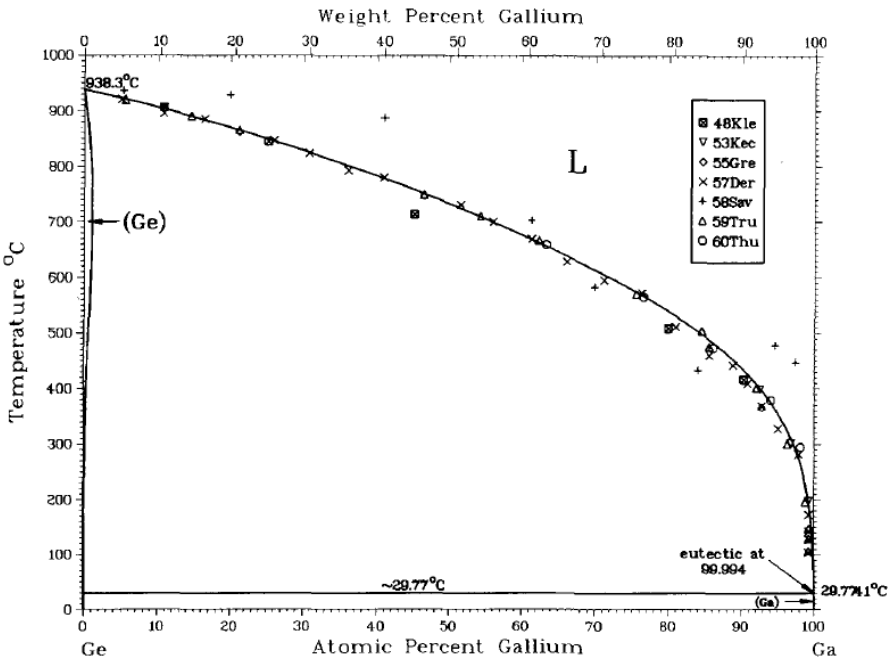

Figure 22: Ga-Ge binary phase diagram. Reprinted with permission from reference[242].

To enable low-temperature growth, a Ge precursor must be found, which decomposes at temperatures as low as possible. The usage of easily decomposable germanes such as di- or trigermane was avoided due to the pyrophoric nature of this compounds and the resulting additional protective equipment which is necessary when working with these chemicals. A less hazardous alternative is *t*BG, which is liquid and stable at room-temperature. *t*BG had been reported as a germanium source feasible for thin film growth of pure Ge,[243] GeSn[244] and GeSbTe[245] at low temperatures via CVD. The reported thin films showed a high crystallinity and exhibited just small carbon contamination on the surface, whereas no carbon was detected inside the material.

5.2.1. Gallium Seeds

Besides the Ge source, a supply of suitable Ga seeds must be ensured. In a first attempt, seed generation should be conducted via an *ex situ* strategy. Therefore, the synthesis of Ga nanoparticles according to He *et al.* had been conducted.[246] In this hot-injection method, Ga-amide is formed *in situ* from $GaCl_3$ and lithium dioctylamide, which is subsequently decomposed via thermolysis:

$$Oct_2NH + n\text{BuLi} + GaCl_3 \xrightarrow{\text{ODE;250 °C}} \text{Ga NPs} \qquad \textbf{(II)}$$

Besides providing the amine group for Ge amide formation, the long-chained amine should stabilise the emerging nanoparticles, which should inhibit uncontrolled growth, agglomeration as well as oxidation. As a result, the obtained Ga particles are amine-terminated. The synthesis using dioctyl amine is an alternative one-pot route, as the usual strategy for Ga particles makes use of presynthesised tris(dimethylamido) gallium (III).[247]

Synthesis according to the aforementioned procedure led to a brownish- to grey-coloured precipitate, which could be separated by centrifugation and redispersed in toluene. SEM micrographs as well as EDX measurements revealed that the obtained precipitate contained rather organic compounds than Ga nanoparticles. Also attempts to modify synthesis parameters such as temperature or the amount of Ga did not lead to Ga nanoparticles. As a result, a different synthesis strategy towards Ga nanoparticles was pursued.

In a second attempt, Ga particles were synthesised by irradiating the bulk metal using ultrasound. This synthesis strategy had been reported for a wide variety of nanoparticles from metals[248-254] including Ga,[255] metal-alloys,[256] as well as for various transition metal oxides[257]. The irradiation of a solution by ultrasound introduces a large amount of energy into a relative small volume, which could lead to chemical reactions such as radical generation, oxidation or reductions, as well as to physical phenomena such as friction, cavitation or micro jet generation.[258] As Ga is already provided as bulk metal, a sonochemical reaction is not required in the applied particle synthesis. The ultrasound irradiation should only apply enough energy to comminute the bulk metal into nanoparticles. In a typical synthesis ~20 mg of Ga metal were immersed in 15 mL toluene. To prevent aggregation of the particles dodecylamine or polyvinylpyrrolidone hexadecyl copolymer was added as surfactant. To prevent oxidation, synthesis had been conducted under argon atmosphere. The solutions turned instantly turbid as they were irradiated with ultrasound and became grey-coloured after one minute of irradiation time.

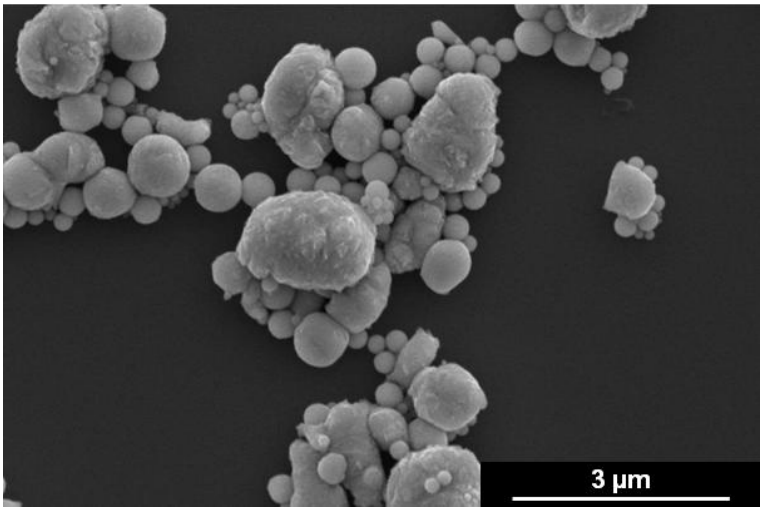

Figure 23: SEM micrograph of gallium particles obtained from the ultrasonic method.

SEM micrographs (Figure 23) of the purified products showed particles with diameters ranging from ~100 nm up to ~2 µm. Contrary to expected, a longer irradiation time did not alter the size distribution towards smaller diameters. Sudo *et al.* in contrast, had reported the synthesis of Ga nanoparticles with diameters of about 20 nm, by a similar synthesis method.[249] However, an additional filtration step using a 0.5 µm PTFE filter was applied in the procedure reported, which explains the absence of particles with larger diameters in their product. Furthermore, the applied irradiation power/energy was not reported, which makes a comparison difficult. In a different publication by Yamaguchi *et al.* a similar product was obtained when applying ~100 W of irradiation power.[254] With our setup, a maximum irradiation power of 30 W could be achieved, which is three-times less. Therefore it must be concluded that it was not possible to apply the amount of energy necessary to obtain particles with diameters <100 nm efficiently. Another aspect could explain the observation of larger particles rather than nanoparticles. Due to the liquid state of these particles at room temperature, they show a distinct tendency for coalescence, if they are not sufficiently stabilised by surfactants.[254] Rough particle surfaces as observed in SEM micrographs indicated at least a partial oxidation of the particles, as pure Ga particles usually show nearly perfect spherical shapes.[247, 249] Whether surface oxidation occurred during particle synthesis, storage or SEM sample preparation could not be clarified. However, the presence of an oxide shell indicates an insufficient capping, which would also explain the assumed particle coalescence.

As both *ex situ* methods did not led to the desired products, the synthesis strategy was modified towards an *in situ* method. Ga seeds were generated directly in the NW growth solution, using pentamethyl cyclopentadienyl gallium (I) (GaCp*), a gallium (I) metallocene derivative.[259, 260] Basically, the thermal decomposition of metallocenes leads to the formation of pure metal due to the cleavage of the metal-cyclopentadienyl bond and an organic by-product:[166, 261]

A similar decomposition route can be expected for the applied pentamethyl cyclopentadienyl complex. As the Ga seeds are generated directly in the NW growth solution prior to the NW growth process, a seed deactivation due to surface oxidation can be excluded, as the particles are not exposed to ambient atmosphere. Additionally, no surfactant had been used to stabilise the emerging seeds, which can lead to potential side reactions with the Ge precursor.

Preliminary experiments regarding the decomposition of GaCp* had been conducted in squalane using microwave heating. After 15 minutes reaction time at 250 °C, a grey-coloured precipitate could be isolated from the yellow reaction solution via centrifugation.

5.2.2. Nanorods

Thermal decomposition of *t*BG and GaCp* in toluene at temperatures between 170 °C and 230 °C resulted in the formation of a greyish-brown precipitate, which could be easily separated via centrifugation from the clear yellow supernatant. Only a clear yellow solution with no precipitate could be obtained when a decomposition temperature was chosen below 170 °C, which indicated an insufficient decomposition of the precursors. Successful growth experiments were conducted in closed steel vessels heated in a tube furnace. Experiments conducted in glass vials heated by microwave radiation in contrast, did only result in the formation of Ga particles with few heterodimer-like structures included. This behaviour could be related to the microwave vials, which were sealed by a rubber plate retained by a plastic ring. During heating to the growth temperature, the sealing started to leak, which resulted in the loss of the Ge precursor.

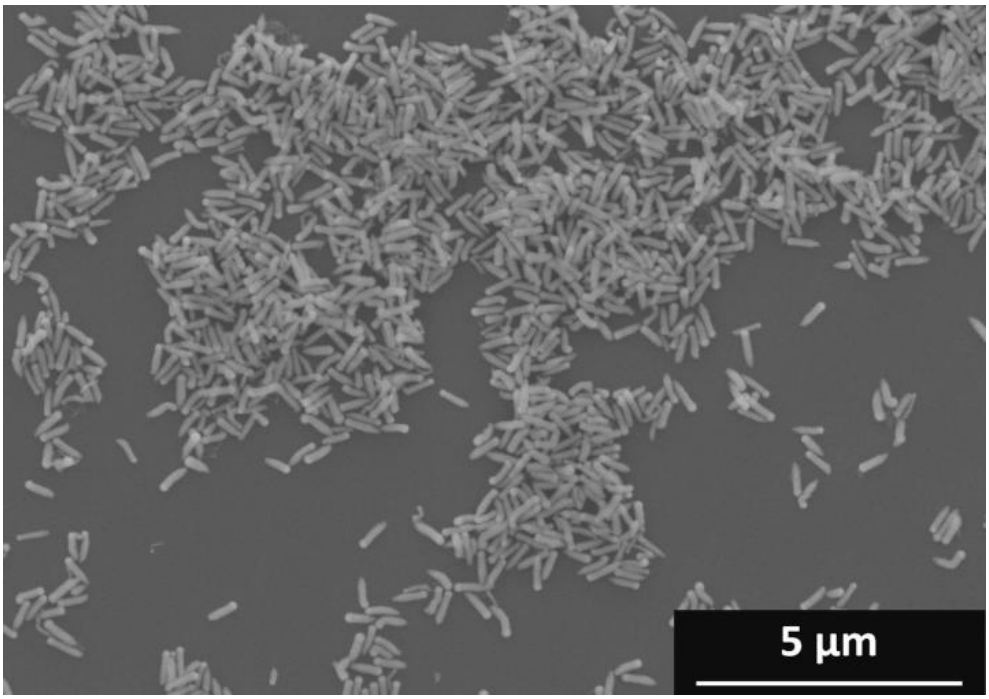

Figure 24: SEM image of a representative Ge NR sample.

As shown in Figure 24, SEM measurements revealed elongated nanostructures with a hemispherical tip exhibiting a different Z-contrast. This shape is very common for 1D structures grown via a metal-assisted growth process. The colour of the purified solids correlated with the length of the nanostructures determined from SEM images. Shorter rods or heterodimer-like structures showed a rather greyish colour, while longer rods were brown. Also differences in the dispersibility and sedimentation behaviour of the obtained products were observed. Smaller structures like the obtained heterodimers sedimented significantly slower than larger rod-like structures, whereas they were easier to disperse in toluene.

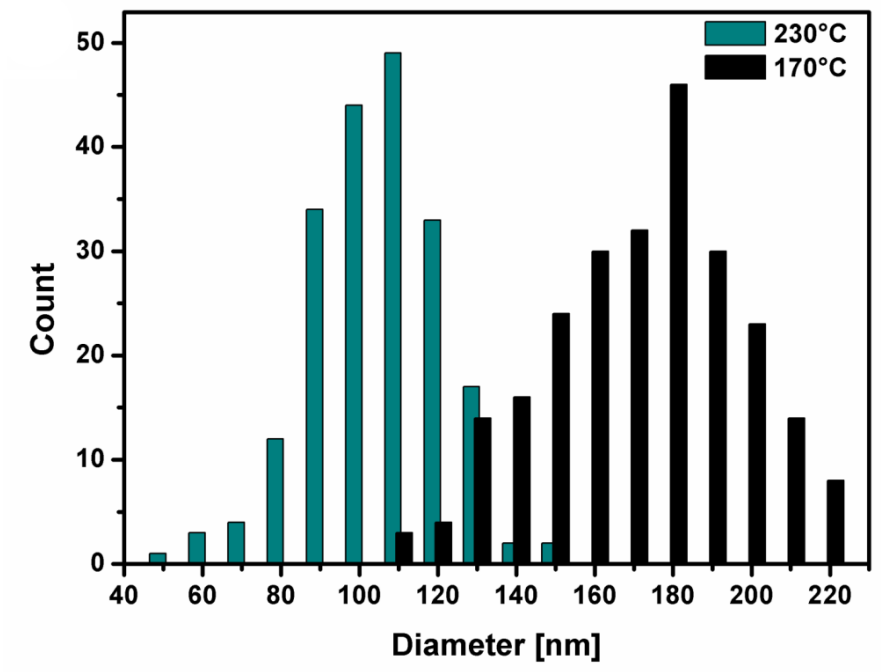

Figure 25: Diameter distribution of Ge NR grown at 170 °C and 230 °C.

Figure 25 depicts the diameter distributions of nanorod samples grown at 170 °C and 230 °C. As there was no stabilisation provided for the *in situ* generated Ga seeds, the diameter distribution of the seeds and as a result of the nanorods was broader than it is known for synthesis methods making use of a proper size control. Seeds as well as nanorods, grown at 230 °C exhibited a ~50 nm smaller mean diameter, compared to nanorods grown at the lowest growth temperature (170 °C). When regarding the seed formation- and the subsequent metal-assisted growth process, the diameters are influenced by two major causes:

First, the size of the growth promoter is influenced by its nucleation process, which can be explained by the LaMer model.[81] A schematic of the concentration evolution during the nucleation process for a lower (dotted) and higher (solid) growth temperature is shown in Figure 26. GaCp* starts to decompose when a certain temperature is reached (t=0 and t=1). The decomposition leads to Ga atoms, which diffuse through the reaction solution and form clusters when colliding with other Ga atoms (red coloured lines). However, these temporary emerging clusters are not stable and dissolve very fast. Due

to missing nucleation sites, the Ga concentration in the solution can be further increased by further GaCp* decomposition and an oversaturation is reached. At a certain point a critic concentration (C_{critic}) is reached, where stable nuclei emerge due to self-nucleation (blue). The nucleation processes occur very fast among the entire reaction solution. As a result, the supersaturation decreases rapidly until the Ga concentration drops below the critic concentration, where no further nucleation occurs. The remaining supersaturation is further decreased to the solubility limit (C_{sat}) by diffusion of the remaining atoms to the arisen particles (green).

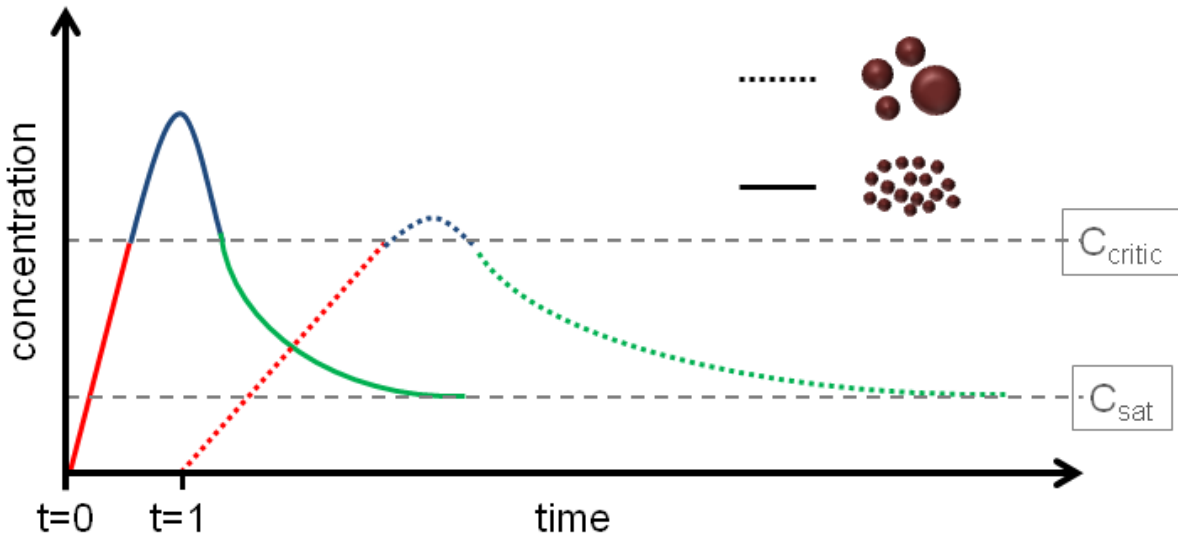

Figure 26: The LaMer model for two different temperatures.

Regarding the applied growth process, where the assembled reaction vessels were placed into the preheated tube furnace, a higher growth temperature led to a higher heating rate and thus to a faster precursor decomposition, which can be seen as the main influence on the obtained size distributions. The fast precursor decomposition rate led to a fast increase in Ga concentration in the heated reaction solution. Due to limited amount of Ga precursor, almost all seed precursor had been depleted, when the nucleation process stopped and growth due to diffusion of atoms could only occur over a short period. In contrast to this, a lower growth temperature led to a later decomposition onset (t=1) and a slower composition rate. Therefore, precursor depletion did not occur during or swiftly after the nucleation phase. Diffusive growth could occur over a longer period as Ga atoms were generated longer by the decomposition of remaining GaCp*. As a result a smaller number, but larger seeds emerged in the reaction solution.

Second, the growth promoter increases in diameter due to agglomeration, induced by collisions with other seeds in the reaction solution. As the applied growth process did not include an additional stabilisation with capping molecules, seed agglomeration is very likely to occur. Only the emerging Ge nucleus provides a small degree of stabilisation, as it covers a certain surface area of the seed. However, the Ge segment emerges not before the growth promoter is supersaturated with Ge, which de-

pends on the decomposition rate and therefore on the growth temperature. As a lower growth temperature results in a longer period for enhanced agglomeration, seeds and nanorods grown at lower temperatures exhibited a larger diameter.

A deeper insight into the growth dynamics of these nanorods is provided by a growth study. Therefore, a fixed precursor ratio of Ge:Ga= 6:1 was decomposed at temperatures between 170 °C and 230 °C for one to eighteen hours and the aspect ratio (i.e. length/diameter) of the obtained nanostructures is correlated with the decomposition duration. The aspect ratio is a good possibility to measure the progressive elongation of a 1D nanostructure, as it is not influenced by the diameter distribution of the seeds. To ensure statistical significance, ~200 rods were measured for each sample.

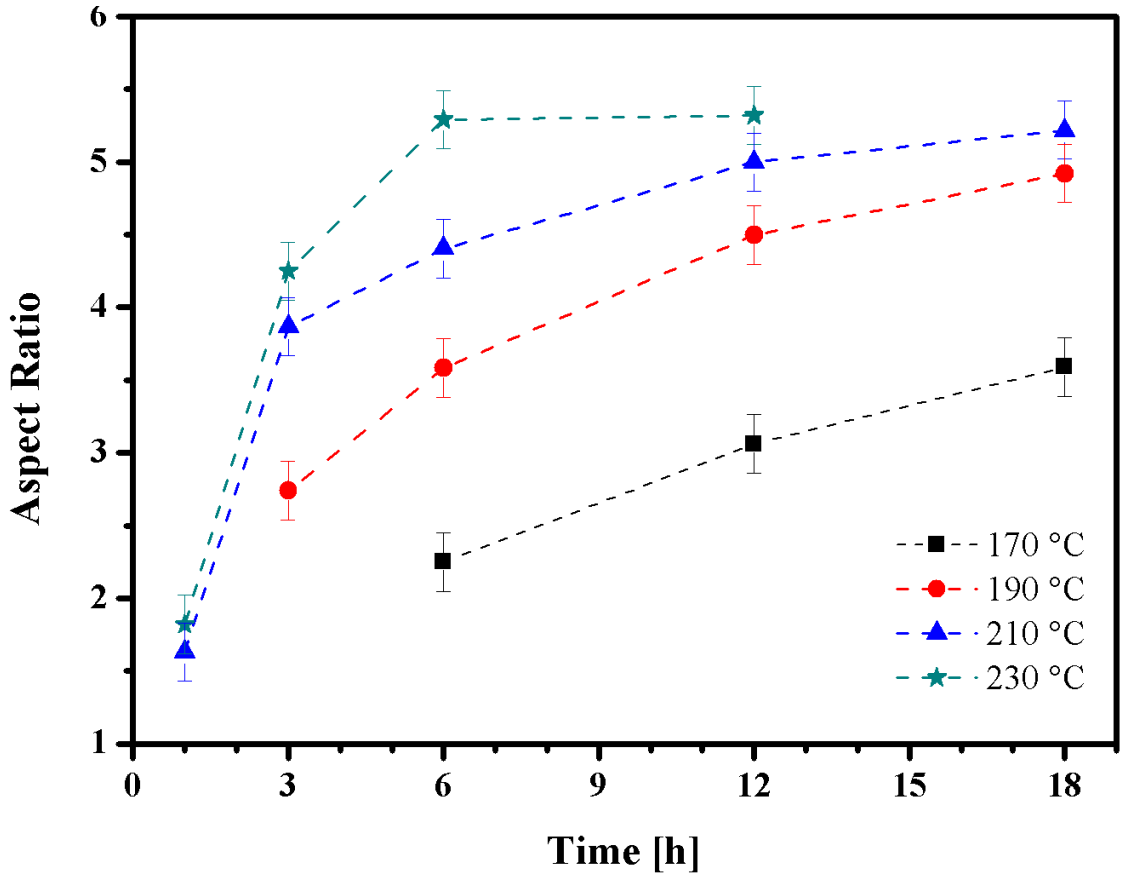

Figure 27: Aspect ratio of obtained Ge NRs correlated with growth durations for temperatures between 170 °C and 230 °C.

Figure 27 illustrates the obtained results: Nanorods grown at 230 °C and 210 °C required an initiation period of <1 h while experiments conducted at lower temperatures (190 °C and 170 °C) did not show any product formation after this growth duration. While short nanorods had been observed after 3 hours at 190 °C, the first product for the lowest conducted growth temperature of 170 °C could be isolated after six hours. During the initiation period the cell is heated to the desired growth temperature and the nucleation of the growth promoter occurs. The formation of Ga seeds showed to be mandatory for the decomposition of *t*BG at low temperatures, as no decomposition of pure precursor in

toluene had been observed at temperatures below 250 °C. CVD processes using *t*BG for thin film growth (no metal as growth promoter involved), require minimum 275 °C to maintain a sufficient precursor decomposition.[245] A period of progressive nanorod elongation occurred subsequently to the initiation step. During this period, a constant growth rate is expected, as the precursor decomposition rate could determine the elongation velocity.[199] Due to the limited amount of data points, this regime is only clearly visible for the lowest temperature. However, the temperature-dependence of the growth rates is clearly recognisable, as nanorods grown at higher temperatures showed higher growth rates. Following to this growth period, a limitation regime had been reached, where nanorod elongation decelerated and finally stopped most likely due to the depletion of precursor in the growth solution. For the highest temperature, this regime was reached between three and six hours, whereas the regime was not reached for nanorods grown at 170 °C after 18 h.

Figure 28 illustrates a typical progress in nanorod evolution over time. For a better illustration, the data points are linked to the corresponding SEM micrographs, showing the emerging of the nanostructures from heterodimer structures (yellow) to fully evolved nanorods.

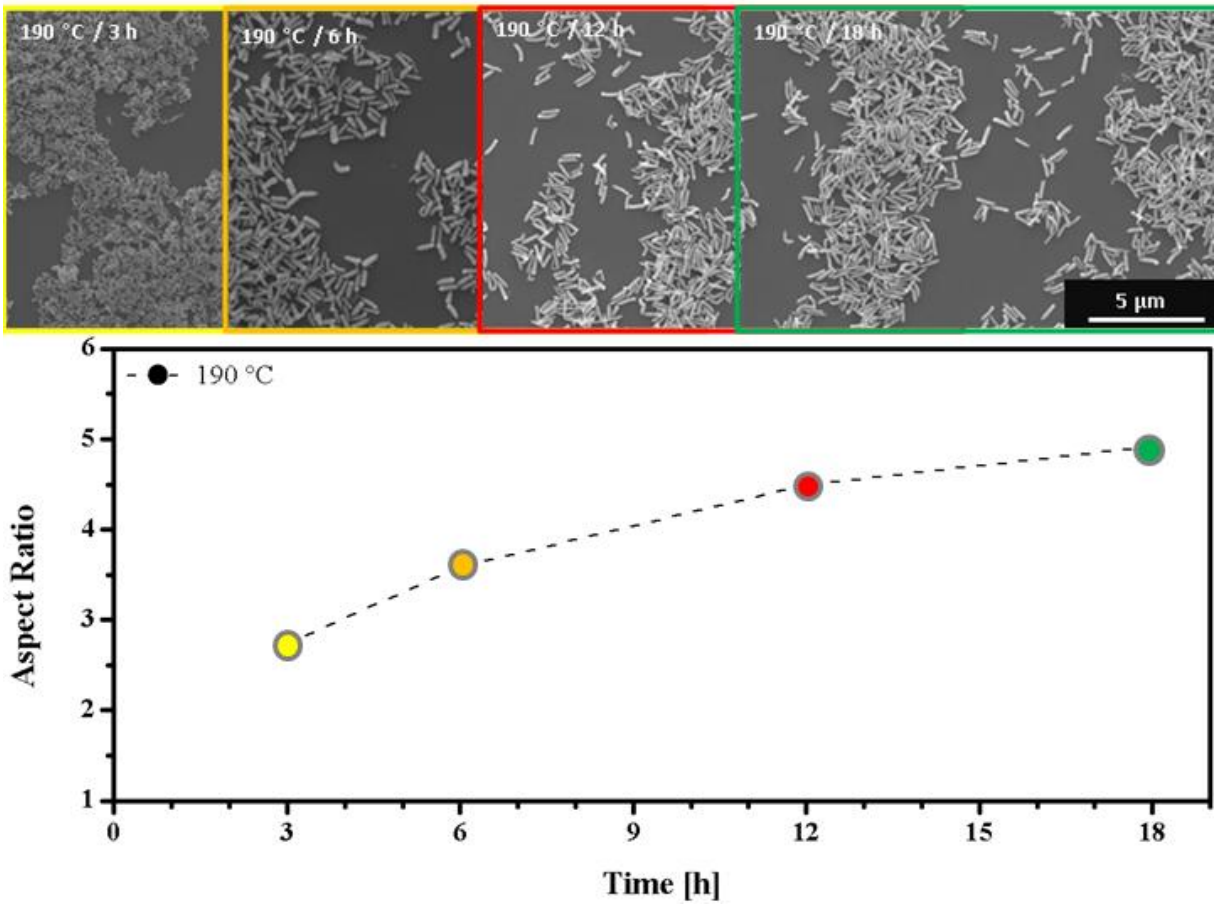

Figure 28: Evolution of the aspect ratio and corresponding SEM micrographs for Ge NRs grown at 190 °C.

Figure 29 illustrates the XRD pattern of a nanorod sample grown at 210 °C for one hour. The observable reflections mach well with the Ge reference and no amorphous background is visible, which is

often the case for low temperature grown nanostructures.[262] The definite shape of the reflections suggests a high crystallinity of the nanorods. The <111> reflection is slightly more pronounced which is the result of the elongated nanorod structure. The absence of Ga reflexes is expected due to its low melting point and the size of the seed particles.

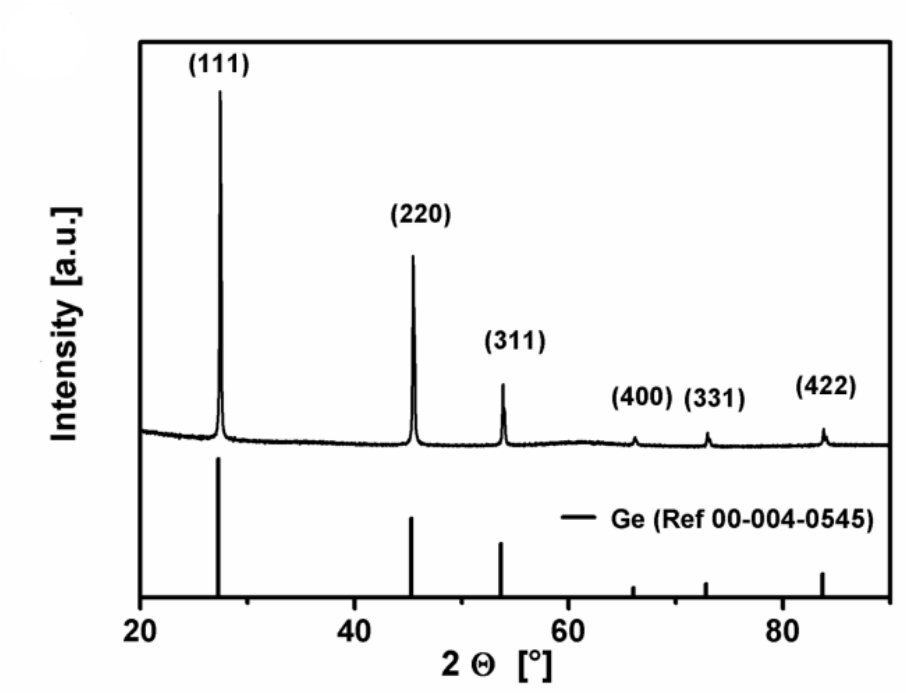

Figure 29: XRD pattern of Ge NRs obtained from a synthesis at 210 °C for 1 hour.

TEM micrographs of the nanorod samples exhibited a high crystallinity, which was already expected from XRD results. FFTs of the obtained high resolution images exhibited that nanorods grew mainly in <111> direction, which is the favourable growth direction for elongated Ge nanostructures with diameters above 20 nm.[263] However, a small fraction had been observed which showed <211> or <110> growth direction. TEM images exhibited also dark lines, which are related to diffraction contrast facilitated by twin planes in the nanostructure. These twin planes are supposed to be kinetically induced during the growth process, due to fluctuations in the contact angle at the TPB.[193, 264] Fluctuations can be induced by minimal changes in the local temperature, precursor concentration, pressure or mass transport.

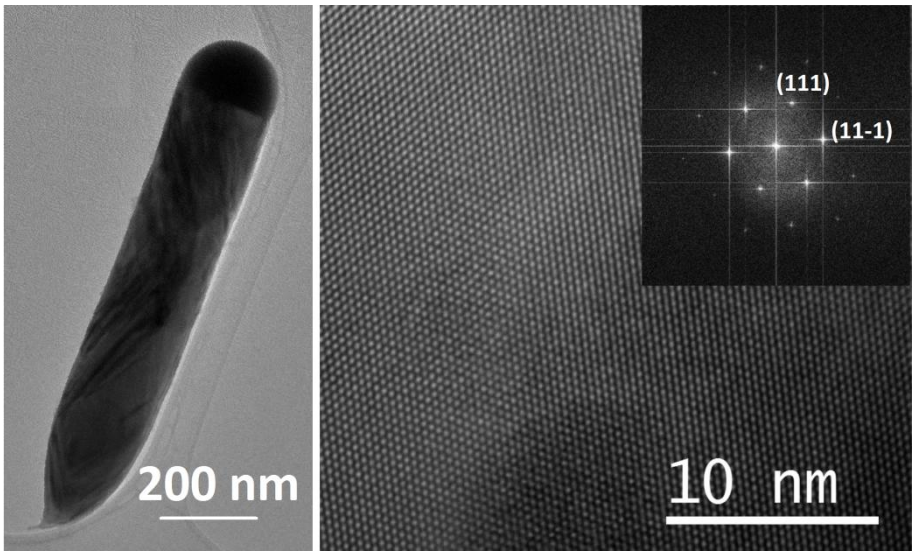

Figure 30: TEM and HRTEM micrograph with corresponding FFT of a Ge NR grown at 190 °C for 16 hours.

For a potential application of the obtained material it is beneficial if the Ga growth promoter can be removed from the NW tips. This can be maintained by treating the purified nanorods with 2% hydrofluoric acid. As shown in Figure 31, the acid-treatment removed the growth promoter while the germanium structure remained unaffected.

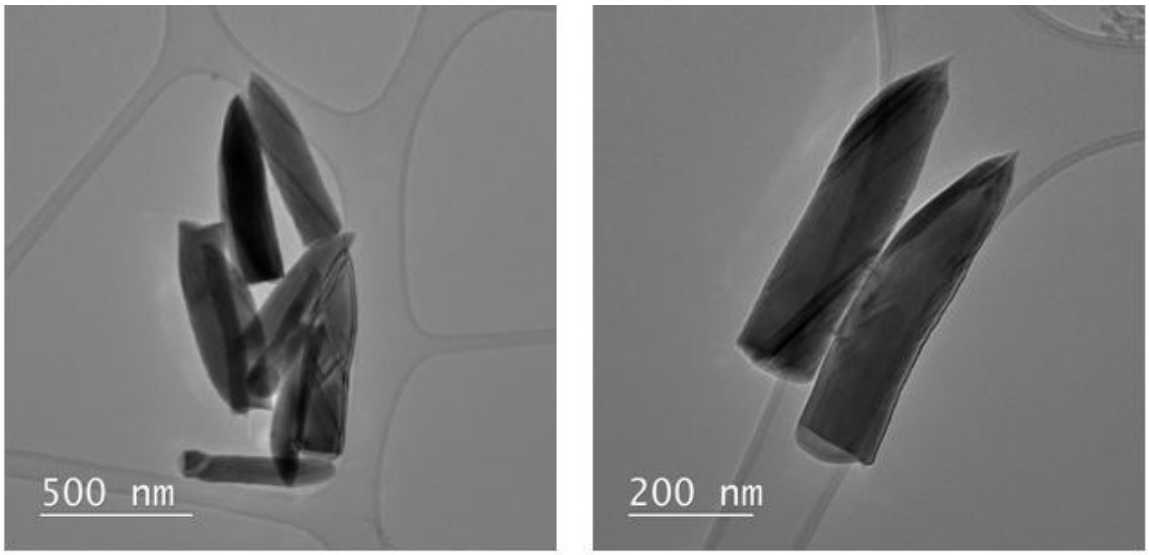

Figure 31: TEM images of Ge NRs after the hydrofluoric acid treatment.

5.2.3. Nanowires

After obtaining nanorods from experiments using low Ge:Ga ratios, the precursor composition was modified towards a higher Ge amount (30:1). Decomposition durations and growth temperatures were chosen according to the results obtained from the nanorod growth study. Isolated products were dark brown in toluene solution and showed a lighter brown colour when the solvent was evaporated. Com-

pared with the nanorod synthesis, a higher amount of precipitate could be isolated from the reaction solution and its redispersion during the purification was more difficult.

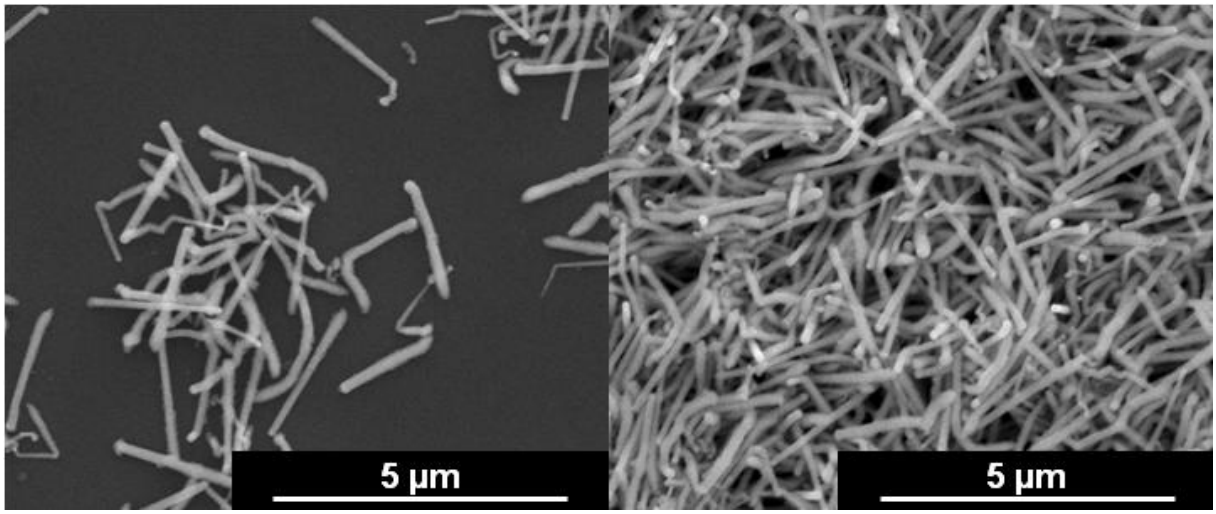

Figure 32: SEM micrographs of gallium-seeded Ge NWs grown at 210 °C for 18 hours.

SEM investigation of the obtained product (Figure 32) exhibited NWs with lengths up to 3 µm. Some NWs showed randomly distributed kinks. A slight tapering could be observed, especially for longer NWs. The related XRD spectra of NWs revealed a significantly more pronounced <111> reflex when being compared with nanorod samples, which is the result of the elongated nanostructure. Similar to the nanorod samples, no amorphous background was visible and the sharp reflex shape indicated a high crystallinity of the product.

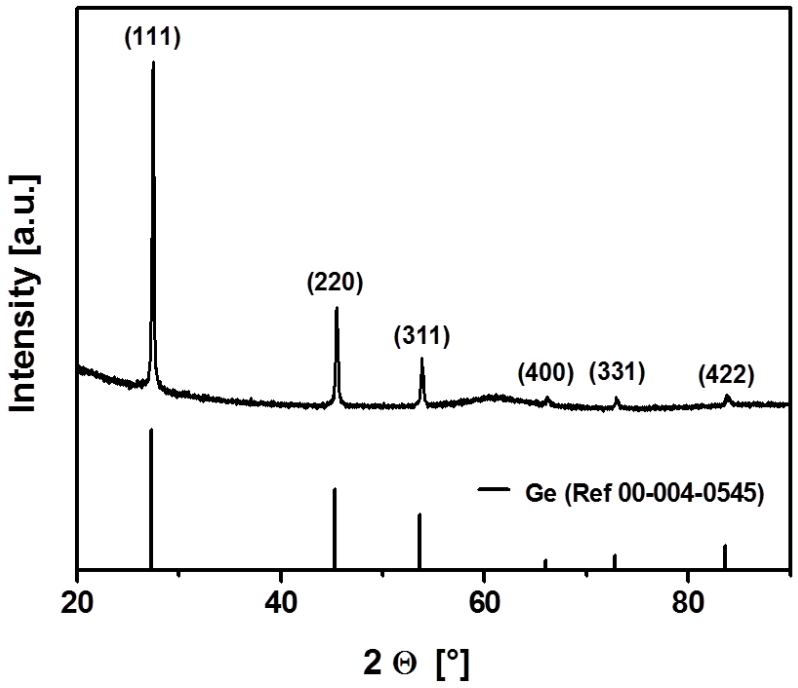

Figure 33: X-ray diffractogram of Ga-seeded Ge NWs grown at 210 °C for 18 hours.

NWs could be also obtained from a two step growth process. Step one included a simple nanorod growth at 210 °C for 1 h, using a Ge:Ga ratio of 6:1. For the second step, the reaction cell was removed from the furnace and opened in the glove box, where additional 18 Eq. of *t*BG were added. The tightly sealed cell was placed again into the furnace, where it was left at 210 °C for 18 hours. A representative SEM micrograph of the product is depicted in Figure 34. As shown in the inset the obtained product exhibited NWs with two different segments. The slightly broader part of the NW can be attributed to the first growth step, while the longer part exhibiting the growth promoter on its tip grew during the elongation step.

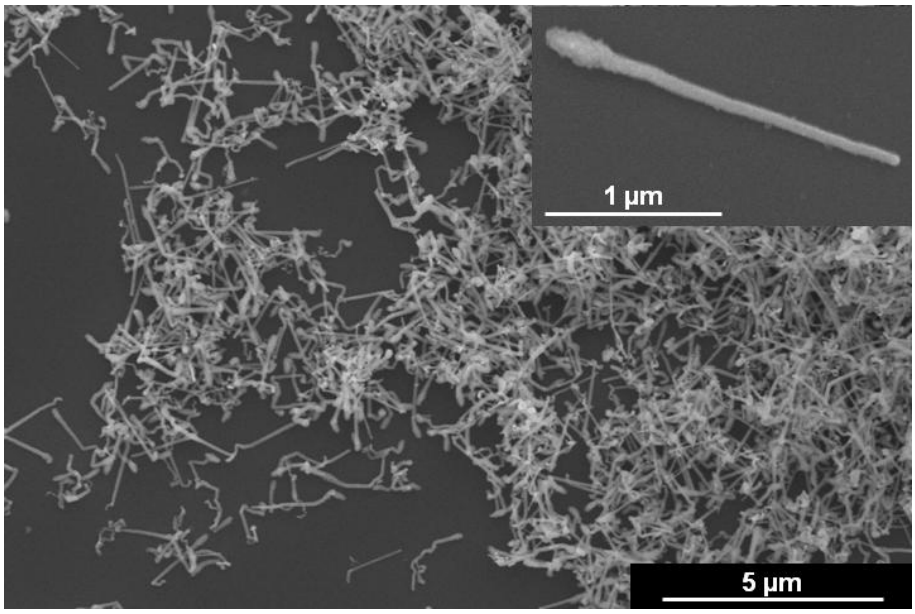

Figure 34: SEM micrograph of Ge NWs grown via the two step growth method.

The low temperatures which could be achieved for NW growth enable the usage of flexible polymer substrates such as silicone. However, polysiloxanes tend to swell when being exposed to toluene at higher temperatures.[265] As a result it was necessary to adapt the growth process towards toluene-free conditions. In order to overcome this aspect, growth via VLS mechanism in a hot wall reactor had been investigated. Therefore, the steel cell acted as a hot-wall CVD reaction chamber, where the NWs grew in a batch process. A silicone substrate was infiltrated with GaCp* and placed into the reaction cell together with the Ge source. The tightly sealed cell was then placed into the furnace at 200 to 230 °C for 12-18 h. The reaction cell was allowed to cool down and opened to obtain a brown-coloured substrate.

A typical SEM micrograph of NWs grown on a silicone substrate is shown in Figure 35. It exhibits nanostructures with similar diameters as obtained from solvent-based approaches. However, the NWs from CVD-based growth exhibited higher lengths and less kinking. In the inset, the flexibility of the substrate after the NW growth process is demonstrated. The silicone substrates lost a certain degree of

their flexibility during the growth. Nevertheless, the remaining flexibility was high enough to enable bending, even at low radii.

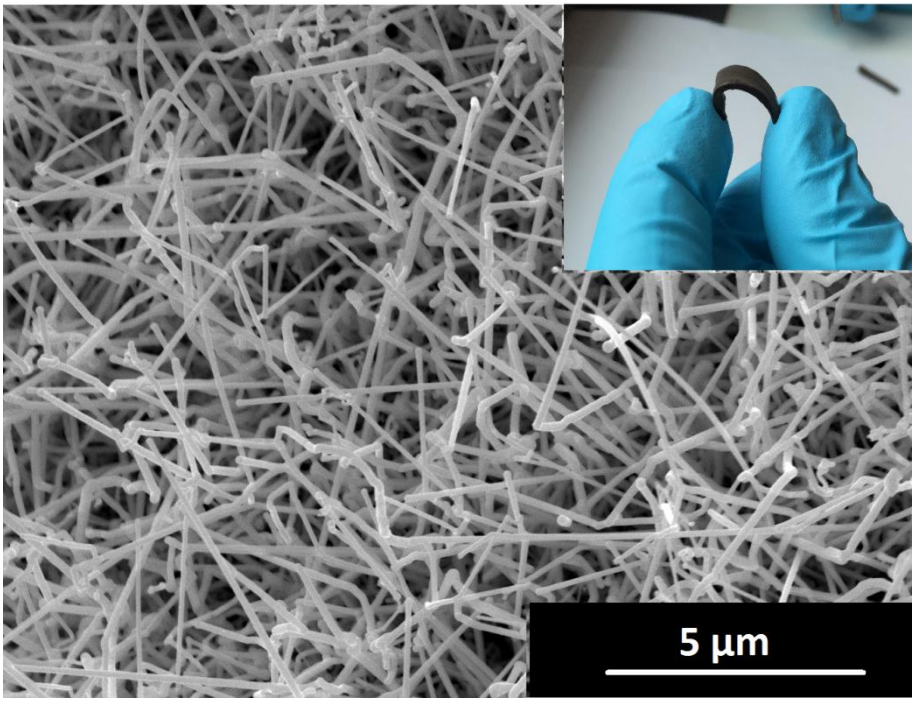

Figure 35: Ge NWs grown via vapour phase on silicone. The inset depicts that the substrate is still flexible after the growth process.

Although growth via VLS as well as SLS mechanism let to similar nanostructures, there are distinct differences between growth in solution and via vapour phase. First, both processes have a different growth environment. VLS growth is performed in a closed reactor, where the vapour phase contains mainly argon. The pressure in the cell is mainly determined by the precursor vapour pressure, i.e. the amount of precursor in the cell. The growth environment influences also the precursor diffusion, which is significant higher in the vapour phase than in solution. As a result, structures grown via VLS are less influenced by precursor fluctuations and grow therefore with less kinks and defects. The SLS mechanism in contrast is performed in toluene. As growth temperatures are too low to generate a supercritical fluid, the pressure in the cells remains rather low when being compared to supercritical fluid environments, but much higher than in the VLS growth.

Regarding the SLS mechanism, growth occurs via seeds being dispersed in a liquid phase. In contrast to this, growth via VLS mechanism makes use of a growth promoter being attached to a substrate. In the SLS mechanism, the nucleation of the Ge crystal occurs at the solution-liquid interface of the Ga droplet and the surrounding solution. As the seed is almost a perfect sphere, the nucleation of the Ge crystal occurs at a random position on the droplet surface. In VLS growth, the nucleation of the Ge structure occurs preferentially at the interface between the Ga droplet and the substrate. The segregation of NW atoms at the substrate-seed interface is energetically favoured, compared to the seed-

vapour interface and therefore the nucleation of the NW is located at the substrate seed interface.[266, 267]

TEM investigation of the obtained NWs showed similar results to the nanorod samples, though the observed structures showed higher aspect ratios. The NWs preferential growth direction agreed with the NR samples, as no change in growth direction was expected and observed. As already observed in the solvent-based growth methods, tapering occurred also in CVD-growth. As growth temperatures are very low, tapering due to sidewall nucleation is very unlikely and can be therefore excluded.[156] Another cause for tapering is the incorporation of seed atoms into the NW matrix.[227] The loss of seed materials leads to a decreasing diameter of the growth promoter, which than alters the diameter of the emerging NW.

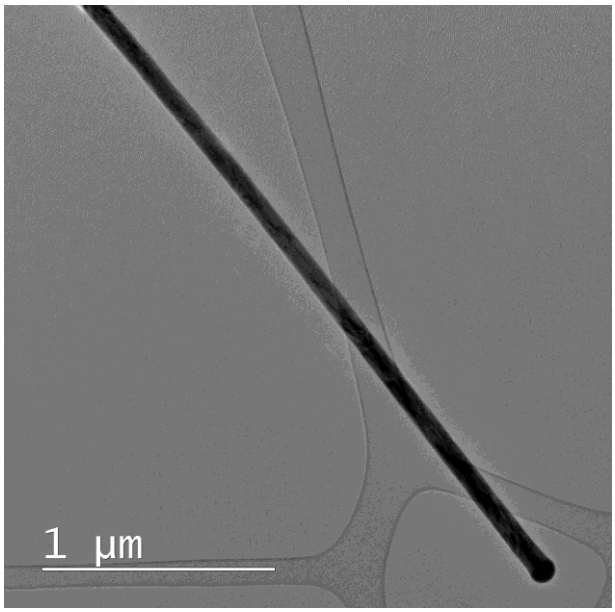

Figure 36: TEM micrograph of a Ga-seeded Ge NW grown at 210 °C via VLS mechanism.

5.2.4. Elemental Mappings

To obtain an insight into the elemental distribution in the material, STEM EDX analysis had been conducted. A representative mapping of an obtained nanorod is depicted in Figure 24. Gallium seeds exhibit no measureable Ge concentration, which is also proposed by the phase diagram, as the concentration of Ge at the eutectic point is 0.006 % and the solubility limit at growth temperature still <1 %.[242] In contrast to this, nanorod bodies contain up to 3.6 % Gallium which is homogenously distributed along the entire nanorod body. No decoration of the surface with metallic Ga droplets could be observed. Regarding the binary phase diagram of the Ga-Ge system, the solubility of Ga in solid Ge is limited to ~1.1 % at 750 °C.[242] At room-temperature, the solubility decreases even to lower per

mille-levels.[268] Therefore, the obtained germanium/gallium alloy can be denoted as a metastable solid solution.

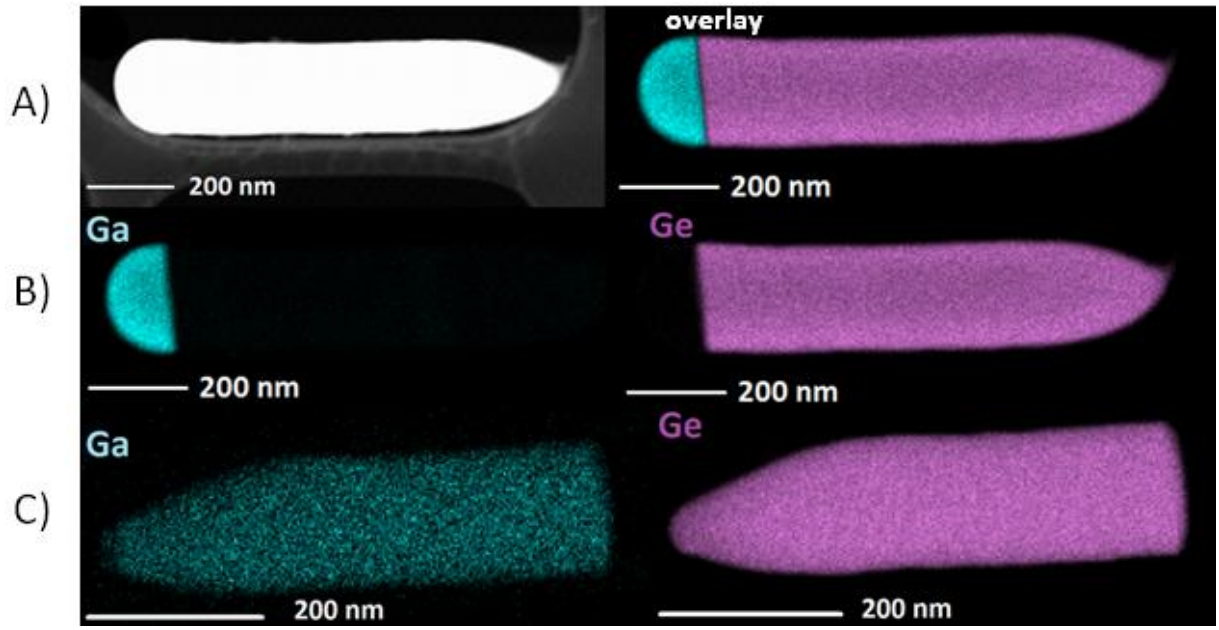

Figure 37: A) HAADF STEM and STEM EDX overlay; B) EDX mapping of pristine Ge NRs; C) EDX mapping of HF-treated Ge NRs.

STEM EDX mappings of HF-treated nanorods showed similar results despite to the absence of the seed. The Ga incorporation in the Ge matrix was not influenced by the HF-treatment. Nevertheless a distinct difference in the Ga distribution is visible when comparing the mapping results of untreated and treated nanorods. In the illustration, untreated nanorods seem to have no Ga incorporated. This artefact is attributed to the limited intensity range available for graphical illustrations. As the tip contains only pure Ga, the maximum achievable colour intensity is adjusted among this area. Nanorod bodies in contrast contain ~3 % Ga, which is than correlated to ~3% of the tips colour intensity. Such low colour intensities cannot be displayed properly.

STEM EDX mapping of single NWs grown via VLS mechanism (illustrated in Figure 38) as well as in solution (depicted in Figure 39) showed similar results regarding the element distribution in the nanostructures. NW tips contained almost pure gallium as the Ge concentration was below the quantification limit. NW bodies in contrast, consisted of Ge alloyed with up to 3.6 % Ga atoms distributed homogenously along the entire structure.

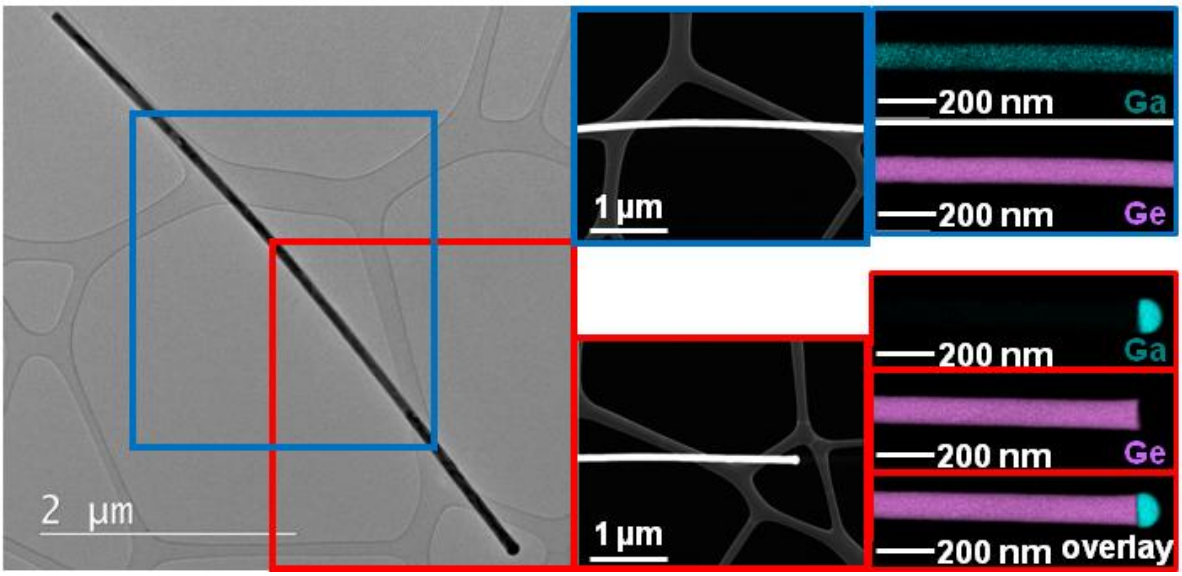

Figure 38: HAADF image of a Ga-seeds GE NW grown via VLS, illustrates the position of STEM EDX mappings and corresponding elemental mappings.

The subsequent incorporation of Ga into the NW matrix leads to a loss of metal in the growth seeds. As Ga is only provided once during the nucleation period the growth seed starts to shrink during the entire NW growth. This effect is marginal for structures with a lower aspect-ratio such as NRs and thereby not visible, but can be observed at structures with a higher aspect-ratio. The NW illustrated in Figure 39 shows significant tapering over the entire length of ~10 µm. While the amount of seed material is steadily reduced and therefore the diameter shrinks, the Ga concentration in the NW body remains the same. A diameter-dependence of the concentration had been reported for metastable alloy NWs with high differences in atomic radii such as GeSn.[236] Incorporation of atoms with different radii leads to strain in the crystal lattice. The strain can relax via the NW surface, which prevents phase segregation. As smaller structure have a higher specific surface, more lattice strain can be relaxed and therefore a higher concentration of foreign atoms can be incorporated. In the case of Ga-seeding, the atomic radii differ only in 2 pm[226] thus, lattice stress can be neglected.

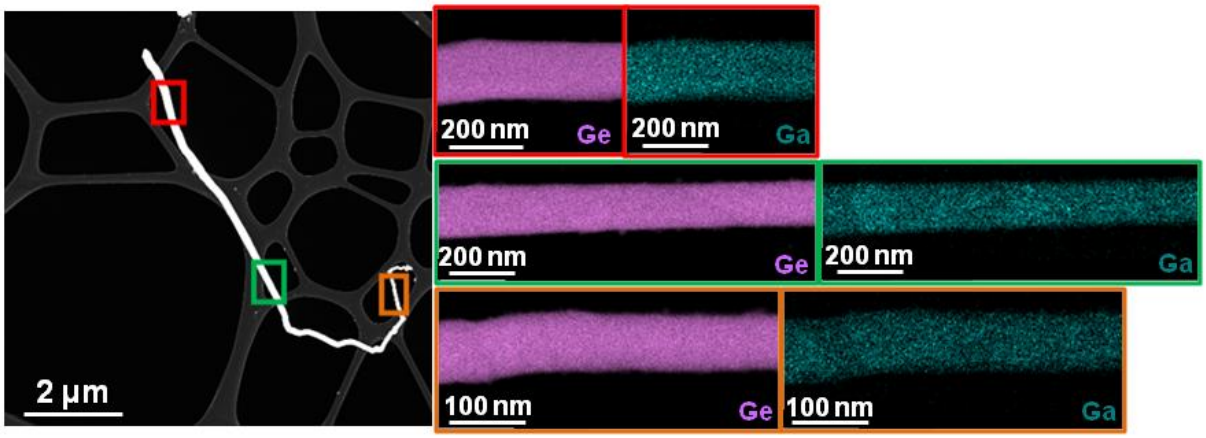

Figure 39: HAADF micrograph of a ~10 µm long Ge NW grown in solution, illustrating the positions of mappings and corresponding STEM EDX mappings.

Further analysis of samples grown at different temperatures pointed out that the amount of incorporated Ga was not influenced by the growth temperature (170-230 °C). However, metal-assisted synthesis of metastable alloys can be very temperature sensitive, as these systems tend to segregate, if the environment allows the system to equilibrate. The achievable compositions of the aforementioned GeSn system for instance, show a high temperature-dependency. Tin seeded growth at 430 °C did not show any tin incorporation[179], whereas growth conducted at lower temperatures (270-230 °C) led to an incorporation of up to 28 % of seed material into the NW.[98, 180, 211]

Similar to the Ge-Sn system, the binary phase diagram of Ge and Ga does not predict the incorporation of high amounts of seed material into the NW. However, phase diagrams represent only the thermodynamic behaviour of a bulk system, they are not feasible to quantify kinetic processes such as the metal-assisted growth of nanoscaled objects. Surface effects, capillarity and related nanoscale stresses could alter boundaries in phase diagrams and therefore shift solubility limits.[269]For instance, the pressure in a seed droplet is depending on its curvature.[111] According to Le Chateliere's principle, a higher pressure in the seed suggests an enhanced incorporation. However, the influence of these thermodynamic effects is favourable for the incorporation of seed material, but too low to explain an incorporation which is orders of magnitudes higher than in equilibrium.

As thermodynamic effects failed to explain the formation of metastable alloys in metal-assisted growth, kinetic effects were considered. Supersaturated solids for instance, were obtained from so-called "solute trapping" experiments, where a melt is ultra-rapidly cooled. When solidification begins, it emerges from its origin like an interface, with very high velocity through the material. To inhibit segregation in this process efficiently, the interface velocities must be in the range of meters per seconds.[270-272] Metal-assisted growth in contrast, is a step-growth process, which occurs via bilayer-formation with growth rates of nm/s to nm/min. According to solute trapping models, such a slow crystallisation velocity should lead to growth near thermodynamic equilibrium and therefore the formation of a metastable phase should not occur. However, these models describe bulk systems, whereas

NWs are nanoscaled objects. In 2013, a quantitative model for the incorporation of seed atoms into NWs had been reported by Moutanabbir *et al.*.[227] They investigated the incorporation of high amounts Al atoms into Si NWs. Their model considers the step growth process with its incubation period between the formation of bilayers at a finite growth front. The incubation period represents the period where the supersaturation in the seed is increased until bilayer formation occurs. In contrast to solute trapping models, atoms become trapped in the crystal during bilayer formation with one side still exposed to the nanowire/seed interface, not just when the atom is covered by the next bilayer. They also considered the reduction of seed atoms in the growth promoter, which means that the seed supersaturation is faster reached and the incubation period decreases. With this model, it became possible to describe the formation of a metastable Si-Al phase via metal-assisted growth, hence it can be adapted to other systems.

Literature concerning metastable Ge-Ga alloy NWs is very limited too few reports. NWs grown from pure gallium seeds via electrodeposition, showed a significant seed incorporation.[182] The growth mechanism of these NWs is supposed to occur similar to the VLS mechanism via cyclical bilayer formation.[183] Despite to reporting any quantity, the dissolution of seed material into the Ge matrix could be already assumed by the high tapering of the investigated nanostructures.[185] Furthermore, electrical measurements revealed a very high conductivity, which also suggests high concentrations of impurities, most likely due to incorporated seed material.[186] Germanium microwires grown via electrodeposition from InGa alloys exhibited Ga concentrations even up to 8.1 % while indium concentrations remained below 0.1 %.[273]. The significant lower indium concentration can be related to the larger atomic radius of In (142 pm)[226], which inhibits the incorporation into the Ge lattice. As mentioned before, the atomic radius of Ga in contrast, differs only 2 pm from Ge.[226] The tremendous high Ga concentration in electrodeposited Ge NWs can be related to the lower growth temperature of ~80 °C. At such low temperatures, phase separation due to segregation can be neglected. However, when annealing these NWs at 250 °C, which is slightly above our applied growth temperatures, Ga atoms started to segregate and form metal islands on the NW surface. As a result, the Ga content in the NWs is reduced to 3.3 %, which is similar to the Ga concentrations observed in our nanorods.

Germanium NWs grown via plasma assisted vapour transport growth have not been investigated regarding the metal-incorporation. However, synthesis temperatures above 300 °C suggest a rather thermodynamic-driven growth regime and therefore only a minor incorporation.[241]

Besides the incorporation of Ga from the growth promoter during the growth process, a subsequent incorporation via focused ion beam had been reported.[26] Focused ion beam technique enables control over the implanted amount, thus the achievable Ga concentrations (~10^{18} cm^{-3}) are well below the concentrations obtained from SLS or VLS growth using Ga seeds(~10^{21} cm^{-3}). Higher ion doses led also to defect generation and amorphisation of the NWs due to beam damage.[26, 208]

5.2.5. Electrical Characterisation

The incorporation of gallium into the NW matrix leads to the formation of acceptor states near the valence band and therefore to a p-doping of the material.[274-276] As the high amount of incorporated Ga is supposed to alter the electronic properties of the NW, an electronic characterisation was performed. Therefore, NWs were transferred onto a substrate using a dry-transfer technique. The NWs were contacted via e-beam lithography using Al electrodes and I-V curves of single NWs were measured, via two-point measuring method.

To ensure the understanding of the characterisation results, a short introduction into electrical characterisation and the necessary metrics is given prior:

The transport of charge (Q) along a certain route can be quantified by the electric current per time according to:

$$I = \frac{dQ}{dt} = \left[\frac{\text{coulomb}}{\text{second}}\right] = [\text{ampere}] \quad \textbf{(III)}$$

As we are going to investigate the charge carrier transport through a material having a finite geometry, the electric current must be related to its cross section, which is ensured by the current density (J):

$$\vec{J} = \frac{I}{A} = \left[\frac{\text{ampere}}{\text{area}}\right] \quad \textbf{(IV)}$$

To generate a current through a conductor, the charge carriers must be attracted or retracted by an electric field, i.e. they must have a certain electric potential (V)

$$V = \int \vec{E} \cdot ds = [\text{ volt}] \quad \textbf{(V)}$$

Electric potential and current are linked according to Ohm's law introducing a constant of proportionality (R) also called resistance:

$$R = \frac{V}{I} = \left[\frac{\text{volt}}{\text{ampere}}\right] = [\text{ohm}] \quad \textbf{(VI)}$$

Similar to the current density mentioned before, a relation to the geometry (cross section, length) of the conductor must be given for the resistance, called resistivity (ρ):

$$\rho = R \cdot \frac{A}{l} = \left[\Omega \frac{cm^2}{cm}\right] = [\Omega \cdot \text{cm}] \quad \textbf{(VII)}$$

Besides resistivity, the conductivity is often reported to describe the conducting behaviour of a material. The conductivity is the reciprocal resistivity:

$$\gamma = \frac{1}{\rho} = [\Omega \cdot \text{cm}]^{-1} \quad \textbf{(VIII)}$$

Figure 40 illustrates the J-V curves of five individual NWs with diameters between 75 nm and 120 nm measured at room-temperature. The linear behaviour of the curve indicates ohmic contacts between Al-electrodes and NW, which could be expected due to the fact that Ga should act as p-dopant and metal contacts with p-type Ge should show ohmic behaviour independent from the metals work function.[277] Regarding the slope of the curves, a specific resistivity including of ~$1.2 \cdot 10^{-4}$ Ωcm can be calculated. The resistivity and corresponding concentration of Ga incorporated (~10^{21} cm^{-3}) fit very well to the fitted values of the resistivity/impurity-concentration curves reported by Cuttriss.[278] However, due to the fact that the resistivity had been determined via 2-point measurement technique and the NW resistivity is very low a slight uncertainty concerning contact resistance must be assumed.

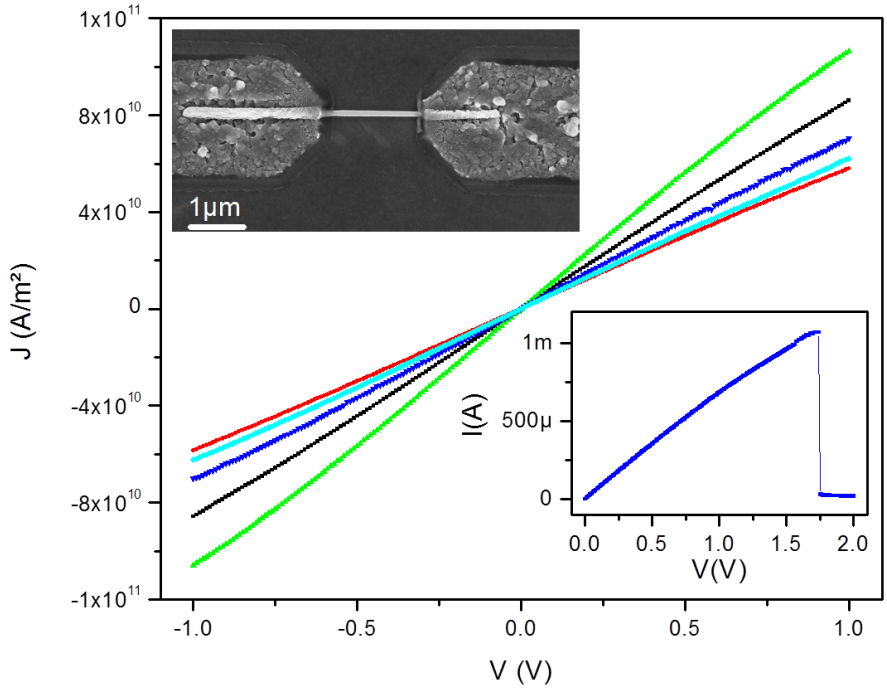

Figure 40: Single-wire electrical characterisation results of Ge NWs grown from Ga seeds via VLS mechanism.

The measured specific resistivity is up to five orders of magnitude lower than the value reported gold-seeded NWs ($1.4 \cdot 10^{-2}$ -30 Ωcm[279-282]). The broad distribution of reported resistivity's can be explained by the different growth methods and temperatures which were applied and led to incorporation of different gold concentrations. Compared to Ga-seeded NWs, the reported gold-seeded NWs have much lower amounts of seed material incorporated, but are not completely gold-free as the specific resistivity of pure germanium is slightly higher (60 Ωcm)[283] . Another aspect which must be considered is that the incorporation of gold does not lead to a p-doping similar to gallium and therefore to a different electrical behaviour. Gold impurities usually create deep level trap states in the inner region of the bandgap.[158]

Electrical measurements of Ge NWs grown via electrodeposition from Ga seeds on n-type Ge substrates did not show a similar ohmic behaviour. The reported I-V curves showed attributes of a Schot-

tky-junction, therefore a rectifying character. This aspect can be related to the applied measurement. The nanostructures had been contacted via a Pt/Ir atomic force microscopy probe directly on the n-doped growth substrate. Measurements of fractured NWs as well as of the substrate revealed that the contribution of the NW to the overall resistance was negligible compared to the p-type-NW/n-type substrate interfacial-resistance.

The electrical characterisation of Ge NWs doped with Ga via FIB revealed a decrease in resistivity of three orders of magnitude compared to pristine NWs.[26] Regarding the comparative lower amount of incorporated Ga ($2 \cdot 10^{18} cm^{-1}$), the reported resistivity ($\sim 10^{-2}$ Ωcm) is well above values obtained for Ga-seeded NWs. Attempts to incorporate higher amounts of Ga into the NWs, led to an increase of the resistivity, which disagrees with the observed results. However, this aspect can be related to the increased amount of defects and starting amorphisation of the NWs due to beam damage.

Four-point-probe measurements of Ge microwires grown from InGa alloys via electrodeposition showed specific resistivity's (1.5 Ωcm) in the range of gold-seeded NW.[186] As no In was found in the NWs via EDS analysis, the decrease in resistivity was completely related to incorporated Ga. However, regarding the equilibrium concentration of Ga in Ge at the applied growth temperatures, (<0.1 %) the measured resistivity seems significantly too high.

For Ge NWs grown from pure In particles also grown via electrodeposition in contrast, a significant lower resistivity($4 \cdot 10^{-5}$ Ωcm) was reported, whereas In concentration in the NW was as low as 0.14 %.[284] However, the reported resistivity was calculated from the determination of the carrier density via the Moss-Burstein shift. This method requires the determination of the bandgap via an absorption measurement and has therefore a larger inaccuracy, when being compared with a direct electrical characterisation.

The measured resistivity of Ga-seeded NWs grown via VLS show a significant higher value when being compared with metal NWs such as aluminium ($3 \cdot 10^{-5}$ Ωcm)[285] or silver ($1.3 \cdot 10^{-5}$ Ωcm)[286] as well as Ge-alloy NWs like Cu_3Ge ($3.4 \cdot 10^{-5}$ Ωcm)[287], which was expected as these materials also lower bulk resistivity's[288, 289].

Regarding the resistivity, the obtained Ga-seeded NWs can be denoted as degenerately p-doped semiconductor. However, the term "doping" is not fully appropriate for the material, as doping describes the incorporation of trace amounts of impurities into a material. The term "trace amounts" is defined by IUPAC as concentrations less than 100 ppm.[290] Therefore, the material should be rather denoted as a solid solution or Ga-Ge alloy than Ga-doped germanium. Usually Ge with high Ga concentrations is produced via thermal diffusion from solid sources in sealed ampoules[291] or via ion implantation[27]. Also the production via thermal diffusion using spin-on dopants had been reported.[292] Low resistivity of these materials can be attributed to the high amount of Ga incorporated into the NW, which leads to the introduction of acceptor states into the valence band. As a result, the amount of free charge carriers

(holes) is drastically increased. Regarding the amount of Ga determined via STEM EDX a “dopant” concentration of ~$1 \cdot 10^{21}$ atoms/cm^3 can be calculated for the obtained NW, which is two orders of magnitude higher than usually reported Ga-dopings in degenerative semiconductors.[292] Another idea of the high conductivity of the material is given by the I-V curve in the inset of Figure 40. The graph shows the increase of current when increasing the applied bias voltage until device failure occurs due to excess joule heating. Regarding the NW diameter was 120 nm a peak current density of 9.4 MA/cm^2 can be calculated. Compared to a former investigations of gold-seeded Ge NWs[293] with similar dimensions, this value is ~33-times higher which emphasizes the high conductivity of the Ga-seeded NWs.

5.3. Defect Transfer from Silver Seeds to Germanium Nanowires

5.3.1. Silver Bipyramid Synthesis

Silver bipyramids appear to be ideal growth promoters for VSS growth of bicrystalline Ge NWs. During growth, the single twin plane could be theoretically transferred to the emerging nanostructure, which would result in the formation of NWs intersected by one twin plane. As the synthesis of this Ag structure via the polyol method is very sensitive to trace impurities as well as growth conditions[294], it was necessary to adapt the synthesis described by Wiley *et al.*.[127]

Attempts to replicate the synthesis method published by Wiley *et al.*[127] did not lead to the desired Ag bipyramids. As the precursor solutions were continuously added to the preheated glycol, the reaction solution became almost instantly strong yellow-coloured, followed by a fast change to turbid, beige-grey during a time period of 10-15 minutes. The described colour-fade due to oxidative etching during the first minutes could not be observed in the conducted experiments. The fast colour evolution indicated the formation of Ag nuclei which grew subsequently without shape-control. SEM micrographs of the isolated products (depicted in Figure 41) revealed a mixture of Ag nanoparticles with different shapes as well as the presence of a high fraction of NWs, which proved the suspected absence of reaction control using oxidative etching.

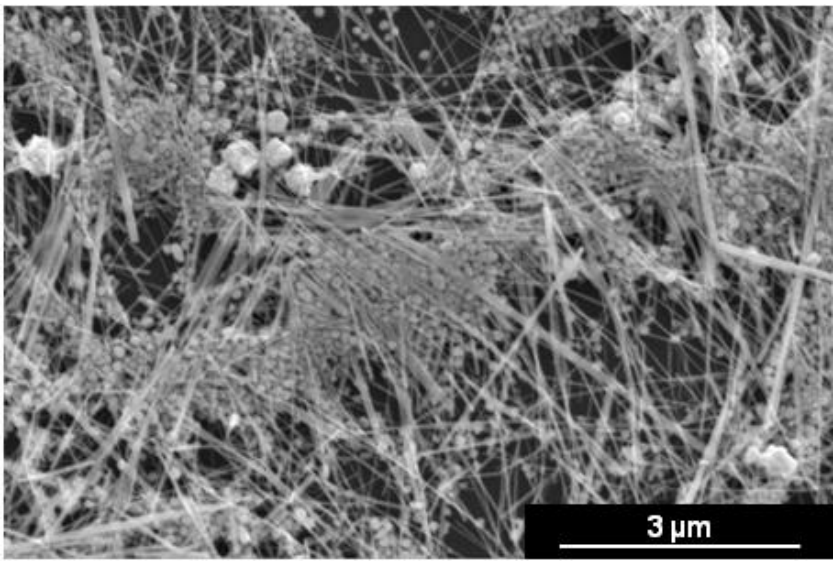

Figure 41: Representative SEM micrograph of a product obtained from a growth reaction according to Wiley *et al.*[127], with insufficient oxidative etching.

In further experiments variations of the amount of $AgNO_3$ as well as the increase of the NaBr content were conducted to induce etching rates high enough to facilitate shape control. Additionally, PVP with higher M_w had been used to enhance the capping of emerging Ag seeds, which should decrease the growth rate. Even the obtained glycol was additionally purified via three-fold distillation. Nevertheless, the fast colour-change of the reaction solution due to insufficient oxidative etching remained the

same. Only in cases of very low Ag precursor concentrations and the additionally purified EG, a delayed blurring of the reaction solution was observed after 50 minutes reaction time.

Regarding these results, the synthesis process was further modified towards an improved oxidative etching. Therefore, the oxygen concentration of the reaction solution should be enhanced by bubbling O_2 (10 sccm) through the solution. This technique had been reported for the synthesis of single crystalline Ag nanocubes via the oxidative etching-assisted polyol method.[130] Usually, Ag nanocubes are synthesised via the polyol process using chloride ions as etchant. Chloride ions are the stronger etchant compared to bromide, which results in an enhanced oxidative etching.[295] During the growth process, chloride ions are capable to dissolve Ag nuclei with all kinds of defects incorporated. As a result only perfect single crystalline nuclei remain, which grow in nanocubes. The addition of oxygen further enhances the etching potential. In the case of bromide, the addition of oxygen could enhance the etching behaviour to obtain single crystalline nanocubes.[130] In the case of chloride, the addition of oxygen results in a corrosion of the nanocubes corners, leading to truncated nanocubes.[128]

The modification led to a distinct change of the colour evolution during synthesis. Similar to the observations before, the reaction solution started to turn yellow during the addition of the precursors, but the colour changed to completely colourless approx. ten minutes after the injection of the precursor solutions had been completed. This behaviour could be related to the starting oxidative etching, which dissolved the emerged Ag nuclei. In contrast to observations made before, the reaction solution remained colourless still 8 hours after reaction start. As a result, no product could be isolated from the reaction solution. Regarding the absence of any nanoparticles, it had been concluded that the process of oxidative etching was enhanced too much by the increased oxygen concentration in the reaction solution. To overcome this drawback, the oxygen flow rate was stepwise decreased until the lower limit of the mass flow controller (0.8 sccm) was reached. At this point, still no formation of nanoparticles occurred.

The oxygen saturation of the growth solution must be further decreased, which was facilitated by replacing pure oxygen by compressed air, dried through a drying unit containing P_2O_5.

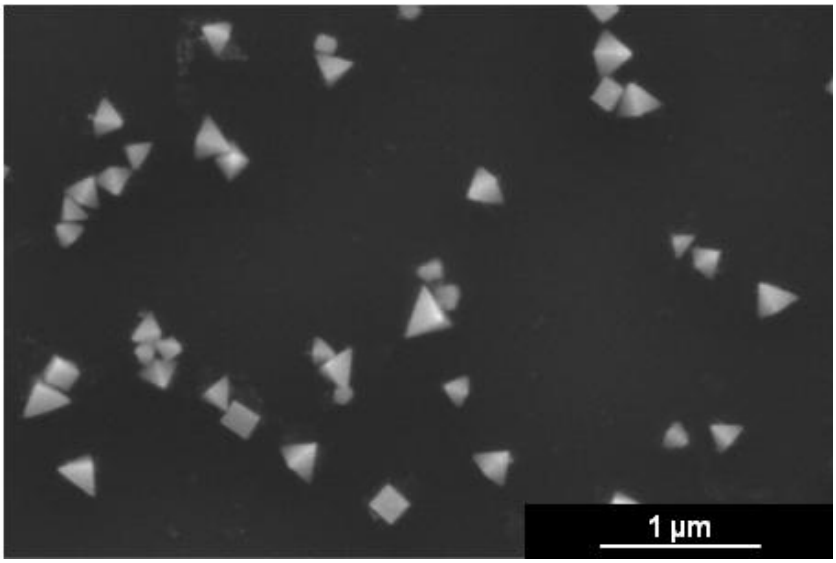

Figure 42: SEM micrograph of the obtained Ag bipyramids, using a gas flow of 2 sccm dry air bubbled through the reaction solution.

With this modification, the desired Ag bipyramids could be obtained at an air flow rate of 2 sccm. At this flow rate, the oxidative etching potential appeared sufficiently low to dissolve only multiple twinned Ag seeds, whereas single twinned and single crystalline seeds remained unaffected. As a result, the product contained mainly bipyramids with a slight contamination of nanocubes. A SEM micrograph of the obtained bipyramids is illustrated in Figure 42. An increase of the flow rate to ~4 sccm yielded in the formation of exclusively nanocubes similar to the results reported by Taguchi *et al*..[130] A representative SEM micrograph of the obtained nanocubes is depicted in Figure 43.

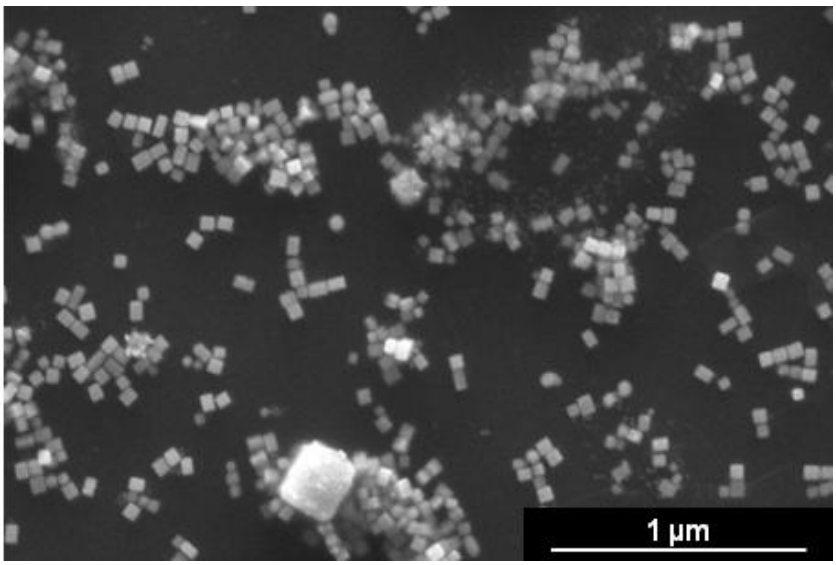

Figure 43: SEM micrograph of obtained Ag nanocubes, formed by bubbling 4 sccm of dry air through the reaction solution.

A decrease in flow rate below 2 sccm led to bipyramid formation, which were contaminated with nanorods and NWs. A successful synthesis could be already recognised by the colour evolution of the

growth solution. The injection of the precursor solutions led to a slight yellow colour of the solution, which reached its maximum in intensity approx. 5 minutes after finished injection. Subsequently, the colour started to fade until a colourless slightly turbid reaction solution was reached after ~25 minutes. This colour remained constant for the next 2 hours, just the turbidity slightly increased. Synthesis with one hour growth duration led to the formation of Ag bipyramids with approx. 180 nm diameters. As this particle size was too large for an efficient NW growth, smaller bipyramids were required. A decrease of the growth duration to 40 minutes led to the formation of smaller bipyramids (~80-120 nm). However these seed diameters appeared to be still on the upper limit to obtain straight NWs. A further reduction of the growth duration did no longer lead to the desired bipyramids. The product isolated from reaction solutions after 30 or 20 minutes reaction time showed almost spherical shaped particles.

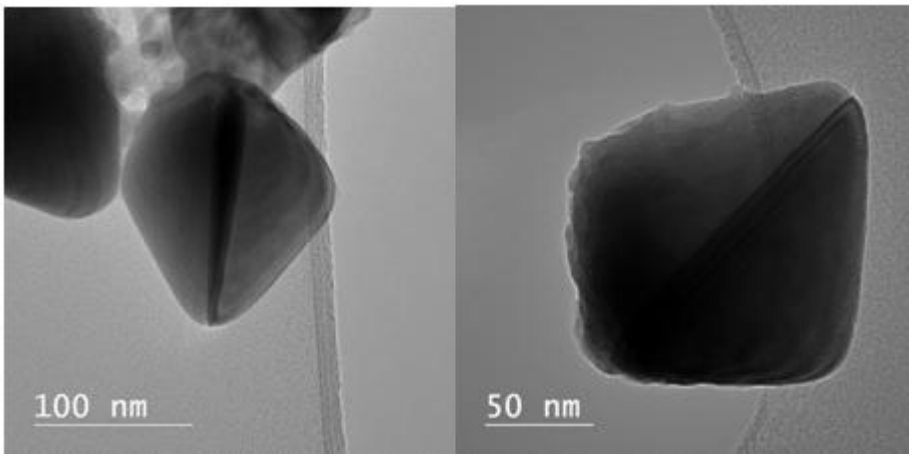

Figure 44: TEM micrograph of Ag bipyramids.

TEM investigation of the obtained product (Figure 44) exhibited bipyramids <120 nm in diameter. The twin plane is clearly visible at the mirror plane intersecting the pyramid halves. The surface of the particles still showed contamination derived from PVP, even after ten purification cycles.

Figure 45 summarises the findings of the conducted Ag nanoparticle syntheses. Besides the optimisation of process parameters, such as air-flow and bromide concentration further aspects were mandatory to facilitate a successful and reproducible bipyramid-growth. The used EG must be as pure as possible. Even new purchased reagent grade (>99 %) EG should be distilled two times. Additionally, the contamination of the growth solution with ions such as iron must be strictly avoided (injection via plastic tubes instead of syringe needles, intact PTFE coatings of stir bars, etc.) It showed to be mandatory to heat the EG to 160 °C for at least one hour before precursor injection. Wiley *et al.* attributed this fact to the removal of trace amounts of water.[127] However, regarding the fact that the mainly reductive species is glycol aldehyde, which is formed due to thermal activated oxidation from EG[296], it can be concluded that the pre-heating is also required to produce enough of this species. The temperature of the reaction solution must be also maintained precisely, as oxidation and reduction kinetics appeared to be highly temperature sensitive. Rycenga *et al*. for instance, reported that already a 5 °C tempera-

ture deviation of the growth solution led instantly to a change in the products morphology.[121] Therefore, a large silicone oil bath was used for heating the growth solution, which provided a large thermal reservoir to smooth temperature fluctuations especially during the injection of the precursor solutions. The air, which was bubbled through the reaction solution to increase the oxygen saturation, had to be moisture-free and exactly dosed. Therefore, the obtained compressed air was dried using a P_2O_5 tower before being dosed via a mass flow controller. Deviations of 0.2 sccm led already to totally different product morphologies, i.e. the contamination with NWs in the case of a lower flow rate and the presence of a higher number of cubes in the case of a too high flow rate. The injection of the precursors had to be maintained in a controlled reproducible way with an injection rate of 45 mL/h. Therefore, the injection was carried out using a modified syringe pump. Finally, purification of the obtained nanoparticles required up to 10 centrifugation and redispersion steps, as excess PVP polymer tended to agglomerate to the Ag nanostructures. Wiley *et al.* insinuated difficulties during particle purification, as TEM sample preparation required an additional, extensive washing step using a gravity-feed flow cell after drop-casting the particle solution onto the TEM grid.[127]

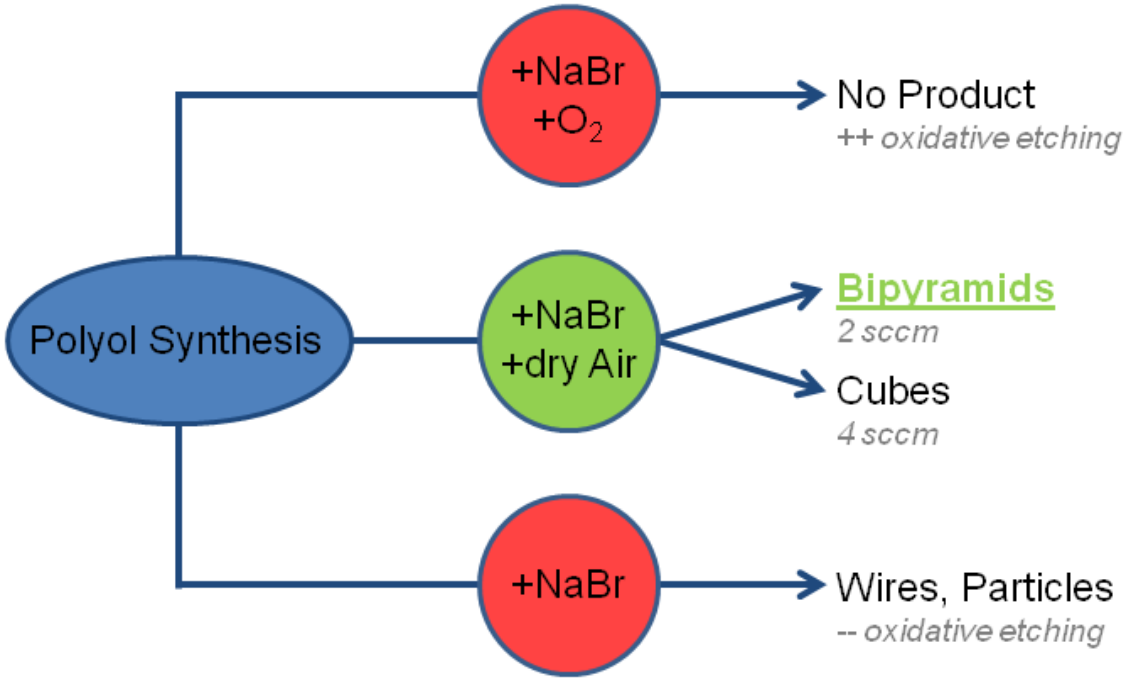

Figure 45: Growth conditions related to the obtained nanostructures for the synthesis of Ag nanostructures via the polyol method.

5.3.2. Germanium Nanowire Growth using Solid Silver Seeds

As shown in Figure 46, the binary phase diagram of silver and germanium exhibits an eutectic point at 651 °C with 75.5 % Ag.[197] The ability to grow Ge NWs via solid Ag seeds is maintained by the pocket at the silver rich site, which implies a solubility of Ge in the silver crystal. To ensure solid-seeding as well as stability of the seeds crystal structure, the growth temperature must be maintained significantly below the eutectic temperature.

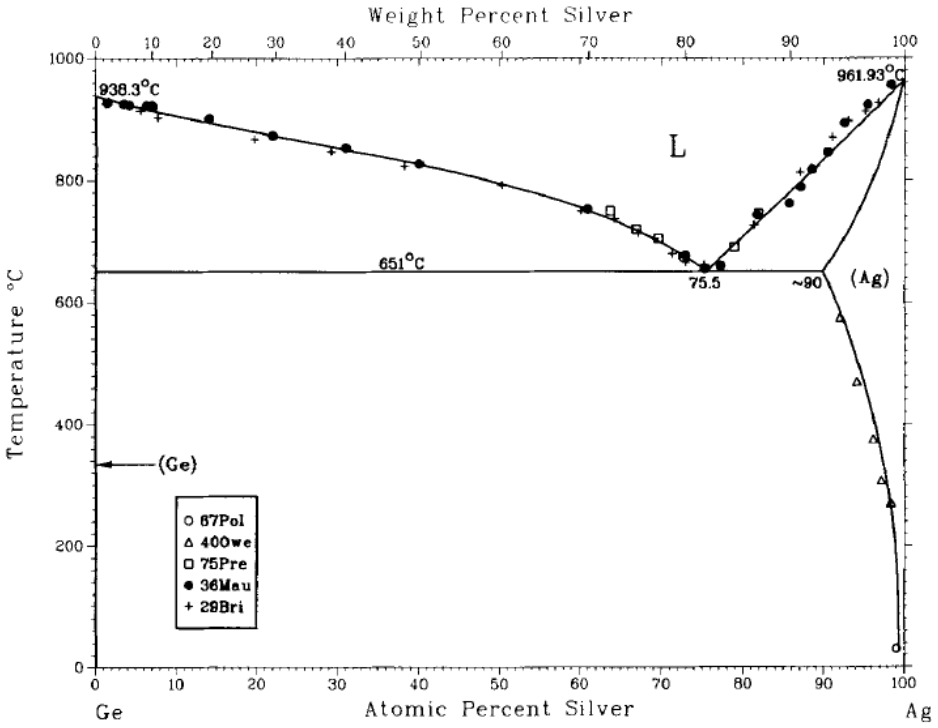

Figure 46: Ag-Ge binary phase diagram. Reprinted with permission.[197]

5.3.2.1. Cold-Wall Chemical Vapour Deposition

Several attempts were made to grow Ge NWs from biscyclopentadienyl germanium(II) ($GeCp_2$) in a cold-wall CVD setup. Germanocenes are reported to be Ge sources feasible for thin film growth[297] as well as for NWs.[166] The decomposition of $GeCp_2$ had been investigated by Mathur *et al.*.[166] Mass spectrometry indicated that thermolysis induces the breakdown of the Ge-cyclopentadienyl bond, which leads to pure Ge and organic by-products. $GeCp_2$ already decomposes sufficiently at 325 °C to obtain NWs. However, the high carbon loading of these molecules can lead to deposits with a higher carbon contamination compared to germanes.

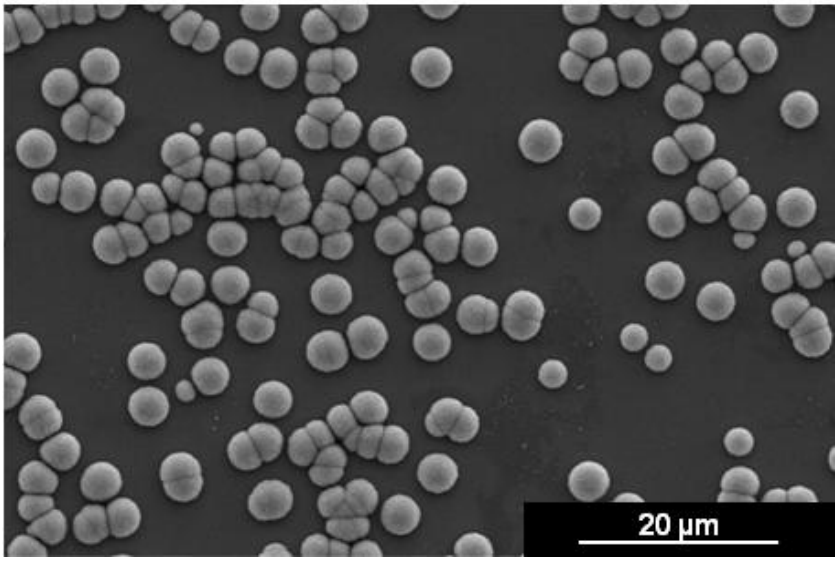

Figure 47: SEM micrograph of the deposit grown from $GeCp_2$ grown at 450 °C

Growth experiments were conducted at substrate temperatures between 350 °C and 500 °C with ~20 mg Ge precursor at pressures $<10^{-3}$ mbar). Due to the high vapour pressure of $GeCp_2$ the precursor was cooled using an ice/water bath. After approx. ten minutes a greyish/brown deposit became visible on the substrate surface. SEM investigation of the obtained substrates showed spherical aggregates with diameters between 500 nm and 5 µm, grown at the areas where Ag particles were drop-casted and some NWs, also contaminated with secondary deposit. However, the majority of substrates exhibited spherical aggregates and no NWs visible.

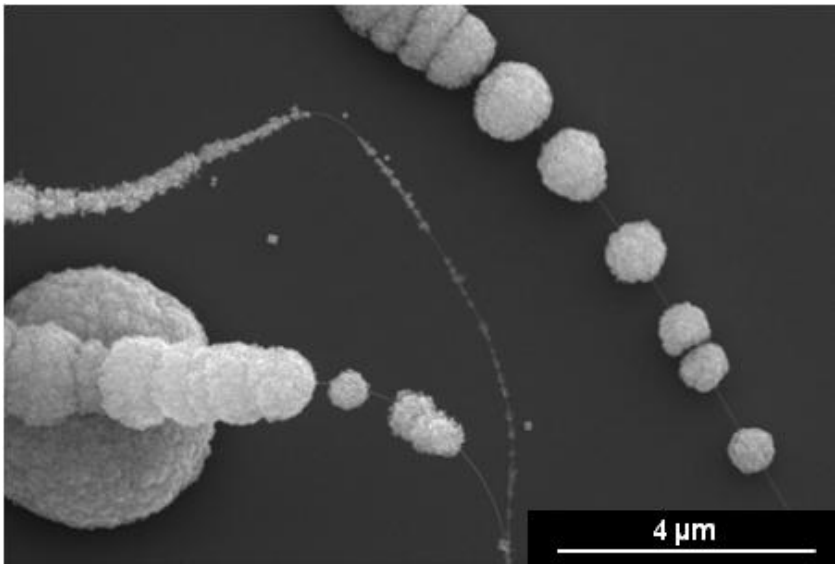

Figure 48: SEM micrograph of Ge NWs derived from GeCp2 decomposition.

XRD analysis of the obtained deposit (depicted in Figure 49) identified its amorphous nature. The morphology of the deposit was reproducible over the whole temperature range (350-500 °C). Even the reduction of precursor flow by an intensified cooling of the precursor flask to -10 °C did not alter the morphology towards NWs. The morphology of the obtained deposit appeared similar to a deposit of

amorphous Ge reported for an electroless deposition method using Ag nanoparticles and GeI_2.[298] In the reported method act silver nanoparticles as sacrificial templates, which are oxidised and dissolved, whereas Ge-ions are reduced and grow as an amorphous phase around the Ag nanoparticles. The formation of an amorphous phase was attributed to the low reaction temperature (200 °C), as an increase of growth temperature to 350 °C showed already the formation of crystalline germanium. Nevertheless, a similar formation mechanism is rather unlikely. The electroless depositon reaction requires the formation of AgI, which can be certainly excluded for the CVD process. Another aspect which becomes noticeable is that growth temperatures in the conducted CVD experiments were significantly higher than the temperatures where Nolan *et al.* observed the formation of crystalline Ge. Nevertheless, CVD still resulted in the formation of an amorphous deposit. Therefore, an additional effect must have supported the crystallisation during electroless deposition at 350 °C, which could be a template effect induced by emerging cubic AgI, which is the stable structure at this temperature.[299]

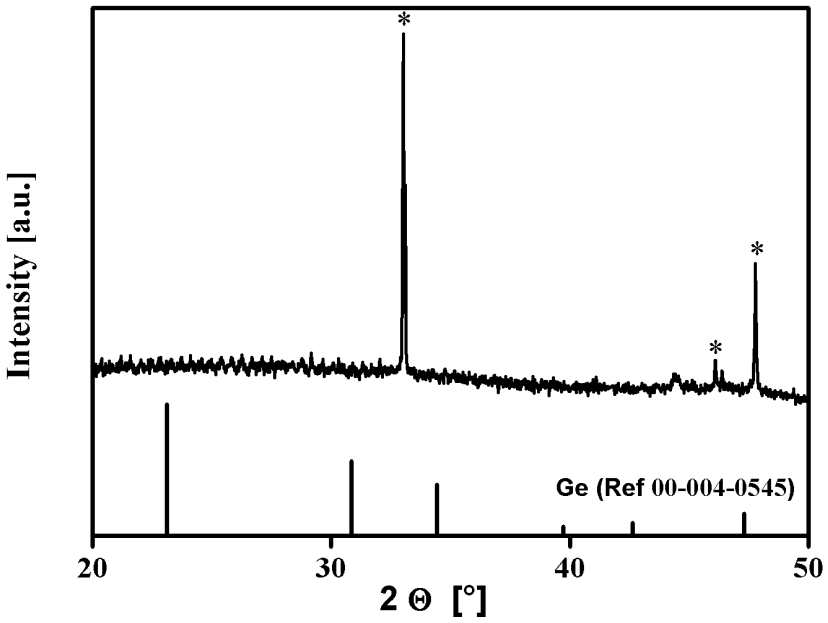

Figure 49: XRD pattern of the obtained deposit. Reflexes marked with * derive from the Si substrate.

Another aspect which should be discussed is the influence of the surface passivation of the silver bipyramids on the crystallisation of Ge during NW growth. Growth strategies which do not use a substrate for NW growth are less demanding regarding the NW nucleation. As long as Ge atoms which derive from the decomposed precursor can reach the growth promoter, a subsequent incorporation into the NW lattice and therefore NW growth should be possible. The defect transfer in contrast requires additionally a clean interface between seed and substrate. Otherwise, adatoms would not be capable to attach heteroepitactically at the interface. PVP which was used to stabilise the Ag bipyramids, could have hindered emerging Ge atoms to reach the growth seeds. As a result, the crystallisation as well as NW growth was inhibited, which would explain the formation of an amorphous deposit. Unfortunately, PVP is necessary during the synthesis, as it selectively stabilises the required <100> facet and

therefore enables bipyramid formation. Therefore, it could not be replaced by a capping agent which is easier to remove or less shielding. Due to its sterically demanding, polymeric nature, including multiple binding sites per molecule, an efficient removal or replacement is also difficult.

Besides $GeCp_2$, growth experiments had been also conducted using diphenyl germane as Ge source. The change in precursor required also an adjustment of some process parameters. Whereby growth temperatures retained unchanged, the precursor concentration in the vapour phase must be increased, as attempts conducted at a dynamic vacuum ($<10^{-3}$ mbar) resulted in no deposit formation. An increase of the precursor temperature to 40 °C resulted in a fast evaporation of the precursor, whereas the expected thin film formation due to the fast and tremendous increase in precursor concentration did not occur. To overcome this drawback, growth had been conducted under static vacuum conditions. Therefore, the growth chamber as well as the precursor flask was evacuated to10^{-3} mbar base pressure. Next, the valves to vacuum pump as well as to the precursor flask were closed and the apparatus was heated to 50-80 °C. During the time the system required to reach the desired temperature the substrate was heated to growth temperature. When all components reached their desired temperatures, the valve to the precursor flask was carefully opened. As a result, a slow increase of the pressure towards 10^{-1} mbar could be observed. The increase in pressure could be attributed to the evaporated precursor as well as to minor leaks in the system. To terminate the growth process, the precursor valve was closed and the system was fully evacuated. To ensure the complete removal of DPG from the reaction chamber, the system remained for 15 minutes under dynamic vacuum, before the substrate was cooled to room temperature.

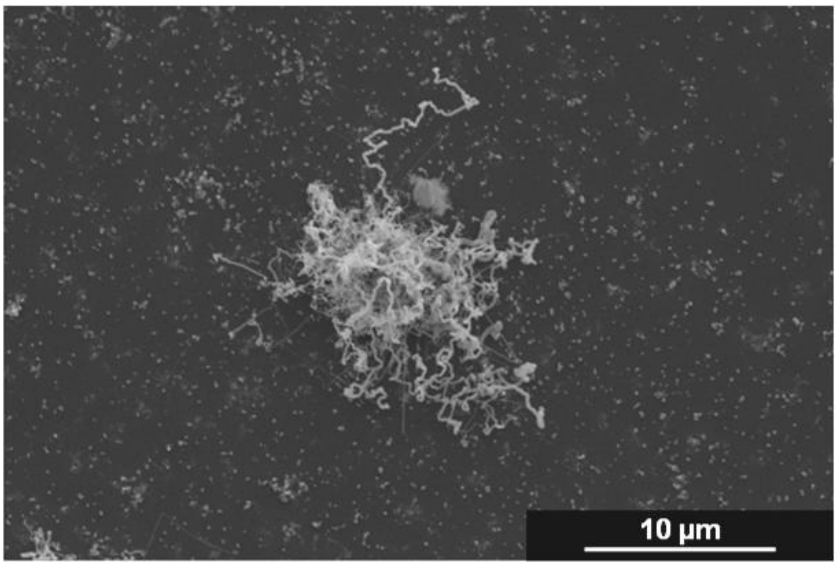

Figure 50: SEM micrograph of a spot where Ge NWs grew from Ag bipyramids in cold-wall CVD under static vacuum at 500 °C for 10 minutes.

Using the optimised growth procedure, a small number of Ge NWs could be obtained and the formation of an amorphous deposit was no longer observed. However, the majority of silver seeds remained

inactive. NW growth did only occur at a small number of individual areas, especially where evaporation marks due to the drop-casting process remained. A SEM micrograph of such an area where NW growth occurred surrounded by a large number of inactive silver seeds is depicted in Figure 50. Similar to the results obtained from the cold-wall CVD using $GeCp_2$, the PVP polymer seemed to inhibit the NW nucleation. Only on spots where less PVP remained, NW nucleation could occur.

To improve NW nucleation it seemed mandatory to remove remaining PVP from the bipyramids and substrate. As the dissolution of PVP in solvents such as water or ethanol is a rather time consuming process and limited to the boiling points of the solvents, a cleaning step at elevated pressure using supercritical toluene was implemented. Therefore, a bipyramid-coated substrate was placed into a high pressure cell together with 4 mL toluene. The reaction vessel was tightly sealed and placed into a tube furnace where it was heated to 400 °C. When the temperature was reached, the supercritical toluene was purged via a valve. Remaining toluene was removed by blowing nitrogen through the reaction vessel. Subsequently, the valves were closed and the cell was allowed to cool to room temperature. The substrate was then removed and mounted on the susceptor for NW growth in the CVD chamber. A significant difference in NW density could be observed, if a substrate decorated with crude bipyramids and a substrate with bipyramids cleaned in supercritical toluene were compared. As depicted in Figure 51, growth substrates which were treated with supercritical toluene showed dense NW growth, whereas untreated substrates showed a rather low NW density.

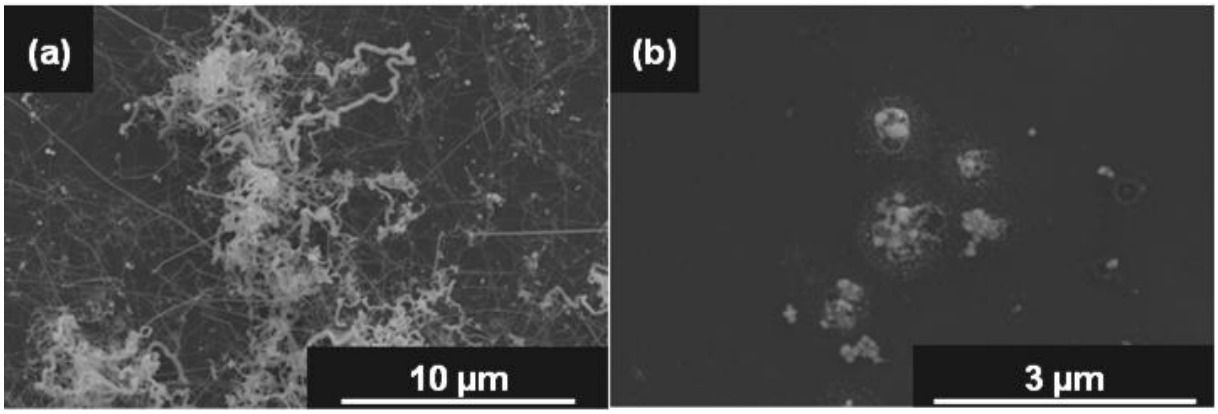

Figure 51: SEM micrographs of Ge NWs grown at 470 °C on a SCF treated (a) and an untreated (b) substrate.

The significant difference in NW density between a SCF-treated and a pristine growth substrate proofed the negative influence of remaining PVP on the NW. Despite to the fact that PVP is almost insoluble in toluene at room temperature, a significant solubility can be expected above the critical point.[300] When the supercritical toluene was drained from the high pressure cell it took dissolved PVP along. The majority of bipyramids remained on the substrate as they are larger and are therefore not so easy to be washed-away. SEM micrographs depicted in Figure 51 illustrate the influence of the SCF

cleaning step. Both samples derived from the same growth experiment at 470 °C, thus sample (a) had been treated with supercritical toluene before. On the substrate with SCF-treated bipyramids, a high number of NWs is visible, whereas on the substrate with untreated bipyramids (b), no NW growth occurred. The experiment confirmed the assumption that the capping polymer significantly inhibited the NW nucleation.

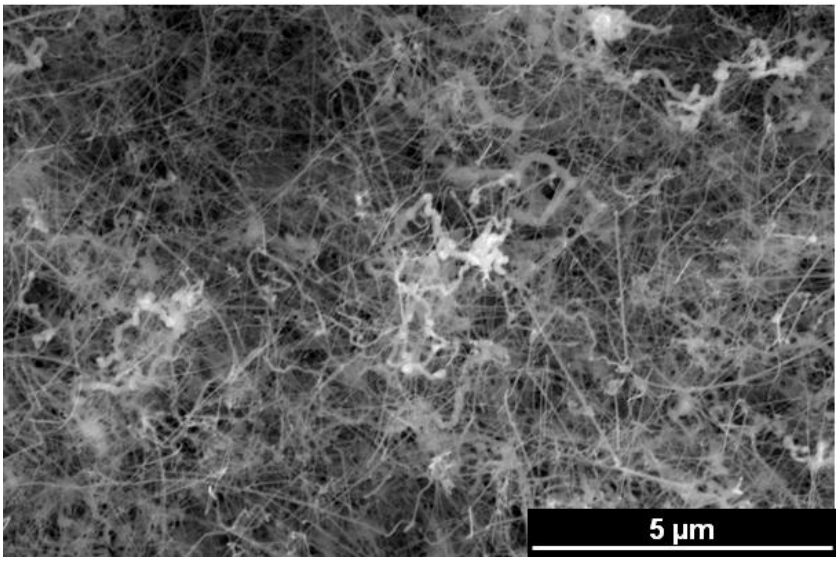

Figure 52: Ge NWs grown via cold-wall CVD at 470 °C.

Further SEM investigation of the obtained Ge NWs revealed a broader diameter distribution than expected from silver bipyramid samples. The observable morphology depended on NW diameter and growth temperature. The fraction of thinner NWs(~20 nm), which derived from irregular shaped seeds, was almost always straight and showed no kinking over the entire investigated temperature range (350-500 °C). Medium thick NWs (40-100 nm) which were suspected to derive from smaller bipyramids, revealed curved growth and a higher number of kinks at lower temperatures. An increase in growth temperature reduced this morphology significantly. NWs with diameters above 120 nm showed always kinking and torturous growth, also at growth temperatures as high as 500 °C. Kinking is a frequently observed phenomenon reported for Ge NWs grown from solid seeds such as Ni[199, 301, 302] or Cu[303] as well as for Si NWs[90, 95]. NW kinking at growth via solid seeds can be explained by various effects. First, different diffusion velocities of Ge atoms within the seed and near the surface cause different deposition rates along the growth interface. The inhomogenous mass flow through the seed leads to spontaneous plastic deformation of the NW. Such a mechanism had been observed for carbon nanotubes by Amelinckx *et al.*[304] but was also proposed for Si NWs by Arbiol *et al.*.[90] The findings reported by Arbiol *et al.* (kinking occurs predominantly at NWs with longer diameter and at lower growth temperatures) agree very well with the observed behaviour. A second explanation for kinking was proposed by Tuan *et al.*, who suggested that the polycrystallinity in NW seeds could cause tortuous growth.[305] Nevertheless, this explanation is rather unlikely for Ge NWs grown from silver bipyramids, as these particles exhibit bicrystalline morphology rather than polycrystallinity. A

third explanation had been reported by Thombare *et al.*[302] They attributed the distinct kinking behaviour to the preferential <111> growth direction and the low energy, required for the introduction of <111> stacking faults and twin boundaries. The formation of a twin leads to a new direction with a different (111) growth facet. As the twin plane propagates, the NW can re-twin facing another (111) growth facet and changing the growth direction again. This process occurs multiple times on several sets of <111> planes resulting in torturous growth and kinking. Regarding Ge NWs grown from silver seeds, a similar explanation is definitely possible, due to the fact that these NWs grow most likely in <111> direction.

Besides NWs with diameters matching to the size of the bipyramids, a high number of NWs with smaller diameters could be observed. However, Ag bipyramid samples did not show any contamination with smaller nanoparticles. Therefore, the small Ag seeds were supposed to emerge during heating to the NW growth temperature from remaining Ag-ions which coordinate to PVP. During nanoparticle synthesis, small amounts of Ag-ions are not reduced and remain bonded to lone pairs of the carboxyl-groups and nitrogen atom in the pyrrolidone rings.[306] Potential coordination sites are illustrated in Figure 53.

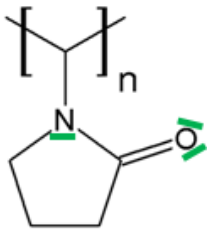

Figure 53: Chemical structure of the PVP repeating unit. Lone pairs for a potential coordination to Ag-ions coloured in green.

During purification, only free or weakly bound polymer can be removed, whereas partially bound PVP molecules with Ag-ions coordinated to free pyrrolidone rings remain in the product. During heating to NW growth temperature the remaining Ag-ions could be reduced by PVP,[307] to form small nanoparticles, which could then off-course act also as NW growth promoter. Certainly, the nanoparticles which emerged during the heating step did not show the single twinned bipyramid-shaped morphology, as their growth took place without any shape control. Therefore, these small particles were not suitable for the controlled defect transfer. Unfortunately, a removal of these nanoparticles was not possible, hence the samples showed always contamination with a high fraction of small-diameter NWs.

SEM micrographs revealed also that NWs with smaller diameters grew faster, than thicker NWs. As a result, the fraction of small diameter NWs appeared significantly larger. Higher growth rates for thinner NWs had been reported for nickel-seeded Ge NWs,[308] whereas liquid-seeded growth revealed higher growth rates for larger seed diameters.[75, 82, 309, 310] Slower growth rates for thicker NWs grown from solid seeds can be related to solid state diffusion of Ge atoms through the growth promoter. Lar-

ger seeds require longer diffusion distances, which adatoms must travel to reach the growth front. This effect is further increased, as diffusion rates are significantly lower in solid-state than in liquid phase.

TEM investigation of a single NW grown at 500 °C (depicted in Figure 54) exhibited multiple twins instead of a single twin boundary along the NW growth axis. The seed exhibited a rather hemispherical than bipyramidal shape, which was expected due to the high temperature environment during growth. The red arrow marks a single planar defect in the seed which exhibited an orientation similar to the twins in the NW. This feature highly suggested a relation between the twin planes in the NW and the planar defect in the growth seed. However, the presence of a ~100 nm segment between NW exhibiting no planar defect structure interfered with this theory. Furthermore, a layer of remaining PVP with smaller Ag particles incorporated could be observed at the growth seed. The origin of these Ag particles had been discussed on the previous page.

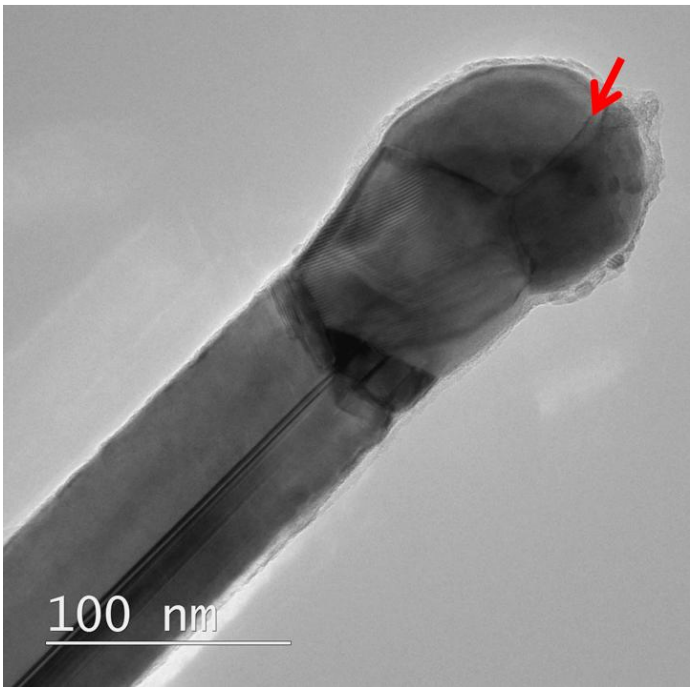

Figure 54: TEM micrograph of the tip of a Ge NW grown via cold-wall CVD at 500 °C.

5.3.2.2. Hot-Wall Chemical Vapour Deposition

Besides growth via low pressure cold wall CVD, defect transfer experiments had been conducted in a hot wall CVD setup under ambient pressure. The CVD process was carried out in stainless steel cells heated by a tube furnace, which allowed the removal of excess capping polymer using supercritical toluene before the NW growth process itself. As DPG is not volatile under ambient conditions, it was introduced as toluene solution, using a syringe pump to control the precursor feed rate. The precursor solution already evaporated in the hot tubing towards the chamber inlet and the toluene/DPG vapour had been carried through the CVD chamber with a nitrogen carrier gas flow, controlled by a mass flow controller. To avoid premature decomposition inside the inlet tube, the feed line was insulated up to ~3 cm before the chamber inlet. However, temperatures in the insulated areas were already sufficiently

high to enable the complete evaporation of toluene and DPG under ambient pressure. The chamber outlet was also connected to a high pressure tube, which ended in a water bath to capture solvent and decomposition products. Inlet as well as outlet could be manually opened and closed via needle valves located outside the tube furnace. In a typical experiment the apparatus was assembled, filled with toluene and placed into the furnace. To maintain a good reproducibility, substrates were always placed at the inlet side inside the CVD chamber. When the furnace was heated to the desired growth temperature (400-500 °C), the pressure inside the cell reached ~350 bar, which is far above the critical pressure of toluene ($p_{critical}$=41.1 bar).[233] To drain toluene and dissolved capping polymer the outlet needle valve was opened. Following this, the nitrogen flow (2-5 sccm) was established and the growth process was initiated by the controlled injection of the precursor solution.

Substrates obtained from NW growth experiments looked slightly different compared to cold-wall experiments. Usually deposits were only located on the side where Ag bipyramids were drop-coated and deposited areas exhibited similar shapes as the Ag particle coating after solvent evaporation. In minor cases, the substrates backside showed brown-coloured deposits as well, mainly located at the end, which pointed towards chamber outlet. SEM investigation of these areas exhibited particles due to secondary deposition. However, in some cases a small fraction of NWs could be also observed. These NWs were supposed to grow from particles which were washed to the substrate backside during the supercritical cleaning step.

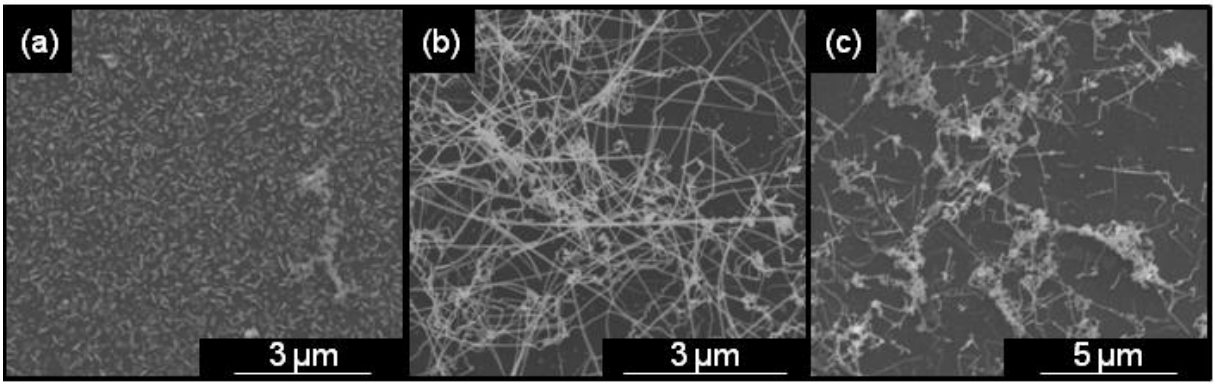

Figure 55: SEM micrographs of observed morphologies near the inlet (a), towards the centre (b) and near the outlet (c).

For lower growth temperatures (400-450 °C) and durations (<30 minutes) a colour evolution along the substrate length was visible. The deposit at the substrate area which pointed towards the chamber inlet showed a greyish colour, which changed to a brown colour along the substrate length. Longer growth durations (>30 minutes) and higher growth temperatures (>450 °C) led to homogenously looking brown-coloured deposits. SEM investigation of the distinct areas exhibited different morphologies. As depicted in Figure 55, the region near the chamber inlet (a) contained mainly particles or short nanorods. When moving towards substrate centre, the morphology of the deposit changed towards NWs (b). NWs located closer to the chamber outlet exhibited a strong contamination with particles (c)

which derive from the homogenous gas-phase reaction. The entire morphology evolution occurred over a substrate length of ~4 cm and might be the result of temperature anisotropy. In the cold-wall CVD, the substrate was mounted onto the susceptor using silver conductive ink, which ensured a good thermal conductivity between susceptor and substrate. In the hot-wall setup in contrast, the flat silicon substrate was placed into the cylindrical CVD chamber. Therefore, heat transfer was mainly maintained via the substrate edges. However, the overall thermal conductivity was rather poor compared to the cold-wall CVD setup. The temperature of incoming precursor feed flow (N_2, DPG- and toluene vapour) was much cooler than the substrate temperature, which led to a local temperature decrease of the substrate area near the inlet. As the gas flow temperature approached the growth temperature, the cooling effect diminished and NWs could grow. The applied high growth temperatures led also to precursor decomposition in the vapour phase, which could be observed as particles contaminating the NW product at substrate regions farer away from the chamber inlet.

Another aspect which should be discussed is the precursor depletion in the vapour phase with increasing distance from the chamber inlet. As the entire CVD chamber is heated in a hot-wall reactor a significant precursor amount is decomposed on reactor side walls. As a result, the vapour phase depletes steadily in precursor, when passing through the CVD chamber. Regarding the results obtained from cold-wall CVD experiments, a certain precursor concentration in the vapour phase was necessary to facilitate NW nucleation. Therefore, an inhibited NW growth at substrate areas further away from the chamber inlet was expected. However, such areas were not observed during the conducted experiments.

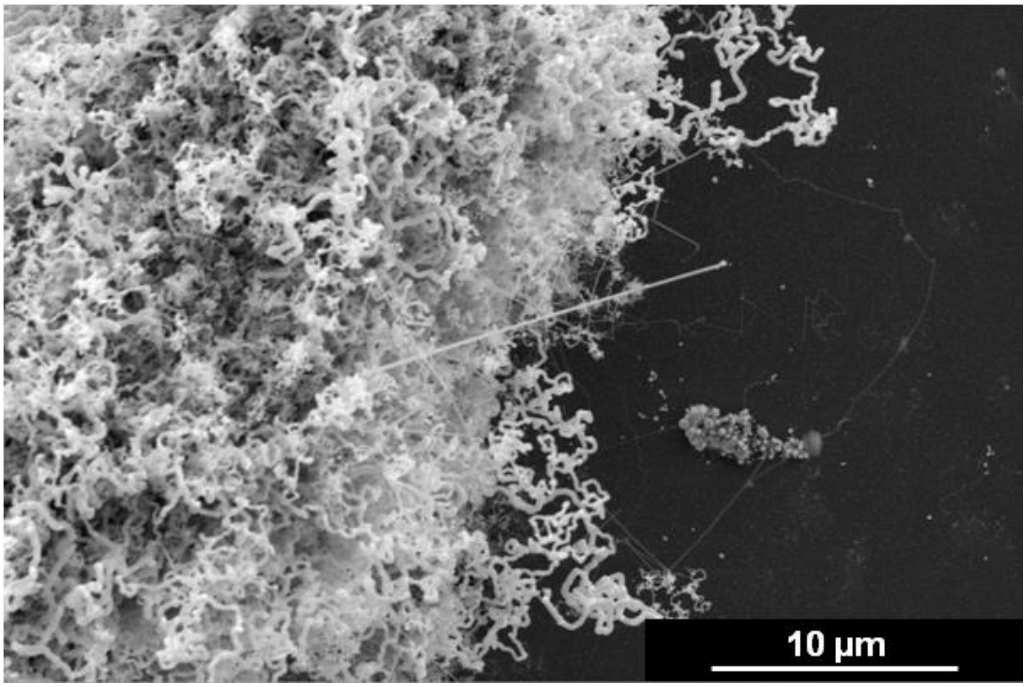

Figure 56: Representative SEM micrograph of straight and kinked Ge NWs obtained from hot-wall CVD growth.

A typical SEM micrograph of the obtained NWs is illustrated in Figure 56. Similar to the results obtained from cold-wall CVD, the obtained NWs showed a much broader diameter distribution than expected from the Ag seeds. NWs with diameters in the size of the Ag bipyramids exhibited strong kinking, whereas NWs with smaller diameters had a rather straight morphology. The formation of the small-diameter Ag seeds is discussed in chapter 5.3.2.1.

An increase of the growth temperature led to less kinking of the targeted NW fraction, however the amount of particle contamination due to secondary decomposition as well as NW tapering increased tremendously. The SEM micrograph in Figure 57 exhibits NW tapering due to secondary deposition on the side walls at higher growth temperatures (500 °C). High growth temperatures (>480 °C) led also to a change in the silver particle morphology. As a result, NW tips appeared spherically, which indicated rather a VLS than a VSS growth. Regarding the binary phase diagram, the applied maximum growth temperature (500 °C) is still 150 °C below the melting point of the Ge/Ag eutectic.[197] Therefore, classical melting of the Ag seeds and resulting VLS growth appears very unlikely, also because melting point depression due to the Gibbs Thomson effect is negligible for particles with ~100 nm diameter. However, binary phase diagrams describe only the thermodynamic behaviour of a bulk system, thus they can be only limited applied to the NW growth process. For instance, the stability of silver nanostructures is highly related to its size and morphology.[311] Gonzáles *et al.* investigated the correlation between morphology, size and stability and reported a temperature-stability chart for Ag nanoparticles with different morphologies. [311] According to his findings, the stability limit for a 30 nm bipyramid is 330 °C. Despite to the fact that the reported diameters of the stability chart are significantly below the obtained bipyramids, the proposed stability limit suggests also a limited for the utilised larger bipyramids. Regarding these findings, a destruction of the seeds crystal structure due to the applied growth temperature and a resulting transformation to spherical or irregular-shaped seeds is easily conceivable.

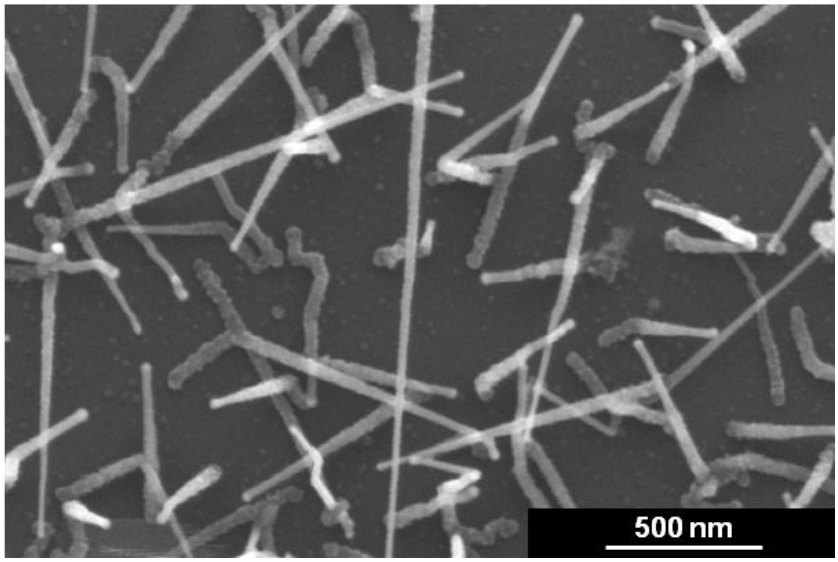

Figure 57: SEM micrograph of Ge NWs grown via hot-wall CVD at 500 °C exhibiting tapering and melted silver seeds.

Needless to say that for a controlled defect transfer the seeds crystal structure must remain stable during the entire growth process. A change in the seeds crystal structure must be prevented under all circumstances. Similar to the results of the cold-wall CVD experiments, two major aspects prevented a successful defect transfer. Low growth temperatures, which ensured the stability of the bipyramids crystal structure led to a kinked NW morphology. Higher growth temperatures in contrast, ensured the growth of straight NWs, but destroyed the seeds crystal structure. A growth temperature where only minor kinking occurred and the silver seeds remained bipyramidal could not be found for hot-wall CVD using DPG.

5.3.2.3. Nanowire Growth in Supercritical Toluene

Besides growth via CVD processes, the defect transfer was also investigated using a solvent-based method. Therefore, NW growth had been conducted in high pressure cells using supercritical toluene as solvent. Due to the closed system, the precursor concentration in the vapour phase can be varied over a much larger range than in CVD. However, the closed system suffered from two big drawbacks. Decomposition products could not be removed and remained in the system, which could affect the proceeding growth process. Second, due to the lack of an injection system, the precursor must be added during cell assembly. As a result, the growth process could not be initiated when the desired growth temperature was reached. The growth process started rather, when the reaction cell reached the decomposition temperature of DPG. Depending on the achievable heating rate and the duration from precursor decomposition onset to NW nucleation, NW growth could already occur at lower temperatures then at the targeted growth temperature. This fact becomes even more important as we observed that the growth of Ag-seeded NWs with ~100 nm diameter required significant higher temperatures to obtain kink-free morphologies.

The SEM micrograph depicted in Figure 58 shows obtained Ge NWs grown in supercritical toluene at 400 °C. Similar to the results obtained from CVD experiments, a diameter deviation between applied Ag bipyramids and obtained Ge NWs could be observed. While Ag bipyramids had diameters around 100-120 nm, the obtained NWs exhibited diameters mostly around 20-30 nm. Compared to CVD experiments, the fraction of broader NWs, matching to the bipyramid diameters appeared significantly less pronounced. This aspect had been attributed to the fact that supercritical growth experiments were conducted using crude Ag bipyramids. As a result, seeds were heavily contaminated with PVP, which included a significant amount of Ag^+ ions coordinated to pyrrolidone groups. During the growth experiments, the Ag^+ ions are reduced and form small Ag nanoparticles, which were responsible for the formation of thin Ge NWs.

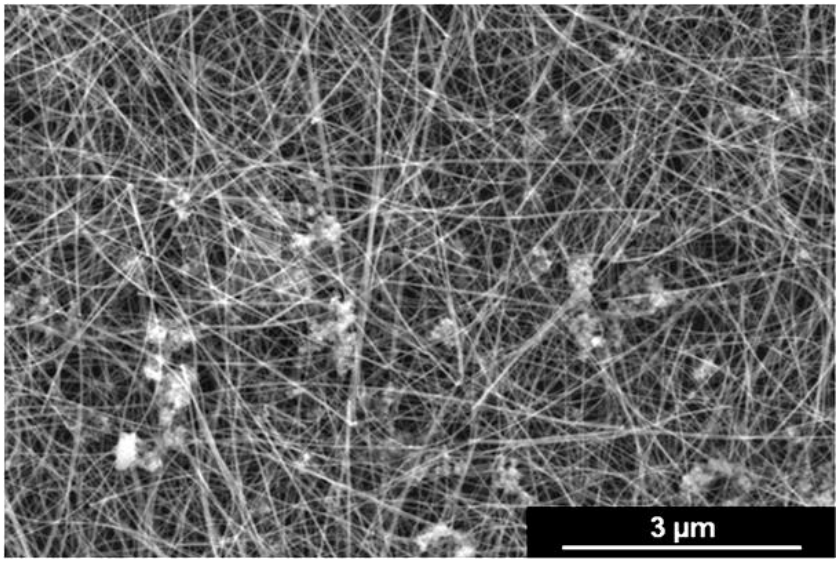

Figure 58: SEM micrograph of Ge NWs grown at 400 °C in toluene under SC conditions.

In some cases, a granular contamination of the NWs was observed, which could be easily removed by washing the extracted substrates with toluene. The contamination occurred intensified under higher growth temperatures as well as when higher DPG concentrations had been applied. The particles derived very likely from secondary decomposition of DPG in the SCF. If Ge atoms emerged too far away from a Ag seed or a suitable surface which could facilitate adsorption, they nucleated as Ge particles in the growth solution.

Figure 59 depicts a SEM micrograph of Ge NWs whose growth was terminated briefly after nucleation. The micrograph exhibits straight NWs with small diameter (~15 nm), whereas thicker NWs show heavy kinking. Similar to the results obtained from CVD experiments, kinking of thicker NWs could be slightly reduced by an increase of the growth temperature.

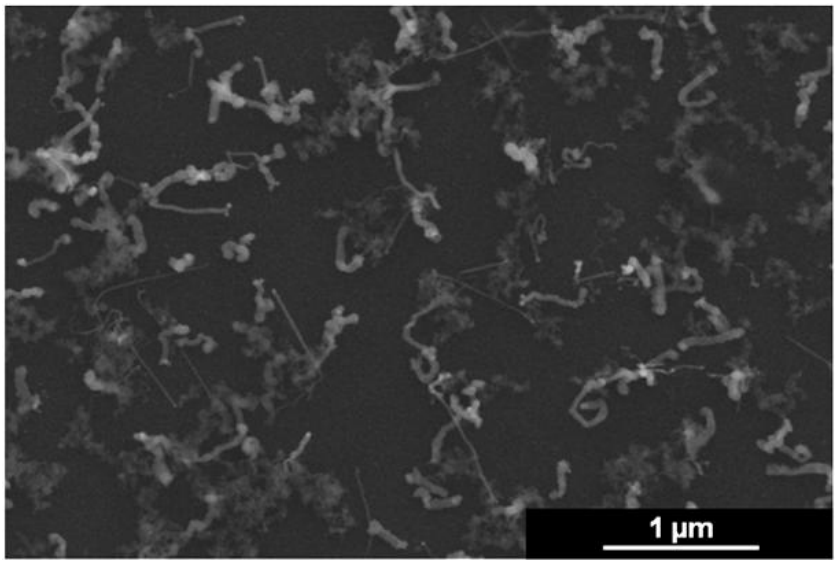

Figure 59: SEM of Ge NWs whose growth process had been terminated briefly after nucleation.

However, even at growth temperatures as high as 500 °C, thicker NWs remained significantly kinked. The SEM micrograph illustrated in Figure 60 depicts Ge NWs grown at 500 °C growth temperature. The thicker NWs which were likely seeded by Ag bipyramids exhibit multiple kinks, whereas thinner NWs showed more often a straight morphology.

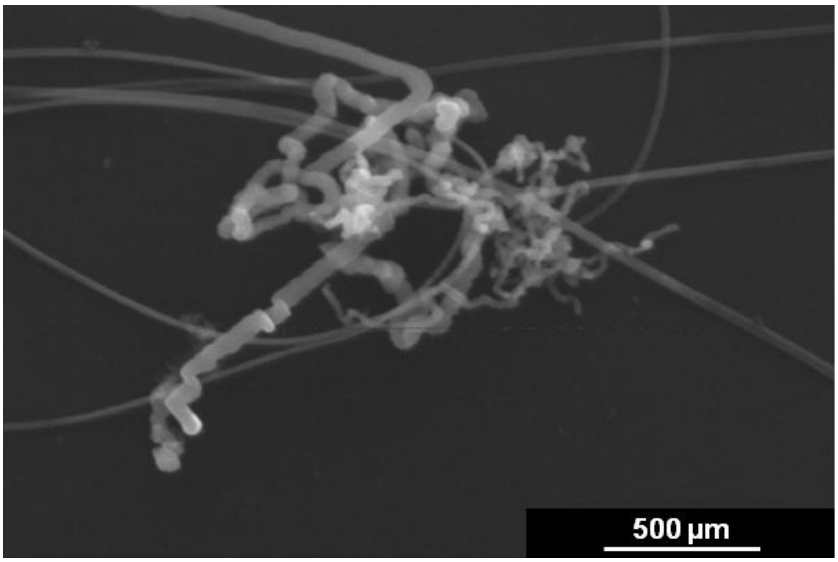

Figure 60: SEM micrograph of kinked Ge NWs obtained from growth in SCF environment.

As TEM investigation of CVD grown NWs at 500 °C revealed spherically shaped silver seeds and therefore a liquid seeded growth, a TEM investigation of NWs grown in SCF at 460 °C had been conducted. To prevent the formation of too long NWs which would have made TEM investigation difficult, growth was conducted for 25 minutes including ~18 minutes for heating to the desired temperature. In accordance to SEM investigation, TEM analysis revealed only a small number of NWs with the targeted diameter of ~100 nm. These NWs were heavily kinked and a successful defect transfer was therefore excluded. However a NW with ~25 nm diameter appeared to have a Ag bipyramid lo-

cated on its top. Figure 61 illustrates a TEM micrograph of the described NW. Despite to the low quality of the micrograph, the projection of the bipyramid can be clearly distinguished at the NW tip. Despite to the fact that SEM investigation of the applied seeds exhibited mainly bipyramids with ~80-100 nm diameter, a fraction of smaller bipyramids similar to the observed 25 nm bipyramid was quite conceivable. Also the intersecting twin plane, connecting both pyramids is slightly visible due to the darker area in the centre region. In one half of the NW lattice planes can be observed, whereas in the second half no planes are visible. This aspect could be attributed to different orientations of the NW halves, which would suggest a bicrystalline NW intersected by a longitudinal twin. Regarding these results, a successfully controlled defect transfer is conceivable. However, the TEM sample contained mainly NWs with irregular or cubic shaped tips, than bipyramid-shaped.

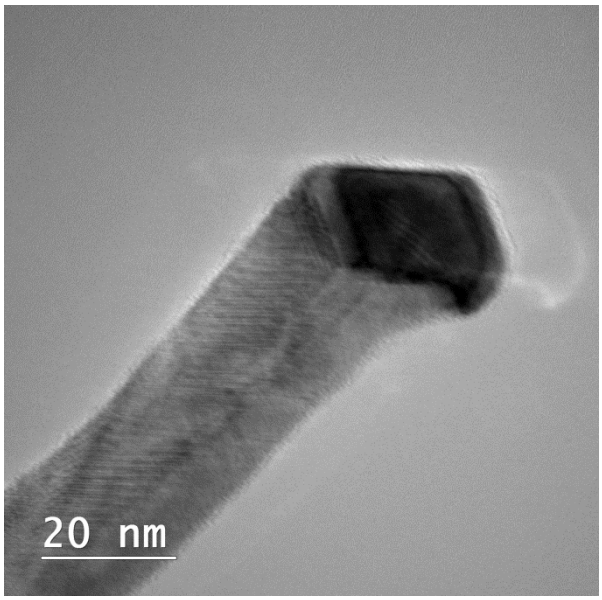

Figure 61: TEM micrograph of a Ge NW grown via SFSS mechanism at 460 °C by a supposed Ag bipyramid.

The HRTEM micrograph illustrated in Figure 62 exhibits a single crystalline silver seed on top of a Ge NW, which was found in the same sample as the NW with the bipyramid tip. The sharp corners and edges of the seed confirmed expected growth via SFSS mechanism. The insets to the right side illustrate FFT patterns of the marked regions in the micrograph. Basically, FFT pattern are a possibility to illustrate the results of a fourier analysis executed on an image. The location of the spots in the FFT pattern indicates in which orientation and distance periodicity occurs, hence it is a facile method to investigate crystal structures by TEM micrographs. The aforementioned insets show same patterns which are moreover similar oriented. Therefore, it can be concluded that the corresponding structures exhibited same crystal structure and orientation, which indicates heteroepitaxy between NW and growth promoter. Heteroepitaxy is a basic requirement for a successful defect transfer, as it ensures the proper orientation of new atomic layers during NW growth.[149]

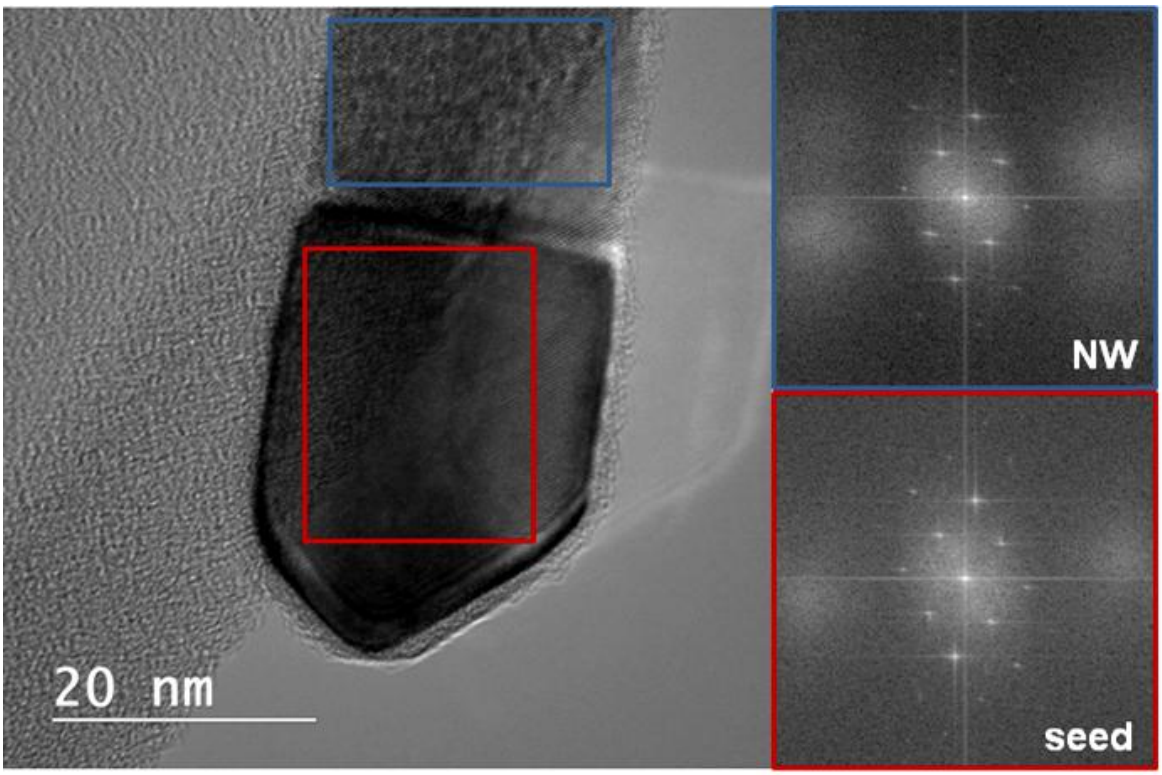

Figure 62: HRTEM micrograph and corresponding FFT patterns of a Ge NW grown from a silver seed via SFSS mechanism at 460 °C.

5.4. Summary and Outlook

Lead-supported Growth

Lead seeds showed to be a feasible growth promoter for Ge NWs. Highly crystalline NWs were obtained from growth in SC toluene via SFLS growth mechanism. Elemental maps revealed that the NWs contained exclusively Ge, whereas the seeds contained only Pb, which is in good agreement with the binary phase diagram.[214] To facilitate growth via solid Pb seeds, the growth temperature was lowered to 250 °C, which is ~80 °C below the eutectic temperature of the Ge-Pb system.[214] Ge NWs grown at 250 °C appeared kinked rather than perfectly straight, which was attributed to the low growth temperature. The NW tips appeared facetted in contrast to the nearly perfect hemispheres on the tips of the NWs grown via liquid seeds, which is a good indication for a solid-seeded growth. Besides the growth using Pb seed particles on Si substrates, NW growth could be also facilitated on Pb foil. In this case, no additional growth promoter must be applied.

As Pb exhibits a very low solubility of Ge, it might be a feasible growth promoter for NW heterostructures with abrupt interfaces. Therefore Pb seeded Ge NWs might be a feasible material for NW electronics such as diodes or transistors. Further research could be done regarding an aimed incorporation of Pb into the Ge NWs. An incorporation of 1 % would already alter the intrinsic indirect bandgap to a direct type[218, 219], which makes the material favourable for optoelectronics such as LEDs or solar cells.

Gallium-Seeding

The growth of elongated Ge nanostructures using Ga seeds exhibited a number of characteristic features, which were investigated. Ga seed growth was attempted via different synthetic routes. Reduction of $GaCl_3$ using a hot-injection method as well as the synthesis strategy using ultrasound irradiation on bulk Ga metal did not result in the formation of feasible Ga seeds. The formation of an oxide shell, during handling had been supposed to passivate the surface of the growth promoter, which inhibited the subsequent growth process. Therefore, the strategy was modified towards an *in situ* approach, utilising the thermal decomposition of GaCp*. This synthesis strategy yielded in the formation of Ga nanoparticles which enabled the subsequent metal-assisted growth. Along with *t*BG, a Ge source which already decomposes at low temperatures, the metal-assisted growth of Ge nanostructures could be demonstrated at growth temperatures as low as 170 °C. Growth experiments were conducted in toluene as well as in vapour phase, directly in the solvent or on substrates such as silicone. To obtain better insight into the growth process a growth study for a fixed Ge:Ga precursor ratio of 6:1 had been conducted. As expected, temperature-depended growth rates could be observed as well as the termination of growth due to the depletion of Ge precursor. Also a temperature dependence of the obtained nanorods could be observed. This aspect had been related to the different heating rates, which influenced the diameter distribution of the emerging Ga seeds.

TEM analysis of the obtained nanorods and wires exhibited a high crystallinity. Growth via a metal-assisted process could be demonstrated as the nanostructures were terminated with a hemispherical tip. Elemental analysis via STEM EDX mappings depicted results which could not be expected from the binary phase diagram of the Ge-Ga system. According to thermodynamic limits, less than 1 % of Ga is soluble in Ge at the applied growth temperatures. However, elemental mappings exhibited Ga concentrations up to 3.6 % which is far beyond the solubility limit. The amount incorporated was not affected by the growth temperature over the investigated temperature range (170-250 °C). The high incorporation was attributed to a kinetic process which was facilitated due to the low growth temperatures. For application in electronic devices the removal of the Ga tips is of interest. Therefore, the treatment of the obtained nanostructures using diluted HF was applied. This method enabled the residue-less removal of the growth promoter, whereas Ga atoms which were incorporated into the Ge matrix remained unaffected.

As Ga is a well-known p-dopant for Ge, the electric properties of the obtained NW were investigated. Therefore, I-V curves of single NWs were measured. Measurements revealed that the material shows a very high conductivity, which is ~five orders of magnitude higher than intrinsic Ge but still below the conductivity values usually obtained for metal NWs. Therefore the material could be denoted as degenerate semiconductor. The results matched very well with the values expected from the amount of incorporated Ga.

In spite of the demonstrated growth of elongated Ge nanostructures using Ga seeds, there remains space for further research on this topic. As this work was aimed to investigate Ga-seeded growth at the lowest temperature possible, further investigations regarding higher growth temperatures should be conducted. Especially, due to the fact that the incorporation of Ga was supposed to be kinetically driven, which should enable control over the Ga concentration via the growth temperature. Furthermore, Ge NWs with gallium tips can act as potential substrates for NW heterostructures with gallium arsenide or indium phosphide. Both materials can grow heteroepitactically on germanium substrates.[312, 313] Additionally, in the case of GaAs, the Ga component is already supplied by the Ga seed. This work demonstrated already successfully that a required two-step growth process using Ga seeds is possible, as the growth promoter remains active during a second elongation step.

Defect Transfer

Silver bipyramids were successfully obtained from a modified polyol method using dry air to enhance oxidative etching. The synthesis method reported by Wiley *et al.* did not lead to silver bipyramids, thus a mixture of different shapes ranging from spherical particles to NWs had been obtained. This aspect was related to insufficient oxidative etching due to contamination of the EG solvent, which could not be removed by purification via distillation. The diameter of the obtained Ag bipyramids could be decreased to 80-100 nm, however further reduction could not be maintained via a decrease in reaction time. The surface of the particles was heavily coated with PVP, which could not be com-

pletely removed via additional purification steps. As a result, the obtained Ag bipyramids which should act as seeds for the subsequent controlled defect transfer were not ideal.

Ag-seeded growth of Ge NWs to facilitate the controlled defect transfer could be maintained via hot-wall, cold-wall CVD as well as in SC toluene, using DPG as Ge source. The usage of $GeCp_2$ in cold-wall experiments led only to amorphous decomposition products. A subsequent cleaning step with SC toluene removed excessive capping polymer, which appeared to be mandatory to facilitate an efficient NW nucleation. Straight NW morphologies were obtained mainly for NWs <30 nm diameter, thicker NWs showed multiple kinks. An increase of the growth temperature reduced the kinking of thicker NWs, thus NWs with 80-100 nm diameter remained kinked. Approaching 500 °C growth temperature, effects such as tapering and particle-contamination increased tremendously, but NWs with diameters around 100 nm still remained kinked. Furthermore, a high contamination with NWs exhibiting diameters ~15 nm was apparent in all NW samples, thus seed particle solutions did not Ag particles with this size. Small silver seeds emerged most likely during heating to growth temperature from silver ions, which were coordinated to pyrrolidone groups of the PVP. As a result, the obtained samples contained rather NWs with irregular shaped seeds than NWs with bipyramidal seeds exhibiting a successful controlled defect transfer.

In order to maintain a controlled defect transfer, further work must be done/ challenges must be met: The size of the bipyramids must be decreased at least below ~60 nm, which should ensure a kink-free growth of the NWs. As a simple reduction of the growth duration for bipyramid growth appeared unrewarding, a modification of the silver precursor concentration seems a good possibility. However, this modification is going to require also the adjustment of the bromide concentration and likely the concentration of the capping polymer as the polyol method is a very sensitive growth process. Furthermore, the purification of the bipyramids should be modified to ensure a good nucleation of the NWs as well as remove silver ions, which could form irregular shaped silver seeds during the NW growth process. From the today's point of view, the implementation of the mentioned modifications should lead to bipyramid-seeded Ge NWs and therefore to a successfully controlled defect transfer.

6. Experimental

6.1. Synthesis

All chemicals were purchased from Sigma Aldrich, abcr or TCI Europe and used as received. Tert buthyl germane was purchased from Gelest. Syntheses were carried out taking stringent precautions against atmospheric moisture and oxygen using nitrogen or argon atmosphere in combination with Schlenk techniques or a glove box. Solvents were dried with sodium/benzophenone and stored over sodium wire if necessary.

6.1.1. Tetraphenylgermane

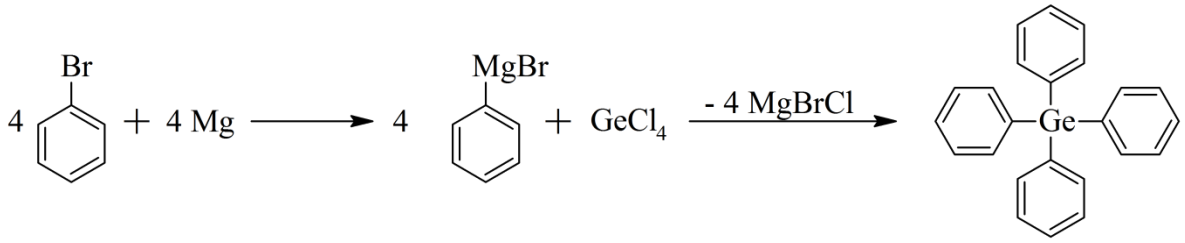

15.9 g (653 mmol, 10 eq.) of magnesium chips were dispersed in a small amount of dry diethyl ether. To start the gringard reaction 103 g (653 mmol, 10 eq.) of distilled bromobenzene were slowly added via the dropping funnel. During the addition, the bromobenzene is diluted with further diethyl ether to provide enough solvent in the reaction solution. Subsequently, the reaction was heated to reflux for 2.5 hours. After cooling to room temperature, 14 g (653 mmol, 1 eq.) germanium tetrachloride were added dropwise. The reaction solution was refluxed two more hours and subsequently quenched with water and diluted HCl. After phase separation the aqueous phase was washed with ether and the solvent of the collected organic phases was removed. The product was purified via crystallisation from toluene. Yield: 17.6 g, (71 %) of a colourless solid.

6.1.2. Diphenylgermane

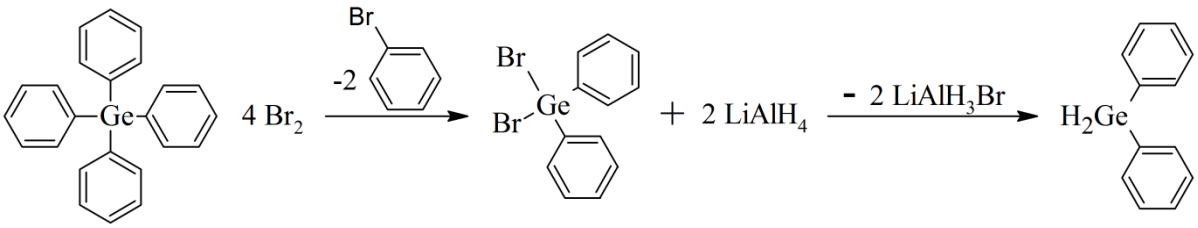

Synthesis had been carried out by a modified procedure published by Johnson *et al.*.[314] 16.2g (42.5 mmol, 1 eq.) tetraphenyl germane were dissolved in 80 mL dichloro ethane followed by the subsequent addition of 15.0 g (188 mmol, 4.4eq.) bromine. The reaction was heated to reflux for three hours. After cooling to room temperature, the volatile components were removed and the remaining

brownish liquid was added to 3.60 g (95 mmol, 2.2 eq.) of $LiAlH_4$ dispersed in dry diethyl ether. The obtained greyish viscous solution was heated to reflux for two hours. The solvent was replaced by pure n-hexane and the solid precipitate was removed by filtration. Finally, the n-hexane was removed and the product recondensed for purification. Yield: 8.15 g (83.8 %) of a colourless liquid.

6.1.3. Germaniumdichloride·Dioxane Complex

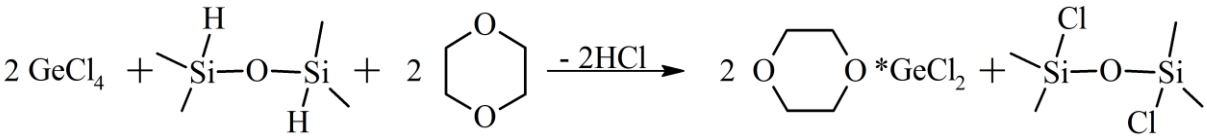

The germaniumdichloride·dioxane complex was prepared according to a synthesis procedure reported by Roskamp *et al.*.[315] 10 g (46 mmol, 1eq.) tetrachloro germane were diluted with 8.6 mL dry 1,4-dioxane and 2.3 mL n-hexane in a 100 mL two-neck schlenk flask equipped with a condenser. Thereafter, 4.4 mL (25 mmol, 0.54 eq.) 1,1,3,3 tetramethyl disiloxane were added dropwise via a nitrogen-purged syringe over a period of 45 minutes. The reaction solution was heated to reflux over night. After cooling to room temperature, the colourless precipitate was isolated via filtration and washed three times with n-hexane. The product is dried under vacuum. Yield: 6.1 g, 57 % colourless crystals

6.1.4. Biscyclopentadienyl Germanium (II)

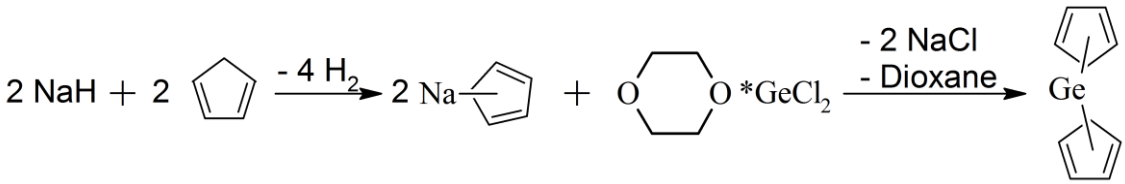

Synthesis had been conducted according to a modified procedure reported by Grenz *et al.*.[316] 1.6 g (65 mmol, 2.4 eq.) of sodium hydride were dispersed in 100 mL dry tetrahydrofurane and cooled using an ice bath. To this dispersion, 14.7 g (72 mmol, 2.6 eq.) of freshly prepared cyclopentadiene were added under vigorous stirring. The reaction solution was left stirring at room temperature for ~12 hours. Subsequently, the reaction solution was added to a solution containing 6.13 g (27.2 mmol, 1 eq.) germaniumdichloride·dioxane complex in 40 mL tetrahydrofurane. The reaction solution was cooled to -78 °C during addition and the following two hours of stirring. The solid byproducts were removed via filtration and the solvent was removed under vacuum. The obtained reddish-coloured crude product was purified via sublimation at $6 \cdot 10^{-2}$ mbar at room temperature. Yield: 1.2 g, 22 % colourless solid.

6.1.5. Bis(trimethylsilyl)amine)Lithium (I)

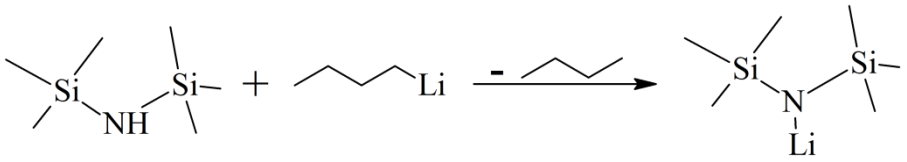

Synthesis had been carried out according to a procedure reported by Golloch *et al.*.[317] 30 mL (0.144 mol, 1.1 eq.) hexamethyldisilazane were frozen in a 250 mL flask equipped with a sublimation tube using liquid nitrogen. Subsequently, 51.5 mL (0.129 mol, 1 eq.) n-buthyl lithium (2.5 M in n-hexane) were added and frozen as well. The solid was allowed to melt and carefully heated until the reaction solution turned from turbid to clear. After two hours, the volatile components were removed by applying vacuum. The resulting colourless crude product was purified via sublimation under vacuum (0.34 mbar) at 100 °C. Yield: 20.8 g, 96 % colourless solid.

6.1.6. Bis(bis(trimethylsilyl)amine) Germanium (II)

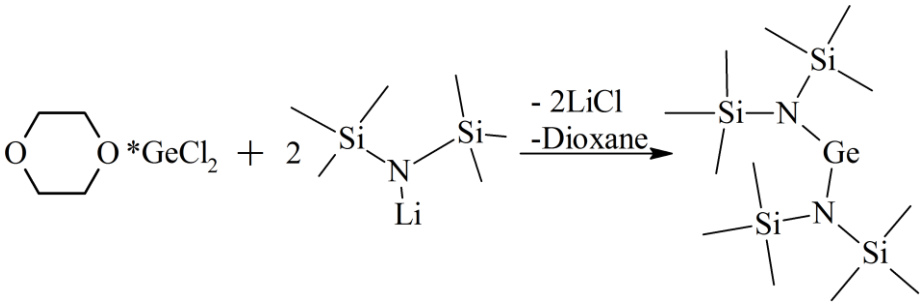

The synthesis had been conducted according to a modified procedure reported by Lappert et al..[318] A solution of 5.61 g (33 mmol, 1.9 eq.) bis(trimethylsilyl)amine) lithium (I) in 15 mL n-hexane and 20 mL tetrahydrofuran was added to a solution containing 4 g (17 mmol, 1 eq.) germanium dichloride dioxane complex in 30 mL dry tetrahydrofuran. The reaction solution was heated to 60 °C for 12 hours. Thereafter, the solvent was replaced by pure n-hexane, a colourless precipitate removed and the solvent entirely removed by vacuum. The obtained orange crude product was purified by vacuum distillation at 65 °C at $6.8 \cdot 10^{-2}$ mbar. Yield: 5.9 g, 88 % orange liquid.

6.1.7. Bis(bis(trimethylsilyl)amine) Lead (II)

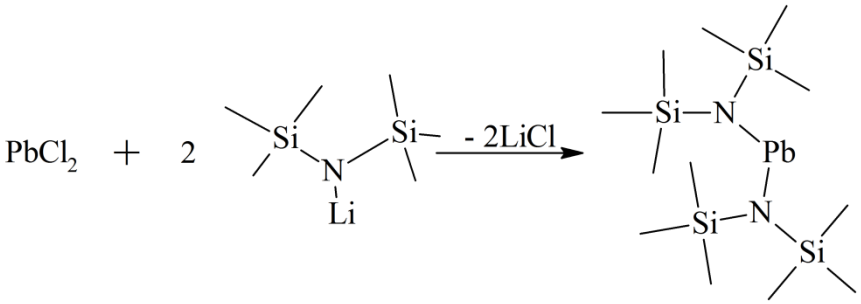

Similar to $Ge(HMDS)_2$, a slightly modified procedure of the synthesis reported by Lappert *et al.* had been used.[318] A solution of 5.61 g (33 mmol, 1.9 eq.) bis(trimethylsilyl)amine) lithium (I) in 15 mL n-hexane and 20 mL tetrahydrofuran was added to a solution containing 4.45 g (16 mmol, 1 eq.) lead dichloride in 30 mL dry tetrahydrofuran. The reaction solution was heated to 60 °C for 12 hours. The solvent was replaced by pure n-hexane and a colourless precipitate removed. After the n-hexane was removed by vacuum the obtained orange crude product is purified by vacuum distillation resulting in a yellow liquid. No yield had been determined.

6.2. Lead-supported Growth

6.2.1. Pb-Particle Synthesis and Substrate Preparation

Lead particles were obtained via photolytic decomposition of $Pb(N(Si(CH_3)_3)_2)_2$ for 14 days in a clear glass vial under inert atmosphere. The particles were separated from the reaction solution and washed with dry toluene. To deposit them onto Si substrates, the particles were dispersed in dry toluene and drop-casted in an Ar-filled glovebox.

6.2.2. Hot-Wall CVD

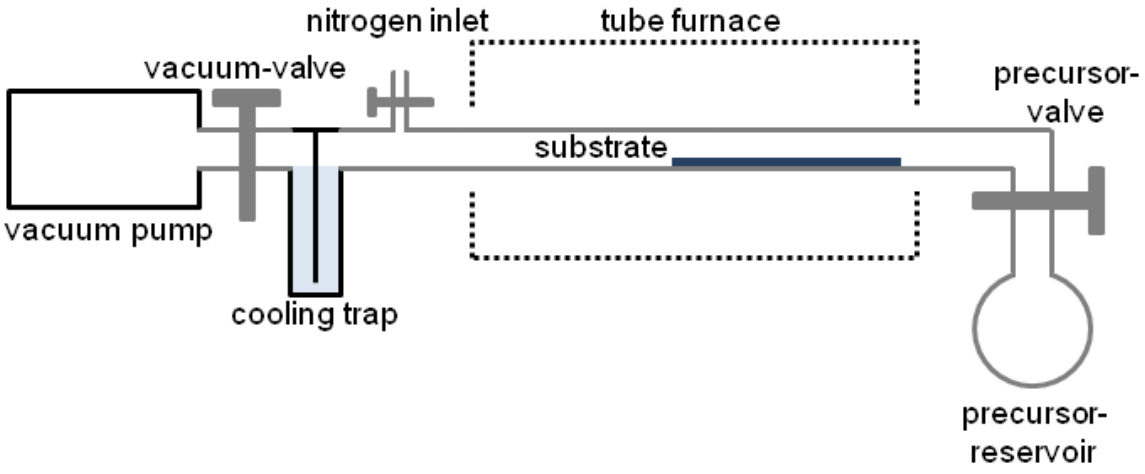

Figure 63: Scheme of the hot-wall CVD reactor used to grow Ge NWs from Pb seeds.

Lead-seeded germanium NWs were grown in a horizontal hot-wall reactor. A scheme of the apparatus is illustrated in Figure 63. Silicon substrates coated with lead particles were placed inside the reactor tube and the evacuated setup ($6 \cdot 10^{-2}$ mbar) was heated to the desired growth temperature (400-430 °C). The precursor reservoir containing 75 mg diphenylgermane could be separated from the growth chamber by a cut-off valve. A slightly raised precursor temperature (35 °C) during deposition was maintained by a water bath. The reactor exhaust was connected to a vacuum system containing a liquid nitrogen cooling trap and a rotary pump. Deposition times ranged from 30 minutes to one hour.

6.2.3. Growth in Supercritical Fluid

Ge NWs have been grown via a batch process in stainless steel high-pressure cells with a volume of 5 mL in toluene (T_C=318 °C). To maintain oxygen- and water-free conditions, assembly was performed in an Ar-filled glove box. The cell was loaded with a particle-coated growth substrate, 3 mL dry toluene and 50 mg diphenylgermane. After sealing, the cell was transferred into a pre-heated tube furnace. Additional temperature control was maintained via a thermocouple connected directly to the cell. Growth temperatures were chosen between 340-420 °C, which leads to a calculated pressure of ~290-320 bar. Growth durations were selected between 40-100 min. The cell was then removed from the furnace and allowed to cool to room temperature. The substrates were removed after draining the growth solution and rinsed with toluene before further characterisation.

Supercritical hexane (T_C=234 °C) was used as solvent for low temperature growth. $Pb(HMDS)_2$ and Ge(HMDS) (Ge:Pb=1:6) were thermally decomposed at 250°C in dry hexane containing small amounts of dodecylamine. Similar to the NW growth in toluene, the cell was assembled and sealed in an Ar-filled glove box and heated to 250 °C for 100 min in a preheated tube furnace.

6.3. Gallium-Seeding of Germanium Nanowires

6.3.1. Nanorod and Nanowire Growth in Solution

Ge NW growth was performed in stainless steel cells with 1.2 mL volume. In a typical growth reaction 0.8 mL dry toluene, 10 µL pentamethylcyclopentadienyl gallium(I) GaCp* and 50 µL *t*BG were filled into the reaction vessel inside an Ar-filled glove box. The tightly sealed cells were placed into a pre-heated furnace for 1-18 h. Growth temperatures were chosen between 170 to 230 °C. After reaching the desired growth time, the cells where put into cold water and allowed to cool to room temperature. The reaction solution was diluted with toluene and the product obtained and purified via multiple centrifugation and dissolution in toluene.

6.3.2. Nanowire Growth on Substrates

Ge NWs were grown on substrates such as <100> oriented Si or silicone in stainless steel vessels with 5 mL volume. To ensure an oxygen and water-free environment, the reaction vessels were assembled in an Ar-filled glove box. The substrate was incubated with GeCp* and placed into the reaction vessel together with 20 µL *t*BG and 1 mL of dry toluene. The vessel was tightly sealed and placed into a preheated tube furnace where it was kept for 12 to 18 hours. The cell was then removed from the furnace and cooled to room temperature using a water bath. The cell was opened and the substrate removed.

6.3.3. Growth Promoter Removal

The purified nanorods were two times washed with ethanol to remove the solvent. The nanorod precipitate was than dispersed in 2 % hydrofluoric acid for 3 minutes, using an ultrasonic bath. Subsequently, the nanorods were separated from the solution via centrifugation and washed with water, ethanol and tetrahydrofurane. Finally, the solvent was replaced by toluene.

6.4. Defect Transfer

6.4.1. Silver Bipyramide Synthesis

In a 25 mL three-neck-flask equipped with condenser and gas inlet 5 mL distilled 1,2-ethanediol were heated to 160 °C. With the gas inlet, 2 sccm of dry air (compressed air dried with phosphorous pentoxide) was bubbled through the reaction solution. Two precursor solutions were prepared one containing 80 mg $AgNO_3$ and 5 mL 1,2-ethanediol, the other 80 mg polyvinylpyrrolidone, a 20 µL drop of 10 mM NaBr solution and 5 mL 1,2-ethanediol. Shortly before reaction start, a 30 µL drop of a 10 mM NaBr solution was added to the preheated glycol. The reaction was started by the simultaneous injection of 3 mL from each precursor solution with an injection rate of 45 mL/h. After one to two hours, the reaction was stopped by removing the oil bath. Nanoparticles were isolated from the reaction solution by adding acetone and subsequent centrifugation. Purification was done by a number of centrifugation and redispersion in iso-propanol.

6.4.2. Germanium Nanowire Growth via Cold-Wall CVD using $GeCp_2$

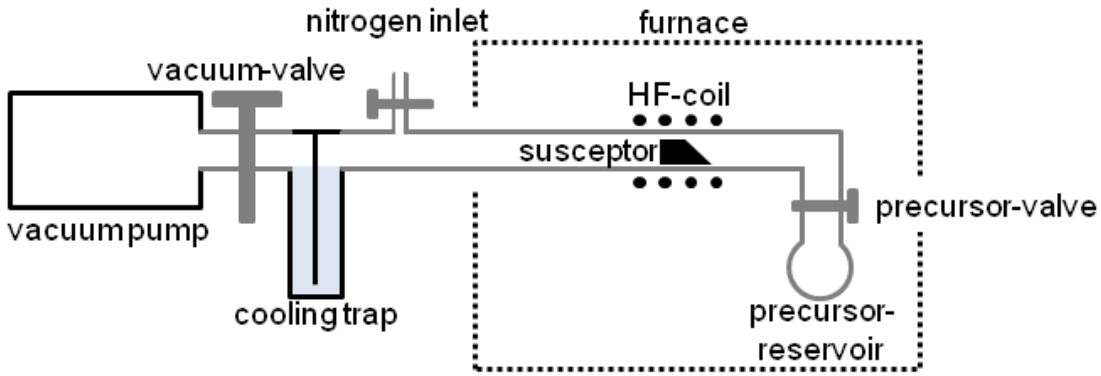

Figure 64: Cold-wall CVD setup used to grow Ge NWs from Ag bipyramids.

Silicon <100> substrates were cleaned in an ultrasonic bath using 2-propanol. Ag bipyramids were coated by dispersing them in 2-propanol and drop-casting the solution onto the cleaned substrates. The substrates were mounted on the top site of a cylindrical graphite susceptor (diameter x length=20x50 mm) using silver conductive paint. The susceptor was placed into a glass tube (~22 mm diameter) inside the coil of the HF-generator and the system was heated to 110 °C under vacuum for one hour to remove moisture. A scheme of the entire CVD apparatus is depicted in Figure

64. The growth process was initiated by heating the susceptor to the desired growth temperature (350-500 °C) and the opening of the valve to the precursor flask, which contained 20-30 mg $GeCp_2$. During the entire growth process, a dynamic vacuum $<10^{-3}$ mbar was applied. The growth process was terminated by closing the precursor valve and cooling the susceptor to room temperature.

6.4.3. Germanium Nanowire Growth via Hot-Wall CVD using DPG

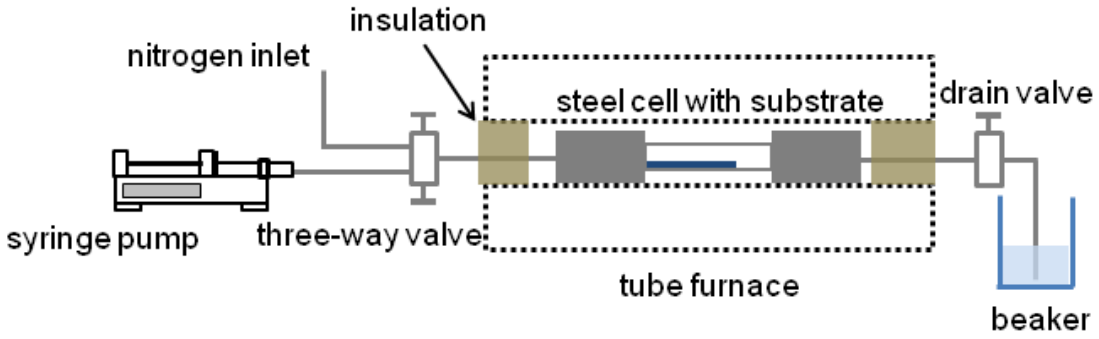

Figure 65: Scheme of the hot-wall CVD setup used to grow Ge NWs from Ag bipyramids.

The nanowire growth process was performed in a custom-made hot-wall CVD setup. A Si substrate with Ag bipyramids (substrate preparation is described in chapter6.4.2) was placed into a stainless steel cell with 5 mL reaction volume. The cell as well as valves and tubing was heated to 120 °C over night and then transferred into a load lock, where it was left to cool to room temperature under vacuum. Further assembly was performed in an Ar-filled glovebox. The reaction cell was filled with 3 mL dry toluene and connected to the tubing. The inlet was sealed with a three-way valve, whereas the outlet was sealed with a simple cut-off valve. The apparatus was placed into a tube furnace with the valves outside and an insulating jacket at the inlet tubing. Subsequently, the furnace was heated to 480 °C and let equilibrate for approx. 15 minutes. Then, the toluene was drained from the reaction chamber via the cut-off valve and a stream of dry nitrogen (2 sccm) through the reaction apparatus was enabled. NW growth was initialized via the injection of 20 µL diphenylgermane in 5 mL toluene with a rate of approx. 3.2 mL/h. To terminate the growth reaction, the precursor injection was stopped and the gas flow was maintained for additional 15 minutes. Afterwards, the reaction cell was cooled to room temperature, opened and the substrate extracted for analysis.

6.4.4. Germanium Nanowire Growth via Cold-Wall CVD using DPG

Silicon substrates were prepared as mentioned in chapter 6.4.2. To remove excess capping polymer, the Ag-decorated substrates were cleaned using supercritical toluene. Therefore the substrate and 3 mL toluene were placed into a stainless steel cell connected to a purge valve. The tightly sealed cells were placed into a tube furnace and heated to 450 °C. After thermal equilibration of the cell, the solvent was purged and the cell removed from the furnace. At room-temperature, the substrates were transferred to a graphite susceptor, which was then placed into the CVD reactor. A scheme of the CVD setup is depicted in Figure 64. To remove moisture from the CVD chamber, the apparatus was heated to 110 °C

under vacuum for at least one hour. The apparatus was primed for NW growth by heating the susceptor to 400-500 °C and the CVD chamber as well as the precursor supply to 60-80 °C. A static vacuum of $<10^{-3}$ mbar was applied. To initiate the growth process the precursor valve was carefully opened, which connected the CVD chamber to the precursor flask containing 50 mg DPG. During the growth process the chamber pressure increased to $>5 \cdot 10^{-1}$ mbar. To terminate NW growth, the precursor valve was closed and the CVD chamber was evacuated once again. After ten minutes hold, the susceptor was cooled to room-temperature.

6.4.5. Germanium Nanowire Growth in Supercritical Toluene

To avoid moisture and oxygen, cell assembly had been carried out in an Ar-filled glove box. A Si substrate coated with Ag bipyramids (preparation described in chapter6.4.2)6.4.3 was placed into a dry high pressure stainless steel cell (1.2 mL volume). The cell was filled with 600 µL of toluene as well as 10 µL diphenyl germane, tightly sealed and placed into a preheated tube furnace. NW growth was maintained between 350-450 °C for 15 to 20 minutes. Thereafter the cell was removed from furnace swiftly cooled to room temperature using a water bath. To remove any contamination, the extracted substrate was carefully rinsed with toluene.

6.5. Material Analysis

6.5.1. X-Ray Diffraction

X-ray diffraction analysis was carried out using a PANalytical X-Pert PRO PW 3050/60 in Bragg-Brentano geometry using Cu-Kα radiation and a X'Celerator detector. Samples were placed onto Si wafers cut in (711) direction and analysis parameters (step size, time per step) were chosen individually to obtain good signal to noise ratio. Data analysis was carried out using HighScore Plus software.

6.5.2. Scanning Electron Microscopy Analysis

SEM analysis has been carried out using a FEI Quanta 200 FEG field emission gun microscope at acceleration voltages between 2 and 20 kV. Dispersions were drop cast onto silicon wafers.

6.5.3. Transmission Electron Microscopy Analysis

TEM analysis has been carried out with a FEI Tecnai F20 field emission microscope. Samples were dispersed in an appropriate solvent such as toluene or iso-propanol and dropcast onto carbon coated copper grids.

6.5.4. Electrical Characterisation of Single Nanowires

The electrical characterisation of single NWs had been conducted at the Institute of solid State Electronics, TU Vienna. Therefore NWs were coated onto sample holders using a dry-transfer technique. Single NWs were contacted by Al electrodes in two-point measurement configuration using an elec-

tron beam lithography technique. For additional information, the interested reader might refer to literature

A. List of Figures

B. Literature

1. Farokhzad, O. C.; Langer, R. *ACS Nano* **2009,** 3, 16.
2. Baer, D. R.; Burrows, P. E.; El-Azab, A. A. *Progress in Organic Coatings* **2003,** 47, 342.
3. Waser, R., *Nanoelectronics and Information Technology*. John Wiley & Sons: 2012.
4. Pokropivny, V. V.; Skorokhod, V. V. *Materials Science and Engineering: C* **2007,** 27, 990.
5. Bardeen, J.; Brattain, W. H. *Physical Review* **1948,** 74, 230.
6. Schubert, E. F.; Gessmann, T.; Kim, J. K., *Light Emitting Diodes*. Wiley Online Library: 2005.
7. Parida, B.; Iniyan, S.; Goic, R. *Renewable and Sustainable Energy Reviews* **2011,** 15, 1625.
8. Hoffmann, M. R.; Martin, S. T.; Choi, W.; Bahnemann, D. W. *Chemical Reviews* **1995,** 95, 69.
9. Brus, L. E. *Journal of Chemical Physics* **1983,** 79, 5566.
10. Smith, A. M.; Nie, S. *Accounts of Chemical Research* **2010,** 43, 190.
11. Edelstein, A. S.; Cammaratra, R. C., *Nanomaterials: Synthesis, Properties and Applications, Second Edition*. Taylor & Francis: 1998.
12. *IBM Research Alliance Builds New Transistor for 5nm Technology*. Press Release, IBM, Albany, NY, 2017.
13. Huang, Z.; Geyer, N.; Werner, P.; de Boor, J.; Gosele, U. *Advanced Materials* **2011,** 23, 285.
14. Huang, Z.; Shimizu, T.; Senz, S.; Zhang, Z.; Zhang, X.; Lee, W.; Geyer, N.; Gosele, U. *Nano Letters* **2009,** 9, 2519.
15. Li, X.; Bohn, P. W. *Applied Physics Letters* **2000,** 77, 2572.
16. Harada, Y.; Li, X.; Bohn, P. W.; Nuzzo, R. G. *Journal of the American Chemical Society* **2001,** 123, 8709.
17. Chartier, C.; Bastide, S.; Lévy-Clément, C. *Electrochimica Acta* **2008,** 53, 5509.
18. Yae, S.; Kawamoto, Y.; Tanaka, H.; Fukumuro, N.; Matsuda, H. *Electrochemistry Communications* **2003,** 5, 632.
19. Tamura, M.; Shukuri, S.; Moniwa, M.; Default, M. *Applied Physics A* **1986,** 39, 183.
20. Rubanov, S.; Munroe, P. R. *Journal of Microscopy* **2004,** 214, 213.
21. Boden, S. A.; Moktadir, Z.; Bagnall, D. M.; Mizuta, H.; Rutt, H. N. *Microelectronic Engineering* **2011,** 88, 2452.
22. Smith, N. S.; Kinion, D. E.; Tesch, P. P.; Boswell, R. W. *Microscopy and Microanalysis* **2007,** 13.
23. Delobbe, A.; Salord, O.; Hrncir, T.; David, A.; Sudraud, P.; Lopour, F. *Microscopy and Microanalysis* **2014,** 20, 298.
24. Giannuzzi, L. A.; Stevie, F. A. *Micron* **1999,** 30, 197.
25. Mayer, J.; Giannuzzi, L. A.; Kamino, T.; Michael, J. *MRS Bulletin* **2011,** 32, 400.

26. Zeiner, C.; Lugstein, A.; Burchhart, T.; Pongratz, P.; Connell, J. G.; Lauhon, L. J.; Bertagnolli, E. *Nano Letters* **2011,** 11, 3108.
27. Riihimäki, I.; Virtanen, A.; Rinta-Anttila, S.; Pusa, P.; Räisänen, J.; Isolde Collaboration, T. *Applied Physics Letters* **2007,** 91, 091922.
28. Patent No: US575,002, Lodyguine, A. D., United States, 1897.
29. Choy, K. *Progress in Materials Science* **2003,** 48, 57.
30. Liu, H.; Dandy, D. S., *Diamond Chemical Vapor Deposition*. William Andrew Publishing: Park Ridge, NJ, 1995.
31. Hou, X.; Choy, K. L. *Chemical Vapor Deposition* **2006,** 12, 583.
32. Doshi, J.; Reneker, D. H. *Journal of Electrostatics* **1995,** 35, 151.
33. Guan, H.; Shao, C.; Liu, Y.; Yu, N.; Yang, X. *Solid State Communications* **2004,** 131, 107.
34. Yang, X.; Shao, C.; Guan, H.; Li, X.; Gong, J. *Inorganic Chemistry Communications* **2004,** 7, 176.
35. Larsen, G.; Velarde-Ortiz, R.; Minchow, K.; Barrero, A.; Loscertales, I. G. *Journal of the American Chemical Society* **2003,** 125, 1154.
36. Li, D.; Wang, Y.; Xia, Y. *Nano Letters* **2003,** 3, 1167.
37. Chronakis, I. S. *Journal of Materials Processing Technology* **2005,** 167, 283.
38. Zhang, Z.; Gekhtman, D.; Dresselhaus, M. S.; Ying, J. Y. *Chemistry of Materials* **1999,** 11, 1659.
39. Erts, D.; Polyakov, B.; Daly, B.; Morris, M. A.; Ellingboe, S.; Boland, J.; Holmes, J. D. *Journal of Physical Chemistry B* **2006,** 110, 820.
40. Brumlik, C. J.; Martin, C. R. *Journal of the American Chemical Society* **1991,** 113, 3174.
41. Zheng, M. J.; Zhang, L. D.; Li, G. H.; Shen, W. Z. *Chemical Physics Letters* **2002,** 363, 123.
42. Xu, J.; Petkov, N.; Wu, X.; Iacopino, D.; Quinn, A. J.; Redmond, G.; Bein, T.; Morris, M. A.; Holmes, J. D. *ChemPhysChem* **2007,** 8, 235.
43. Petkov, N.; Birjukovs, P.; Phelan, R.; Morris, M. A.; Erts, D.; Holmes, J. D. *Chemistry of Materials* **2008,** 20, 1902.
44. Zhang, Z.; Shimizu, T.; Senz, S.; Gösele, U. *Advanced Materials* **2009,** 21, 2824.
45. Lew, K.-K.; Redwing, J. M. *Journal of Crystal Growth* **2003,** 254, 14.
46. Bachmann, J.; Jing, J.; Knez, M.; Barth, S.; Shen, H.; Mathur, S.; Gosele, U.; Nielsch, K. *Journal of the American Chemical Society* **2007,** 129, 9554.
47. Gu, D.; Baumgart, H.; Namkoong, G.; Abdel-Fattah, T. M. *Electrochemical and Solid-State Letters* **2009,** 12.
48. Liu, Z.; Zhang, D.; Han, S.; Li, C.; Lei, B.; Lu, W.; Fang, J.; Zhou, C. *Journal of the American Chemical Society* **2005,** 127, 6.
49. Satishkumar, B. C.; Govindaraj, A.; Vogl, E. M.; Basumallick, L.; Rao, C. N. R. *Journal of Materials Research* **2011,** 12, 604.

50. Mann, S.; Li, M.; Schnablegger, H. *Nature* **1999,** 402, 393.
51. Hopwood, J. D.; Mann, S. *Chemistry of Materials* **1997,** 9, 1819.
52. Li, M.; Mann, S. *Advanced Functional Materials* **2002,** 12, 773.
53. Vayssieres, L.; Beermann, N.; Lindquist, S.-E.; Hagfeldt, A. *Chemistry of Materials* **2001,** 13, 233.
54. Sun, Y. G.; Mayers, B.; Herricks, T.; Xia, Y. N. *Nano Letters* **2003,** 3, 955.
55. Zhu, Y.-J.; Hu, X.-L. *Chemistry Letters* **2003,** 32, 1140.
56. Chen, J.; Herricks, T.; Geissler, M.; Xia, Y. *Journal of the American Chemical Society* **2004,** 126, 10854.
57. Greene, L. E.; Law, M.; Goldberger, J.; Kim, F.; Johnson, J. C.; Zhang, Y.; Saykally, R. J.; Yang, P. *Angewandte Chemie International Edition* **2003,** 42, 3031.
58. Gates, B.; Mayers, B.; Cattle, B.; Xia, Y. *Advanced Functional Materials* **2002,** 12.
59. Gates, B.; Yin, Y.; Xia, Y. *Journal of the American Chemical Society* **2000,** 122, 12582.
60. Gates, B.; Mayers, B.; Grossman, A.; Xia, Y. *Advanced Materials* **2002,** 14, 1749.
61. Mayers, B.; Xia, Y. *Journal of Materials Chemistry* **2002,** 12, 1875.
62. Mayers, B.; Gates, B.; Yin, Y.; Xia, Y. *Advanced Materials* **2001,** 13, 1380.
63. Sears, G. W. *Acta Metallurgica* **1955,** 3, 361.
64. Sears, G. W. *Acta Metallurgica* **1955,** 3, 367.
65. Dai, Z. R.; Pan, Z. W.; Wang, Z. L. *Advanced Functional Materials* **2003,** 13, 9.
66. Zhang, R. Q.; Lifshitz, Y.; Lee, S. T. *Advanced Materials* **2003,** 15, 635.
67. Colli, A.; Hofmann, S.; Fasoli, A.; Ferrari, A. C.; Ducati, C.; Dunin-Borkowski, R. E.; Robertson, J. *Applied Physics A* **2006,** 85, 247.
68. Zhang, Y. F.; Tang, Y. H.; Wang, N.; Lee, C. S.; Bello, I.; Lee, S. T. *Physical Review B* **2000,** 61, 4518.
69. Zhang, R. Q.; Chu, T. S.; Cheung, H. F.; Wang, N.; Lee, S. T. *Materials Science and Engineering: C* **2001,** 16, 31.
70. Shi, W. S.; Zheng, Y. F.; Wang, N.; Lee, C. S.; Lee, S. T. *Advanced Materials* **2001,** 13, 591.
71. Shi, W. S.; Zheng, Y. F.; Wang, N.; Lee, C. S.; Lee, S. T. *Applied Physics Letters* **2001,** 78, 3304.
72. Shi, W. S.; Zheng, Y. F.; Wang, N.; Lee, C. S.; Lee, S. T. *Journal of Vacuum Science & Technology B: Microelectronics and Nanometer Structures* **2001,** 19.
73. Wagner, R. S.; Ellis, W. C. *Applied Physics Letters* **1964,** 4, 89.
74. Okamoto, H.; Massalski, T. B. *Bulletin of Alloy Phase Diagrams* **1983,** 4, 190.
75. Kodambaka, S.; Tersoff, J.; Reuter, M. C.; Ross, F. M. *Science* **2007,** 316, 729.
76. Verheijen, M. A.; Immink, G.; de Smet, T.; Borgstrom, M. T.; Bakkers, E. P. *Journal of the American Chemical Society* **2006,** 128, 1353.

77. Borgstrom, M. T.; Immink, G.; Ketelaars, B.; Algra, R.; Bakkers, E. P. *Nature Nanotechnology* **2007,** 2, 541.
78. Nishizawa, J.-i. *Journal of Vacuum Science & Technology B* **1996,** 14.
79. Persson, A. I.; Fröberg, L. E.; Jeppesen, S.; Björk, M. T.; Samuelson, L. *Journal of Applied Physics* **2007,** 101, 034313.
80. Jensen, L. E.; Björk, M. T.; Jeppesen, S.; Persson, A. I.; Ohlsson, B. J.; Samuelson, L. *Nano Letters* **2004,** 4, 1961.
81. LaMer, V. K.; Dinegar, R. H. *Journal of the American Chemical Society* **1950,** 72, 4847.
82. Givargizov, E. I. *Journal of Crystal Growth* **1975,** 31, 20.
83. Givargizov, E. I.; Sheftal, N. N. *Journal of Crystal Growth* **1971,** 9, 326.
84. Hofmann, S.; Sharma, R.; Wirth, C. T.; Cervantes-Sodi, F.; Ducati, C.; Kasama, T.; Dunin-Borkowski, R. E.; Drucker, J.; Bennett, P.; Robertson, J. *Nature Materials* **2008,** 7, 372.
85. Wen, C. Y.; Tersoff, J.; Hillerich, K.; Reuter, M. C.; Park, J. H.; Kodambaka, S.; Stach, E. A.; Ross, F. M. *Physical Review Letters* **2011,** 107, 025503.
86. Oh, S. H.; Chisholm, M. F.; Kauffmann, Y.; Kaplan, W. D.; Luo, W.; Ruhle, M.; Scheu, C. *Science* **2010,** 330, 489.
87. Gamalski, A. D.; Ducati, C.; Hofmann, S. *The Journal of Physical Chemistry C* **2011,** 115, 4413.
88. Dubrovskii, V. G. *Crystal Growth & Design* **2017,** 17, 2589.
89. Kratzer, P.; Sakong, S.; Pankoke, V. *Nano Letters* **2012,** 12, 943.
90. Arbiol, J.; Kalache, B.; Cabarrocas, P. R. i.; Morante, J. R.; Morral, A. F. i. *Nanotechnology* **2007,** 18, 305606.
91. Lensch-Falk, J. L.; Hemesath, E. R.; Lopez, F. J.; Lauhon, L. J. *Journal of the American Chemical Society* **2007,** 129, 10670.
92. Regolin, I.; Khorenko, V.; Prost, W.; Tegude, F. J.; Sudfeld, D.; Kästner, J.; Dumpich, G.; Hitzbleck, K.; Wiggers, H. *Journal of Applied Physics* **2007,** 101.
93. Wang, G. T.; Talin, A. A.; Werder, D. J.; Creighton, J. R.; Lai, E.; Anderson, R. J.; Arslan, I. *Nanotechnology* **2006,** 17, 5773.
94. Kirkham, M.; Wang, X.; Wang, Z. L.; Snyder, R. L. *Nanotechnology* **2007,** 18.
95. Lensch-Falk, J. L.; Hemesath, E. R.; Perea, D. E.; Lauhon, L. J. *Journal of Materials Chemistry* **2009,** 19, 849.
96. Wang, F.; Dong, A.; Sun, J.; Tang, R.; Yu, H.; Buhro, W. E. *Inorganic Chemistry* **2006,** 45, 7511.
97. Wang, F.; Dong, A.; Buhro, W. E. *Chemical Reviews* **2016**.
98. Seifner, M. S.; Biegger, F.; Lugstein, A.; Bernardi, J.; Barth, S. *Chemistry of Materials* **2015,** 27, 6125.

99. Deng, S. Z.; Fan, H. M.; Wang, M.; Zheng, M. R.; Yi, J. B.; Wu, R. Q.; Tan, H. R.; Sow, C. H.; Ding, J.; Feng, Y. P.; Loh, K. P. *ACS Nano* **2010,** 4, 495.
100. Holmberg, V. C.; Rasch, M. R.; Korgel, B. A. *Langmuir* **2010,** 26, 14241.
101. Yu, H.; Gibbons, P. C.; Buhro, W. E. *Journal of Materials Chemistry* **2004,** 14.
102. Chockla, A. M.; Harris, J. T.; Korgel, B. A. *Chemistry of Materials* **2011,** 23, 1964.
103. Buriak, J. M. *JALA: Journal of the Association for Laboratory Automation* **1999,** 4, 36.
104. Mattox, D. M., *Handbook of physical vapor deposition (PVD) processing*. Elsevier: 2010.
105. Volmer, M.; Weber, A. *Zeitschrift für Physikalische Chemie* **1926,** 119U.
106. Thompson, C. V. *Annual Review of Materials Research* **2012,** 42, 399.
107. Zhu, H. *Philosophical Magazine Letters* **1996,** 73, 27.
108. Lewis, L. J.; Jensen, P.; Barrat, J.-L. *Physical Review B* **1997,** 56, 2248.
109. Zachariah, M. R.; Carrier, M. J. *Journal of Aerosol Science* **1999,** 30, 1139.
110. Hendy, S.; Brown, S. A.; Hyslop, M. *Physical Review B* **2003,** 68.
111. Jose-Yacaman, M.; Gutierrez-Wing, C.; Miki, M.; Yang, D. Q.; Piyakis, K. N.; Sacher, E. *Journal of Physical Chemistry B* **2005,** 109, 9703.
112. Mullins, W. W. *Journal of Applied Physics* **1957,** 28, 333.
113. Guo, D. L.; Huang, X.; Xing, G. Z.; Zhang, Z.; Li, G. P.; He, M.; Zhang, H.; Chen, H.; Wu, T. *Physical Review B* **2011,** 83.
114. Wu, Y.; Yang, P. *Journal of the American Chemical Society* **2001,** 123, 3165.
115. Sun, J.; Cui, F.; Kisielowski, C.; Yu, Y.; Kornienko, N.; Yang, P. *The Journal of Physical Chemistry C* **2015**.
116. Arar, M.; Pein, A.; Haas, W.; Hofer, F.; Norrman, K.; Krebs, F. C.; Rath, T.; Trimmel, G. *The Journal of Physical Chemistry C* **2012,** 116, 19191.
117. Kim, D.; Jeong, S.; Lee, S.; Park, B. K.; Moon, J. *Thin Solid Films* **2007,** 515, 7692.
118. Sharma, V. K.; Yngard, R. A.; Lin, Y. *Advances in Colloid and Interface Sciences* **2009,** 145, 83.
119. Rai, M.; Yadav, A.; Gade, A. *Biotechnology Advances* **2009,** 27, 76.
120. Link, S.; El-Sayed, M. A. *The Journal of Physical Chemistry B* **1999,** 103, 8410.
121. Rycenga, M.; Cobley, C. M.; Zeng, J.; Li, W.; Moran, C. H.; Zhang, Q.; Qin, D.; Xia, Y. *Chemical Reviews* **2011,** 111, 3669.
122. Xue, C.; Metraux, G. S.; Millstone, J. E.; Mirkin, C. A. *Journal of the American Chemical Society* **2008,** 130, 8337.
123. Sun, Y.; Mayers, B.; Xia, Y. *Nano Letters* **2003,** 3, 675.
124. Saidi, W. A.; Feng, H.; Fichthorn, K. A. *The Journal of Physical Chemistry C* **2013,** 117, 1163.
125. Wiley, B.; Sun, Y.; Xia, Y. *Accounts of Chemical Research* **2007,** 40, 1067.
126. Lofton, C.; Sigmund, W. *Advanced Functional Materials* **2005,** 15, 1197.
127. Wiley, B. J.; Xiong, Y.; Li, Z. Y.; Yin, Y.; Xia, Y. *Nano Letters* **2006,** 6, 765.

128. Wiley, B.; Herricks, T.; Sun, Y.; Xia, Y. *Nano Letters* **2004,** 4, 1733.
129. Wiley, B.; Sun, Y.; Xia, Y. *Langmuir* **2005,** 21, 8077.
130. Taguchi, A.; Fujii, S.; Ichimura, T.; Verma, P.; Inouye, Y.; Kawata, S. *Chemical Physics Letters* **2008,** 462, 92.
131. Wang, Y.; Peng, H. C.; Liu, J.; Huang, C. Z.; Xia, Y. *Nano Letters* **2015**.
132. Winkler, C. *Berichte der deutschen chemischen Gesellschaft* **1886,** 19, 210.
133. Xiao, S. Q.; Pirouz, P. *Journal of Materials Research* **2011,** 7, 1406.
134. Macfarlane, G. G.; Roberts, V. *Physical Review* **1955,** 97, 1714.
135. Moontragoon, P.; Ikonić, Z.; Harrison, P. *Semiconductor Science and Technology* **2007,** 22, 742.
136. Maeda, Y.; Tsukamoto, N.; Yazawa, Y.; Kanemitsu, Y.; Masumoto, Y. *Applied Physics Letters* **1991,** 59, 3168.
137. Trwoga, P. F.; Kenyon, A. J.; Pitt, C. W. *Journal of Applied Physics* **1998,** 83, 3789.
138. Peelaers, H.; Partoens, B.; Giantomassi, M.; Rangel, T.; Goossens, E.; Rignanese, G. M.; Gonze, X.; Peeters, F. M. *Physical Review B* **2011,** 83.
139. Sze, S. M.; Irvin, J. C. *Solid-State Electronics* **1968,** 11, 599.
140. Gagliani, G.; Reggiani, L. *Il Nuovo Cimento B* **2008,** 30, 207.
141. Kroemer, H.; Polasko, K. J.; Wright, S. C. *Applied Physics Letters* **1980,** 36, 763.
142. Aksoy, B.; Kalay, Y. E.; Unalan, H. E. *Journal of Crystal Growth* **2014,** 392, 20.
143. Gouveia, R. C.; Kamimura, H.; Munhoz, R.; Rodrigues, A. D.; Leite, E. R.; Chiquito, A. J. *Materials Chemistry and Physics* **2016,** 183, 145.
144. Li, L.; Fang, X.; Chew, H. G.; Zheng, F.; Liew, T. H.; Xu, X.; Zhang, Y.; Pan, S.; Li, G.; Zhang, L. *Advanced Functional Materials* **2008,** 18, 1080.
145. Nguyen, P.; Ng, H. T.; Meyyappan, M. *Advanced Materials* **2005,** 17, 549.
146. Sutter, E.; Ozturk, B.; Sutter, P. *Nanotechnology* **2008,** 19, 435607.
147. Morales, A. M. *Science* **1998,** 279, 208.
148. Schmidt, V.; Wittemann, J. V.; Senz, S.; Gosele, U. *Advanced Materials* **2009,** 21, 2681.
149. Barth, S.; Boland, J. J.; Holmes, J. D. *Nano Letters* **2011,** 11, 1550.
150. Okamoto, H.; Massalski, T. B. *Bulletin of Alloy Phase Diagrams* **1984,** 5, 601.
151. Adhikari, H.; McIntyre, P. C.; Marshall, A. F.; Chidsey, C. E. D. *Journal of Applied Physics* **2007,** 102, 094311.
152. Sivaram, S. V.; Hui, H. Y.; de la Mata, M.; Arbiol, J.; Filler, M. A. *Nano Letters* **2016**.
153. Sivaram, S. V.; Shin, N.; Chou, L. W.; Filler, M. A. *Journal of the American Chemical Society* **2015,** 137, 9861.
154. Jagannathan, H.; Deal, M.; Nishi, Y.; Woodruff, J.; Chidsey, C.; McIntyre, P. C. *Journal of Applied Physics* **2006,** 100, 024318.
155. Adhikari, H.; Marshall, A. F.; Chidsey, C. E.; McIntyre, P. C. *Nano Letters* **2006,** 6, 318.

156. Greytak, A. B.; Lauhon, L. J.; Gudiksen, M. S.; Lieber, C. M. *Applied Physics Letters* **2004,** 84, 4176.
157. Chen, W.; Yu, L.; Misra, S.; Fan, Z.; Pareige, P.; Patriarche, G.; Bouchoule, S.; Roca i Cabarrocas, P. *Nature Communications* **2014,** 5, 4134.
158. Tyler, W. W. *Journal of Physics and Chemistry of Solids* **1959,** 8, 59.
159. Tuan, H. Y.; Lee, D. C.; Korgel, B. A. *Angewandte Chemie International Edition* **2006,** 45, 5184.
160. Geaney, H.; Mullane, E.; Ramasse, Q. M.; Ryan, K. M. *Nano Letters* **2013,** 13, 1675.
161. O'Regan, C.; Biswas, S.; Barth, S.; Morris, M. A.; Petkov, N.; Holmes, J. D. *Journal of Materials Chemistry C* **2014,** 2, 4597.
162. Richards, B. T.; Gaskey, B.; Levin, B. D. A.; Whitham, K.; Muller, D.; Hanrath, T. *Journal of Materials Chemistry C* **2014,** 2, 1869.
163. Geaney, H.; Dickinson, C.; Barrett, C. A.; Ryan, K. M. *Chemistry of Materials* **2011,** 23, 4838.
164. Sun, X.; Calebotta, G.; Yu, B.; Selvaduray, G.; Meyyappan, M. *Journal of Vacuum Science & Technology B* **2007,** 25.
165. Wen, C. Y.; Reuter, M. C.; Bruley, J.; Tersoff, J.; Kodambaka, S.; Stach, E. A.; Ross, F. M. *Science* **2009,** 326, 1247.
166. Mathur, S.; Shen, H.; Sivakov, V.; Werner, U. *Chemistry of Materials* **2004,** 16, 2449.
167. Barth, S.; Koleśnik, M. M.; Donegan, K.; Krstić, V.; Holmes, J. D. *Chemistry of Materials* **2011,** 23, 3335.
168. Lu, X.; Fanfair, D. D.; Johnston, K. P.; Korgel, B. A. *Journal of the American Chemical Society* **2005,** 127, 15718.
169. Park, J.; Kim, K. *Electronic Materials Letters* **2012,** 8, 545.
170. Seifner, M. S.; Pertl, P.; Bernardi, J.; Biswas, S.; Holmes, J. D.; Barth, S. *Materials Letters* **2016,** 173, 248.
171. Geaney, H.; Mullane, E.; Ryan, K. M. *Journal of Materials Chemistry C* **2013,** 1, 4996.
172. Ge, M.; Liu, J. F.; Wu, H.; Yao, C.; Zeng, Y.; Fu, Z. D.; Zhang, S. L.; Jiang, J. Z. *The Journal of Physical Chemistry C* **2007,** 111, 11157.
173. Zaitseva, N.; Harper, J.; Gerion, D.; Saw, C. *Applied Physics Letters* **2005,** 86.
174. Hobbs, R. G.; Barth, S.; Petkov, N.; Zirngast, M.; Marschner, C.; Morris, M. A.; Holmes, J. D. *Journal of the American Chemical Society* **2010,** 132, 13742.
175. Chockla, A. M.; Korgel, B. A. *Journal of Materials Chemistry* **2009,** 19, 996.
176. Gerung, H.; Boyle, T. J.; Tribby, L. J.; Bunge, S. D.; Brinker, C. J.; Han, S. M. *Journal of the American Chemical Society* **2006,** 128, 5244.
177. Hanrath, T.; Korgel, B. A. *Journal of the American Chemical Society* **2002,** 124, 1424.
178. Barrett, C. A.; Gunning, R. D.; Hantschel, T.; Arstila, K.; O'Sullivan, C.; Geaney, H.; Ryan, K. M. *Journal of Materials Chemistry* **2010,** 20, 135.

179. Mullane, E.; Kennedy, T.; Geaney, H.; Dickinson, C.; Ryan, K. M. *Chemistry of Materials* **2013,** 25, 1816.
180. Barth, S.; Seifner, M. S.; Bernardi, J. *Chemical Communications* **2015,** 51, 12282.
181. Mullane, E.; Geaney, H.; Ryan, K. M. *Chemical Communications* **2012,** 48, 5446.
182. Ma, L.; Gu, J.; Fahrenkrug, E.; Maldonado, S. *Journal of the Electrochemical Society* **2014,** 161, D3044.
183. Fahrenkrug, E.; Maldonado, S. *Accounts of Chemical Research* **2015,** 48, 1881.
184. Carim, A. I.; Collins, S. M.; Foley, J. M.; Maldonado, S. *Journal of the American Chemical Society* **2011,** 133, 13292.
185. Fahrenkrug, E.; Biehl, J.; Maldonado, S. *Chemistry of Materials* **2015**, 150420140053005.
186. Fahrenkrug, E.; Gu, J.; Jeon, S.; Veneman, P. A.; Goldman, R. S.; Maldonado, S. *Nano Letters* **2014,** 14, 847.
187. Wang, D.; Dai, H. *Angewandte Chemie International Edition* **2002,** 114, 4977.
188. Kamins, T. I.; Li, X.; Williams, R. S.; Liu, X. *Nano Letters* **2004,** 4, 503.
189. Chou, Y.-C.; Wen, C.-Y.; Reuter, M. C.; Su, D.; Stach, E. A.; Ross, F. M. *ACS Nano* **2012,** 6, 6407.
190. Patent No: US8507381 B2, Renard, V.; Jousseaume, V.; Jublot, M., United States, 2013.
191. Read, C. G.; Biacchi, A. J.; Schaak, R. E. *Chemistry of Materials* **2013,** 25, 4304.
192. Boyle, T. J.; Tribby, L. J.; Ottley, L. A.; Han, S. M. *European Journal of Inoganic Chemistry* **2009,** 2009, 5550.
193. Davidson, F. M.; Lee, D. C.; Fanfair, D. D.; Korgel, B. A. *The Journal of Physical Chemistry C* **2007,** 111, 2929.
194. Algra, R. E.; Verheijen, M. A.; Borgstrom, M. T.; Feiner, L. F.; Immink, G.; van Enckevort, W. J.; Vlieg, E.; Bakkers, E. P. *Nature* **2008,** 456, 369.
195. Dick, K. A.; Thelander, C.; Samuelson, L.; Caroff, P. *Nano Letters* **2010,** 10, 3494.
196. Zuo, J. M.; Li, B. Q. *Physical Review Letters* **2002,** 88, 255502.
197. Olesinski, R. W.; Abbaschian, G. J. *Bulletin of Alloy Phase Diagrams* **1988,** 9, 58.
198. Hanrath, T.; Korgel, B. A. *Small* **2005,** 1, 717.
199. Tuan, H.-Y.; Lee, D. C.; Hanrath, T.; Korgel, B. A. *Chemistry of Materials* **2005,** 17, 5705.
200. Biswas, S.; Singha, A.; Morris, M. A.; Holmes, J. D. *Nano Letters* **2012,** 12, 5654.
201. Wiley, B.; Sun, Y.; Chen, J.; Cang, H.; Li, Z.-Y.; Li, X.; Xia, Y. *MRS Bulletin* **2005,** 30, 356.
202. Simoen, E.; Claeys, C., *Germanium-Based Technologies*. Elsevier: Oxford, 2007; p 67.
203. Levy, R., *Microelectronic Materials and Processes*. Springer Netherlands, 1989.
204. Bracht, H.; Schneider, S.; Kube, R. *Microelectronic Engineering* **2011,** 88, 452.
205. Fuller, C. S. *Physical Review* **1952,** 86, 136.
206. Nastasi, M.; Mayer, J. W.; Walter, K. C., Ion Implantation. In *Kirk-Othmer Encyclopedia of Chemical Technology*, John Wiley & Sons, Inc.: 2000.

207. Duffy, R.; Shayesteh, M.; Kazadojev, I.; Yu, R. *Germanium Doping Challenges*, 13th International Workshop on Junction Technology (IWJT), Kyoto, Japan, 2013; IEEE: Kyoto, Japan.
208. Suzuki, K.; Ikeda, K.; Yamashita, Y.; Harada, M.; Taoka, N.; Kiso, O.; Yamamoto, T.; Sugiyama, N.; Takagi, S.-I. *IEEE Transactions on Electron Devices* **2009,** 56, 627.
209. Olesinski, R. W.; Abbaschian, G. J. *Bulletin of Alloy Phase Diagrams* **1984,** 5, 180.
210. Biswas, S.; Doherty, J.; Saladukha, D.; Ramasse, Q.; Majumdar, D.; Upmanyu, M.; Singha, A.; Ochalski, T.; Morris, M. A.; Holmes, J. D. *Nature Communications* **2016,** 7, 11405.
211. Bodnarchuk, M. I.; Kravchyk, K. V.; Krumeich, F.; Wang, S.; Kovalenko, M. V. *ACS Nano* **2014,** 8, 2360.
212. Lu, X.; Korgel, B. A. *Chemistry - A European Journal* **2014,** 20, 5874.
213. Olesinski, R. W.; Abbaschian, G. J. *Bulletin of Alloy Phase Diagrams* **1984,** 5, 265.
214. Olesinski, R. W.; Abbaschian, G. J. *Bulletin of Alloy Phase Diagrams* **1984,** 5, 374.
215. Koren, E.; Elias, G.; Boag, A.; Hemesath, E. R.; Lauhon, L. J.; Rosenwaks, Y. *Nano Letters* **2011,** 11, 2499.
216. He, G.; Atwater, H. A. *Physical Review Letters* **1997,** 79, 1937.
217. Jenkins, D. W.; Dow, J. D. *Physical Review B* **1987,** 36, 7994.
218. Huang, W.; Cheng, B.; Xue, C.; Li, C. *Physica B* **2014,** 443, 43.
219. Huang, W.; Cheng, B.; Xue, C.; Yang, H. *Journal of Alloys and Compounds* **2017,** 701, 816.
220. Flynn, G.; Palaniappan, K.; Sheehan, M.; Kennedy, T.; Ryan, K. M. *Nanotechnology* **2017,** 28, 255603.
221. Hanrath, T.; Korgel, B. A. *Advanced Materials* **2003,** 15, 437.
222. Barth, S.; Jimenez-Diaz, R.; Sama, J.; Prades, J. D.; Gracia, I.; Santander, J.; Cane, C.; Romano-Rodriguez, A. *Chemical Communications* **2012,** 48, 4734.
223. Dzarnoski, J.; O'Neal, H. E.; Ring, M. A. *Journal of the American Chemical Society* **1981,** 103, 5740.
224. Stanley, A. E.; Johnson, R. A.; Turner, J. B.; Roberts, A. H. *Applied Spectroscopy* **2016,** 40, 374.
225. Schmidt, V.; Senz, S.; Gosele, U. *Nano Letters* **2005,** 5, 931.
226. Cordero, B.; Gomez, V.; Platero-Prats, A. E.; Reves, M.; Echeverria, J.; Cremades, E.; Barragan, F.; Alvarez, S. *Dalton Transactions* **2008**, 2832.
227. Moutanabbir, O.; Isheim, D.; Blumtritt, H.; Senz, S.; Pippel, E.; Seidman, D. N. *Nature* **2013,** 496, 78.
228. Oehme, M.; Kostecki, K.; Schmid, M.; Oliveira, F.; Kasper, E.; Schulze, J. *Thin Solid Films* **2014,** 557, 169.
229. Ramasamy, K.; Kotula, P. G.; Fidler, A. F.; Brumbach, M. T.; Pietryga, J. M.; Ivanov, S. A. *Chemistry of Materials* **2015**, 150626072745006.

230. Esteves, R. J. A.; Ho, M. Q.; Arachchige, I. U. *Chemistry of Materials* **2015,** 27, 1559.
231. Zhou, Q.; Chan, T. K.; Lim, S. L.; Zhan, C.; Osipowicz, T.; Gong, X.; Tok, E. S.; Yeo, Y. C. *ECS Solid State Letters* **2014,** 3, P91.
232. Coombes, C. J. *Journal of Physics F* **1972,** 2, 441.
233. Rebelo, L. P.; Canongia Lopes, J. N.; Esperança, J. M.; Filipe, E. *The Journal of Physical Chemistry B* **2005,** 109, 6040.
234. Gao, L.; Hou, Z.; Zhang, H.; He, J.; Liu, Z.; Zhang, X.; Han, B. *Journal of Chemical & Engineering Data* **2001,** 46, 1635.
235. Gerung, H.; Bunge, S. D.; Boyle, T. J.; Brinker, C. J.; Han, S. M. *Chemical Communications* **2005**, 1914.
236. Seifner, M. S.; Biegger, F.; Lugstein, A.; Bernardi, J.; Barth, S. *Chemistry of Materials* **2015,** 27, 6125.
237. Yuan, F.-W.; Yang, H.-J.; Tuan, H.-Y. *Journal of Materials Chemistry* **2011,** 21, 13793.
238. Dřínek, V.; Fajgar, R.; Klementová, M.; Šubrt, J. *Journal of the Electrochemical Society* **2010,** 157, K218.
239. Thurmer, K.; Williams, E.; Reutt-Robey, J. *Science* **2002,** 297, 2033.
240. Conesa-Boj, S. n.; Zardo, I.; Estradé, S. n.; Wei, L.; Jean Alet, P.; Roca i Cabarrocas, P.; Morante, J. R.; Peiró, F.; Morral, A. F. i.; Arbiol, J. *Crystal Growth & Design* **2010,** 10, 1534.
241. Chandrasekaran, H.; Sumanasekara, G. U.; Sunkara, M. K. *Journal of Physical Chemistry B* **2006,** 110, 18351.
242. Olesinski, R. W.; Abbaschian, G. J. *Bulletin of Alloy Phase Diagrams* **1985,** 6, 258.
243. Suda, K.; Ishihara, S.; Sawamoto, N.; Machida, H.; Ishikawa, M.; Sudoh, H.; Ohshita, Y.; Ogura, A. *Japanese Journal of Applied Physics* **2014,** 53, 110301.
244. Inuzuka, Y.; Ike, S.; Asano, T.; Takeuchi, W.; Nakatsuka, O.; Zaima, S. *Thin Solid Films* **2016,** 602, 7.
245. Machida, H.; Hamada, S.; Horiike, T.; Ishikawa, M.; Ogura, A.; Ohshita, Y.; Ohba, T. *Japanese Journal of Applied Physics* **2010,** 49, 05FF06.
246. He, M.; Protesescu, L.; Caputo, R.; Krumeich, F.; Kovalenko, M. V. *Chemistry of Materials* **2015,** 27, 635.
247. Yarema, M.; Worle, M.; Rossell, M. D.; Erni, R.; Caputo, R.; Protesescu, L.; Kravchyk, K. V.; Dirin, D. N.; Lienau, K.; von Rohr, F.; Schilling, A.; Nachtegaal, M.; Kovalenko, M. V. *Journal of the American Chemical Society* **2014,** 136, 12422.
248. Pokroy, B.; Aichmayer, B.; Schenk, A. S.; Haimov, B.; Kang, S. H.; Fratzl, P.; Aizenberg, J. *Journal of the American Chemical Society* **2010,** 132, 14355.
249. Sudo, S.; Nagata, S.; Kokado, K.; Sada, K. *Chemistry Letters* **2014,** 43, 1207.
250. Li, Z.; Tao, X.; Cheng, Y.; Wu, Z.; Zhang, Z.; Dang, H. *Materials Science and Engineering: A* **2005,** 407, 7.

251. Okitsu, K.; Mizukoshi, Y.; Bandow, H.; Maeda, Y.; Yamamoto, T.; Nagata, Y. *Ultrasonics Sonochemistry* **1996,** 3, S249.
252. Yeung, S. A.; Hobson, R.; Biggs, S.; Grieser, F. *Journal of the Chemical Society, Chemical Communications* **1993**, 378.
253. Nagata, Y.; Watananabe, Y.; Fujita, S.-i.; Dohmaru, T.; Taniguchi, S. *Journal of the Chemical Society, Chemical Communications* **1992**, 1620.
254. Yamaguchi, A.; Mashima, Y.; Iyoda, T. *Angewandte Chemie International Edition* **2015,** 54, 12809.
255. Kumar, V. B.; Gedanken, A.; Kimmel, G.; Porat, Z. *Ultrasonics Sonochemistry* **2014,** 21, 1166.
256. Hohman, J. N.; Kim, M.; Wadsworth, G. A.; Bednar, H. R.; Jiang, J.; LeThai, M. A.; Weiss, P. S. *Nano Letters* **2011,** 11, 5104.
257. Kumar, R. V.; Diamant, Y.; Gedanken, A. *Chemistry of Materials* **2000,** 12, 2301.
258. Mason, T.; Peters, D., Practical Sonochemistry (Second Edition). Woodhead Publishing: 2002.
259. Loos, D.; Schnöckel, H. *Journal of Organometallic Chemistry* **1993,** 463, 37.
260. Loos, D.; Baum, E.; Ecker, A.; Schnöckel, H.; Downs, A. J. *Angewandte Chemie International Edition* **1997,** 36, 860.
261. Dyagileva, L. M.; Mar'in, V. P.; Tsyganova, E. I.; Razuvaev, G. A. *Journal of Organometallic Chemistry* **1979,** 175, 63.
262. Aghazadeh Meshgi, M.; Biswas, S.; McNulty, D.; O'Dwyer, C.; Alessio Verni, G.; O'Connell, J.; Davitt, F.; Letofsky-Papst, I.; Poelt, P.; Holmes, J. D.; Marschner, C. *Chemistry of Materials* **2017,** 29, 4351.
263. Picraux, S. T.; Dayeh, S. A.; Manandhar, P.; Perea, D. E.; Choi, S. G. *Journal of Minerals* **2010,** 62, 35.
264. Madras, P.; Dailey, E.; Drucker, J. *Nano Letters* **2009,** 9, 3826.
265. Bueche, A. M. *Journal of Polymer Science* **1955,** 15, 97.
266. Wacaser, B. A.; Dick, K. A.; Johansson, J.; Borgström, M. T.; Deppert, K.; Samuelson, L. *Advanced Materials* **2009,** 21, 153.
267. Nebol'sin, V. A.; Shchetinin, A. A. *Inorganic Materials* **2003,** 39, 899.
268. Trumbore, F. A.; Porbansky, E. M.; Tartaglia, A. A. *Journal of Physics and Chemistry of Solids* **1959,** 11, 239.
269. Schwalbach, E. J.; Voorhees, P. W. *Nano Letters* **2008,** 8, 3739.
270. Baker, J. C.; Gahn, J. W. *Acta Metallurgica* **1969,** 17, 575.
271. White, C. W.; Wilson, S. R.; Appleton, B. R.; Young, F. W. *Journal of Applied Physics* **1980,** 51, 738.
272. Reitano, R.; Smith, P. M.; Aziz, M. J. *Journal of Applied Physics* **1994,** 76, 1518.
273. Ma, L.; Fahrenkrug, E.; Gerber, E.; Crowe, A. J.; Venable, F.; Bartlett, B. M.; Maldonado, S. *ACS Energy Letters* **2016,** 2, 238.

274. Levinshtein, M.; Rumyantsev, S.; Shur, M., *Handbook Series on Semiconductor Parameters*. World Scientific Publishing Co Pte Ltd: Singapore, 1996.
275. Kesan, V. P.; Iyer, S. S.; Cotte, J. M. *Journal of Crystal Growth* **1991,** 111, 847.
276. Zabidi, N. A.; Kassim, H. A.; Shrivastava, K. N. *AIP Conference Proceedings,* **2011,** 1328, 77.
277. Lieten, R. R.; Degroote, S.; Kuijk, M.; Borghs, G. *Applied Physics Letters* **2008,** 92.
278. Cuttriss, D. B. *Bell System Technical Journal* **1961,** 40, 509.
279. Burchhart, T.; Lugstein, A.; Hyun, Y. J.; Hochleitner, G.; Bertagnolli, E. *Nano Letters* **2009,** 9, 3739.
280. Hanrath, T.; Korgel, B. A. *Journal of Physical Chemistry B* **2005,** 109, 5518.
281. Simanullang, M.; Wisna, G. B. M.; Usami, K.; Cao, W.; Kawano, Y.; Banerjee, K.; Oda, S. *Journal of Materials Chemistry C* **2016,** 4, 5102.
282. Gu, G.; Burghard, M.; Kim, G. T.; Düsberg, G. S.; Chiu, P. W.; Krstic, V.; Roth, S.; Han, W. Q. *Journal of Applied Physics* **2001,** 90, 5747.
283. Serway, R. A., *Principles of Physics*. Saunders College Publications: Fort Worth, Texas, 1997.
284. Mahenderkar, N. K.; Liu, Y. C.; Koza, J. A.; Switzer, J. A. *ACS Nano* **2014,** 8, 9524.
285. Lee, J. W.; Kang, M. G.; Kim, B. S.; Hong, B. H.; Whang, D.; Hwang, S. W. *Scripta Materialia* **2010,** 63, 1009.
286. Sun, Y.; Yin, Y.; Mayers, B. T.; Herricks, T.; Xia, Y. *Chemistry of Materials* **2002,** 14, 4736.
287. Burchhart, T.; Zeiner, C.; Hyun, Y. J.; Lugstein, A.; Hochleitner, G.; Bertagnolli, E. *Nanotechnology* **2010,** 21, 435704.
288. Serway, R. A., *Principles of Physics*. Saunders College Pub.: 1998.
289. Krusin-Elbaum, L.; Aboelfotoh, M. O. *Applied Physics Letters* **1991,** 58, 1341.
290. IUPAC, *Compendium of Chemical Terminology, 2nd ed. (the "Gold Book")*. Blackwell Scientific Publications: Oxford, 1997.
291. Dunlap, W. C. *Physical Review* **1954,** 94, 1531.
292. Sharp, J.; Lee, W. J.; Ploog, K.; Umana-Membreno, G. A.; Faraone, L.; Dell, J. M. *Solid-State Electronics* **2013,** 89, 146.
293. Lugstein, A.; Mijic, M.; Burchhart, T.; Zeiner, C.; Langegger, R.; Schneider, M.; Schmid, U.; Bertagnolli, E. *Nanotechnology* **2013,** 24, 065701.
294. Coskun, S.; Aksoy, B.; Unalan, H. E. *Crystal Growth & Design* **2011,** 11, 4963.
295. Wiley, B.; Sun, Y.; Mayers, B.; Xia, Y. *Chemistry - A European Journal* **2005,** 11, 454.
296. Skrabalak, S. E.; Wiley, B. J.; Kim, M.; Formo, E. V.; Xia, Y. *Nano Letters* **2008,** 8, 2077.
297. Dittmar, K.; Jutzi, P.; Schmalhorst, J.; Reiss, G. *Chemical Vapor Deposition* **2001,** 7, 193.
298. Nolan, B. M.; Chan, E. K.; Zhang, X.; Muthuswamy, E.; van Benthem, K.; Kauzlarich, S. M. *ACS Nano* **2016,** 10, 5391.
299. Binner, J. G. P.; Dimitrakis, G.; Price, D. M.; Reading, M.; Vaidhyanathan, B. *Journal of Thermal Analysis and Calorimetry* **2006,** 84, 409.

300. McHugh, M. A., *Supercritical Fluid Extraction (Second Edition)*. Butterworth-Heinemann: Boston, US, 1994.
301. Lu, X.; Harris, J. T.; Villarreal, J. E.; Chockla, A. M.; Korgel, B. A. *Chemistry of Materials* **2013,** 25, 2172.
302. Thombare, S. V.; Marshall, A. F.; McIntyre, P. C. *Journal of Applied Physics* **2012,** 112, 054325.
303. Kang, K.; Kim, D. A.; Lee, H.-S.; Kim, C.-J.; Yang, J.-E.; Jo, M.-H. *Advanced Materials* **2008,** 20, 4684.
304. Amelinckx, S.; Zhang, X. B.; Bernaerts, D.; Zhang, X. F.; Ivanov, V.; Nagy, J. B. *Science* **1994,** 265, 635.
305. Tuan, H.-Y.; Ghezelbash, A.; Korgel, B. A. *Chemistry of Materials* **2008,** 20, 2306.
306. Wang, H.; Qiao, X.; Chen, J.; Wang, X.; Ding, S. *Materials Chemistry and Physics* **2005,** 94, 449.
307. Wu, C.; Mosher, B. P.; Lyons, K.; Zeng, T. *Journal of Nanoscience and Nanotechnology* **2010,** 10, 2342.
308. Thombare, S. V.; Marshall, A. F.; McIntyre, P. C. *APL Materials* **2013,** 1, 061101.
309. Clark, T. E.; Nimmatoori, P.; Lew, K. K.; Pan, L.; Redwing, J. M.; Dickey, E. C. *Nano Letters* **2008,** 8, 1246.
310. Dubrovskii, V. G.; Sibirev, N. V. *Journal of Crystal Growth* **2007,** 304, 504.
311. González, A. L.; Noguez, C.; Beránek, J.; Barnard, A. S. *The Journal of Physical Chemistry C* **2014,** 118, 9128.
312. Bakkers, E. P.; van Dam, J. A.; De Franceschi, S.; Kouwenhoven, L. P.; Kaiser, M.; Verheijen, M.; Wondergem, H.; van der Sluis, P. *Nature Materials* **2004,** 3, 769.
313. Bobb, L. C.; Holloway, H.; Maxwell, K. H.; Zimmerman, E. *Journal of Applied Physics* **1966,** 37, 4687.
314. Johnson, O. H.; Harris, D. M.; Rochow, E. G.; Tolivaisa, N., *Inorganic Synthesis*. John Wiley & Sons, Inc.: 1957; Vol. 5.
315. Roskamp, C. A.; Roskamp, E. J. *e-EROS Encyclopedia of Reagents for Organic Synthesis* **2001**.
316. Grenz, M.; Hahn, E.; Du Mont, W.-w.; Pickardt, J.; Pickardt, J.; Grenz, M.; Hahn, E. *Angewandte Chemie International Edition* **1984,** 96, 69.
317. Golloch, A.; Kuß, H. M.; Sartori, P., *Anorganisch-Chemische Präparate: Darstellung und Charakterisierung ausgewählter Verbindungen*. De Gruyter: 1985.
318. Lappert, M.; Protchenko, A.; Power, P.; Seeber, A., *Subvalent Amides of Silicon and the Group 14 Metals*. John Wiley & Sons, Ltd: 2008.

C. Curriculum Vitae

Personal data

Name	Dipl. Ing. Patrik Pertl BSc.
Address	Josef Schwarz Straße 10, A-8052 Graz
Date and Place of Birth	July, 12th 1987, Graz
Citizenship	Austrian
Email	patrik.pertl@gmail.com

Education

Since 07/2014	PhD studies (supervised by Privdoz. Dipl. Chem. Dr. rer. nat. Sven Barth) IMC, TU Vienna
04/2012-04/2014	Master studies Technical Chemistry, TU Graz, Thesis: "Lead Sulfide Nanocrystals as Electron Acceptor in Hybrid Solar Cells" (supervised by Assoc.Prof. Dipl.-Ing. Dr.techn. Gregor Trimmel)
09/2008-03/2012	Bachelor studies Chemistry, TU Graz, Thesis: "Calziumzinkat als anodisches Aktivmaterial für die aufladbare Zink-Luft-Batterie" (supervised by Ass.Prof. Dipl.-Ing. Dr.techn. Waltraud Taucher-Mautner)
09/2006-09/2008	Bachelor studies Biomedical Engineering, TU Graz
09/1998-07/2006	Secondary school, BG/BRG Klusemannstraße, Graz

Work experience

07/2014-06/2017	University assistant, Institute of Materials Chemistry, TU Vienna
07/2012-08/2012	Mayr Melnhof Karton, Frohnleiten. F & E, analytics
08/2011-09/2011	Mayr Melnhof Karton, Frohnleiten. F & E, analytics
07/2010-08/2010	JSW Lifescience, Grambach. Histology
07/2010-08/2009	JSW Lifescience, Grambach. Animal Facility

08/2010-09/2009	JSW Lifescience, Grambach. Animal Facility
09/2006-03/2007	Compulsory community service, Red Cross Graz

Competences

Languages	German (mother tongue), English (fluent, spoken and written), French (basics).
Technical Competences	Handling of moisture and oxygen sensitive compounds, Schlenk techniques, glovebox techniques, CVD, XRD, IR, NMR, electrical characterisation (I-V measurements, IPCE, CV), SEM.
IT Competences	MS Office, Origin, LATEX, chemistry related software (ChemDraw, X'Pert Highscore, SciFinder, etc.), image processing (GIMP).
Driving Licenses	Class A and B.

Further Information

Hobbies	sports (soccer, running, ice hockey, cycling), e-guitar, RC models, 3D printing
Memberships	Aero Club Austria, USFC Stainztal, MF Dobl

Publications

- *"Lead-supported Germanium Nanowire Growth"*
  M. S. Seifner, P. Pertl, J. Bernardi, S.Biswas, J. D. Holmes, S. Barth, *Materials Letters*, **2016**, *173, 248.*

Posters:

- *"Microwave-assisted Synthesis of Crystalline Germanium/Tin Alloy Nanostructures"*
  P. Pertl, M. S. Seifner, S. Barth, *16th Austrian Chemistry Days*, **2015**, Innsbruck.

Oral Presentation:

- *"Nucleation and Growth Phenomena of Germanium Nanowires using Unusual Metal Seeds"*
  P. Pertl, *Seminar Series Focus Materials Chemistry*, **2017**, IMC TU Wien